TECHNISCHE UNIVERSITÄT MÜNCHEN

Lehrstuhl für Technische Chemie II

Impact of La^{3+} cations in FAU type zeolites to hydride transfer reactions

Florian Schüßler

Vollständiger Abdruck der von der Fakultät für Chemie der Technischen Universität München zur Erlangung des akademischen Grades eines

Doktor-Ingenieurs (Dr.-Ing.)

genehmigten Dissertation.

Vorsitzender:	Univ.-Prof. Dr. K. Köhler
Prüfer der Dissertation:	1. Univ.-Prof. Dr. J. A. Lercher
	2. Univ.-Prof. Dr. D. Weuster-Botz

Die Dissertation wurde am 16.01.2013 bei der Technischen Universität München eingereicht und durch die Fakultät für Chemie am 07.05.2013 angenommen.

Für meine Familie

„Die Neugier steht immer an erster Stelle eines Problems, das gelöst werden will.“

Galileo Galilei

(1564-1642)

Acknowledgements

During my work on this thesis I worked together with a lot of friendly and highly motivated people. For this time I thank all of you. Your time, support, expertise and attention have been a most valuable contribution to my work. Science is never an achievement of an individual but always a product of the team.

First of all I want to thank Prof. Johannes A. Lercher for supporting me in this interesting project. He always found time for discussion and embraced his knowledge in the most efficient way. Furthermore he gave me the possibility to take part in many international conferences. For this great chance to work on this very interesting topic I thank you a lot.

Further I want to thank Prof. Dr.-Ing. Dirk Weuster-Botz for his role as a secondary reviewer and for evaluating this thesis.

My special thanks go to Erika Ember for her ongoing support. Thanks for the discussions and corrections to the thesis and the papers.

I would like to thank Prof. Andreas Jentys for his help, in particular for fruitful discussions on temperature programmed desorption and spectroscopy.

To work on projects using capacities of different facilities was very interesting. Thanks to Carsten Sievers, that you always gave me the chance to participate in such projects. During these projects I learnt a lot how to argue in conference calls.

Thanks to Evgeny A. Pidko, Emiel J.M. Hensen and Prof. Rutger A. van Santen for discussions and cooperation into DFT calculations. The study in lanthanum cation position and species was very interesting and challenging.
Further I want to thank Sonja Kouva, Jaana Kanervo, Outi Krause and Roberta Olindo. The collaboration in temperature programmed desorption of ammonia in experimental as well as micro-kinetic modeling was very interesting.

I would like to thank Gabriele Raudaschl-Sieber, Stefan Steuernagel and Gerd Gemmecker for support in solid state NMR spectroscopy. My special thanks go to Jiří Dědeček for deepening my knowledge in solid state NMR experiments. Moreover, I am very grateful to Gerhard Althoff-Ospelt for his support in any NMR questions. The support in ^{139}La NMR experiments was also very helpful.

Thanks to Xaver Hecht, Martin Neukamm, and Andreas Marx for technical support and measurements as well as to Steffi, Katarina and Helen for their help with paperwork.

Stefanie Simson, Arne Holtz, Vedat Akcakaya, Eva Schachtl, Heiko Pfisterer, Sabine Pilsl, Sabine Anton, Elena Popp, Sebastian Müller, Marco Giuman, Patrick Kubryk, Andreas Schmidt, André Utrap and Daniel Weiß, who did their Bachelor-, Master-, Semester- or Diploma thesis under my supervision, should consider themselves included in my thanks.

Deep thankfulness goes also to all my colleagues. Working with you was always a pleasure and I enjoyed that a lot. Especially Sabine Wilhelm, Anna Lubinus, Sarah Maier, Stefanie Simson and Ana Hrabar have been a benefit for my work and grew into friends during this time.

I am very grateful for all my friends, especially Jürgen Liebert, Felix Grabher, Sebastian Jerebic, Tobias Ulbrich, Florian Bittner, Georg Simson, Maximilian Peter, Andreas Kossmann and Felix Buth. Their support and understanding has always been a welcome contribution.

Ein besonderer Dank gilt meinem besten Freund Marcus für die immerwährende Unterstützung.

Vielen Dank Kathrin für deine Geduld und Verständnis, vor allem in der Endphase der Dissertation.

Mein spezieller Dank gilt meinen Eltern Lydia und Dieter sowie meinen Schwestern Stephanie und Miriam. Vielen, Vielen Dank für Eure Unterstützung.

Nomenclature

Å	Angström
a_0	Unit cell parameter
B_0	Magnetic Field
bar	Bar
cm^{-1}	Wavenumber
δ	Chemical Shift (NMR)
eV	Electron Volt
h	Hours
Hz	Herz
K	Kelvin
kg	Kilogram
l	Liter
m	Meter
mA	Milliampere
min	Minute
mol	Mol
mol%	Mol per cent
p	Pressure
ppm	Parts per million
s	Second
V	Volt
vol.%	Volume per cent
wt.%	Weight per cent

Abbreviations

AAS	Atomic Absorption Spectroscopy
BEA	Beta zeolite
BAS	Brønsted Acid Sites
BET	Brunnauer, Emmet, Teller
CSTR	Continuous Stirred Tank Reactor
DFT	Density Functional Theory
DMH	Dimethylhexane
EFAL	Extra Framework Aluminium
FAU	Faujasite zeolite
FCC	Fluidized Catalytic Cracking
FID	Flame Ionization Detector
FTIR	Fourrier Transformation Infrared
GC	Gas Chromatography
ICP-OES	Inductively Coupled Plasma – Optical Emission Spectrometry
IR	Infrared
LAS	Lewis Acid Sites
MAS	Magic Angle Spinning
MFI	Mobile Five
MHp	Methylheptane
MQ	Multiple Quantum
MS	Mass Spectrometry, Mass Spectrometer
NMR	Nuclear Magnetic Resonance
Rpm	Rotations per minute
SAS	Strong Acid Sites
SBAS	Strong Brønsted Acid Sites
SBU	Secondary Building Unit
SEM	Scanning Electron Microscopy
SLAS	Strong Lewis Acid Sites
T-atom	Tetrahedrally coordinated Al or Si atom
TBU	Tertiary Building Unit

TEM	Transmission Electron Microscopy
TMP	Trimethylpentane
TOF	Turnover Frequency
TPD	Temperature Programmed Desorption
USY	Ultra stable Y-type Faujasite zeolite
XAS	X-ray Absorption Spectroscopy
XRD	X-ray Diffraction
ZSM5	Zeolite Socony Mobile 5

Table of Contents

Chapter 1

Chapter 2

Chapter 3

Chapter 6

Appendix

Publication

Chapter 1

General introduction

Oil, gasoline and all other refining products are one of the most valuable products. In the last years the worldwide oil consumption was about 90 million barrel a day while it is further increasing. Therefore, the development and use of highly active and selective catalysts is of enormous importance.

The first chapter is devoted to main catalytic processes in refining industry and relevant zeolitic materials used as catalysts. The role of incorporated metal ions, e.g. lanthanum is presented on the catalytic performance and stability of solid acid catalysts is discussed in detail.

1.1. Catalytic processes in refining industry

Since its first industrial use in 1855 as reactant for the production of kerosene, crude oil has become today's most important chemical. Its range of use is as wide as important but still dominated by the production of fuels for transportation use. Nowadays increasing legislative requirements demand lower emissions and therewith cleaner high performance fuels. High octane numbers imply a good effectiveness caused by a clean and controlled burn-up process. Several possible options were examined in the past as blending fuels with MTBE or alcohols. The former however is causing drink water to smell bad even in a concentration of a few ppm while the latter causing high gasoline vapor pressure.[1] Therefore, in near future the main target remains finding an efficient way to synthesize hydrocarbons with high octane numbers, low Reid vapor pressure and nearly no encumbering characteristics for the environment.

The main challenge in modern refining processes is to transfer the acid-catalyzed alkylation of isobutane and C_3 - C_5 alkenes as fluid cracking compounds into a complex mixture of highly branched alkanes. Major products are iso-octanes, such as trimethylpentanes (TMP) and dimethylhexanes (DMH). Most commonly used mineral acids, such as sulphuric and anhydrous hydrofluoric acid, are applied as catalysts.[1,2] As this poses plant engineering and environmental problems, it is of great techno-economical interest to design novel high-efficient solid acid catalysts which are able to replace mineral acids in these processes. In terms of acidity and stability, zeolites are one of the most promising materials of choice, as they provide strong Brønsted acidity and tailor able site density and porosity. In extensive research work devoted to the development of new heterogeneous catalysts for the hydrocarbon activation, it was confirmed that high surface area porous faujasites are the most promising candidates in terms of activity and stability to catalyze these reactions.[3,4] Further thermal and chemical modification of the zeolitic material, especially the introduction of a metal in the main zeolitic channels of a solid acid catalyst can combine the high catalytic activity of transition metals with the shape selective constrains unique to zeolite structures.[1,2]

1.2. Zeolite catalysts

Zeolites are crystalline microporous (alumino-)silicates of natural or synthetic origin with highly ordered porous structures. In nature more than 40 different types of zeolites exist and nowadays there are over 100 artificial ones known. Because of their ordered pore structure

large pore zeolite like beta, faujasite and mordenite are most commonly used in industrial refining processes.[3-5] Depending on the silica-to-alumina ratio of their framework, synthetic faujasite zeolites are divided into X (Si/Al = 1.0-1.5) and Y (Si/Al > 1.5) zeolites. By using thermal, hydrothermal or chemical methods, some of the alumina can be removed from the Y zeolite framework, resulting in high-silica Y zeolites with increased stability.[2] The stability of the zeolite increases with the Si/Al ratio of the framework.[6] Zeolite Y has superseded zeolite X in this field because, due to the higher Si/Al ratio, it is both more active and more stable[6] at high temperatures.

Zeolites belong to the group of tectosilicates (described also as aluminum-silicates) and have a three-dimensional ordered network. They depend on the $[(Al,Si)O_4]$- tetrahedron as smallest structural unit which are corner-linked over oxygen atoms to polyhedrons, layers and chains and form in faujasite-type zeolites cuboctahedrons (sodalite cages/ β-cages) which define the *secondary building unit (SBU)*. Connections of eight sodalite cages by hexagonal prisms build up a supercage (α-cage). The structure formed by linking *secondary building units* is called *tertiary building unit (TBU)*.[1,2]

As a consequence of the replacement of a silicon framework atom with a net +IV charge by an aluminum atom with a net +III charge, a net negative charge is created. To compensate this charge, various cations, such as H^+, Na^+, ect. are used.[7-9] On this way, by using a proton as a counter ion, new strong Brønsted acid sites are created as indicated in Scheme 1.1.

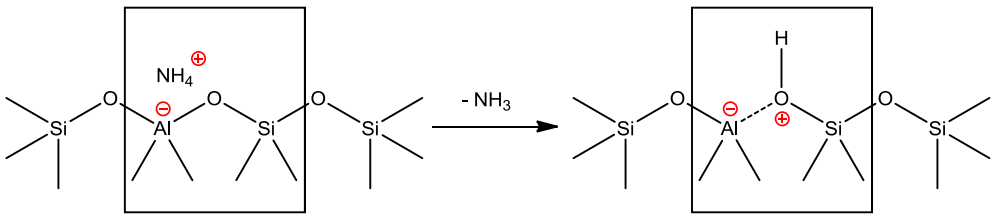

Scheme 1.1: Brønsted acid site generation during calcination

The Brønsted acidity is generated by the steric vicinity of a Si-OH group to a free site of an aluminum ion. As the oxygenium atom coordinates to the aluminum the bond to the hydrogen atom becomes weaker. The elimination of the proton is facilitated and the negative charge is compensated as shown in Scheme 1.2.

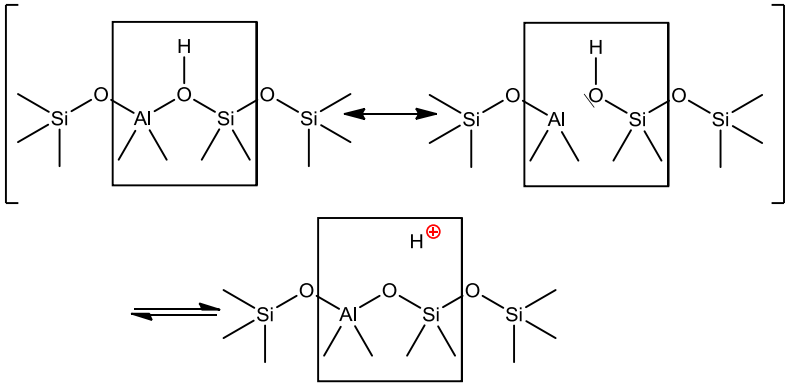

Scheme 1.2: Brønsted acid sites existing in zeolitic material

Besides Brønsted acid sites also Lewis acid sites exist. These are coordinative unsaturated EFAL species which can be produced by dehydration as shown in Scheme 1.3.[9,10]

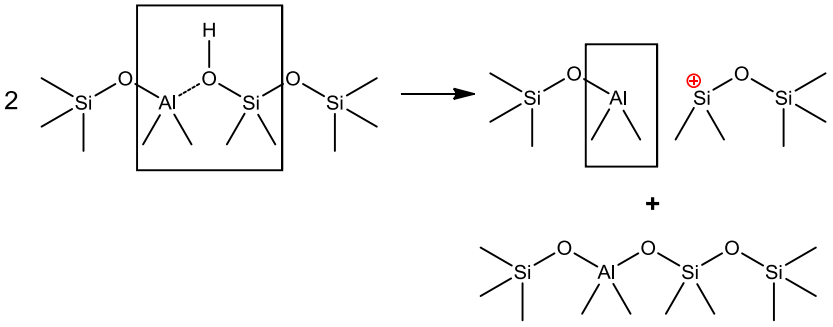

Scheme 1.3: Formation of Lewis acid sites by dealumination

Besides EFAL species also other exchanged cations can form Lewis acid sites. These Lewis acid sites increase the acid strength of neighbored Brønsted acid sites by stabilizing the negative charge of the deprotonated form of the Brønsted acid sites through delocalizing it.

As silicon is stronger electronegative compared to aluminum, the electron withdrawing character of Lewis acidic EFAL species increases with the number of neighbored silicon atoms. This implies that in general a higher concentration of aluminum ions leads to a higher Brønsted acid site concentration but a lower acid strength[11] while the concentration of aluminum is limited by the Loewenstein-Rule which specifies that it is not possible to link two [AlO_4] tetrahedra.[12] Consequently, the lowest possible Si/Al ratio is 1 as the formation of two Si-O-Al-bridge is energetic more beneficial than the formation of one Si-O-Si- and one Al-O-Al-bridge.

As the catalytic effect of zeolites depends on their Brønsted acid sites, increasing acid strength of these positively influences the catalysis.[13] Feller et al. found that increasing lanthanum

concentration in faujasites increases the lifetime in isobutane/2-butene alkylation. Lanthanum causes an increase of the Si-O-Al angle in the lattice leading to a higher ratio of strong Brønsted acid sites (SBAS) to total strong acid sites (SAS).[5] Additionally multivalent lanthanum ions and their electron withdrawing effect causes an increase in the Brønsted acidity as the p-character of the O-H bond is increasing.[14] Especially lanthanum exchanged faujasites showed a great catalytic performance[3,4] as lanthanum ions incorporated into the zeolite lattice stabilize the latter by compensating its negative charge and being involved in the formation of Brønsted acid sites.[15-17] These lanthanum cations are often found in the center of the supercage, the center of the sodalite cage or the twelve-ring window of the supercage.[18] An increasing aluminum concentration in the lattice showed to rise the heat of isobutane absorption.[19] But Sievers et al. found out that lanthanum ions in the lattice affect the heat of absorption even stronger.[20] Lanthanum cation incorporation into faujasite materials is described in the following section.

1.3. Lanthanum speciation and location in faujasite materials

Rare earth exchanged zeolitic materials, like lanthanum exchanged faujasite are well known and often used because of their improved catalytic performance.[21-24] Lanthanum cations incorporated into extra-framework position stabilize the zeolite lattice and involve Brønsted acid sites by hydrolysis.[15-17]

$$[La(H_2O)_n]^{3+} \rightarrow [La(OH)(H_2O)_{n-1}]^{2+} + H^+ \qquad (1)$$

Lanthanum is normally introduced into the lattice by liquid ion exchange. La^{3+} in hydrated form has a kinetic diameter of 7.9 Å while the six-membered ring of the sodalite cage is only 2.5 Å large. During calcinations the hydrated shell is partially removed and lanthanum ions are able to enter the sodalite cage.[18]

In general there are different possible cation positions in faujasite material existing. Figure 1.1 shows the most important position for lanthanum incorporation within sodalite cage as well as supercage.

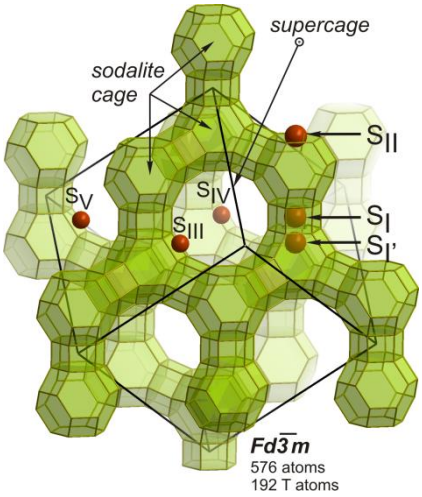

Figure 1.1: Main extra-framework sites in faujasite type zeolites

In hydrated form the cation position is often found in center of twelve-membered ring (site IV) in the supercage as well as in the center of supercage (site V) and sodalite cage (site U).[18] Lanthanum extra-framework positions in sodalite cage after thermal treatment can be close to the six-membered ring of the hexagonal prism or supercage. Lanthanum inside the supercage was often found close to the four-membered ring (site III and III') as well as slightly inside the supercage (site II) close to the six-membered ring of the sodalite cage or shifted to the center of supercage (site II*).[18] Thermal treatment affects the lanthanum species incorporated. Therefore different hydroxylated lanthanum species can exist with different formal charge. In Figure 1.2 three different lanthanum species stabilized (initial state) within the sodalite six-membered ring are shown.

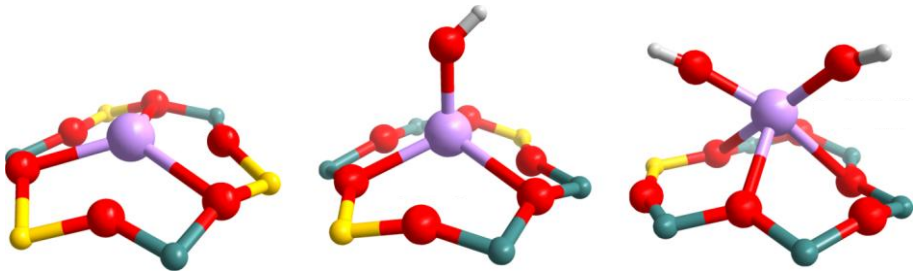

La^{3+} $[LaOH]^{2+}$ $[La(OH)_2]^{+}$

Figure 1.2: La^{3+}, $[LaOH]^{2+}$ and $[La(OH)_2]^{+}$ stabilized within the sodalite six-membered ring

In the case of three aluminum atoms within the sodalite six-membered rings, lanthanum can be stabilized, in the initial state, as La^{3+}. If there are only two ore one aluminum existing in the six-membered ring lanthanum is assumed to be stabilized as $[LaOH]^{2+}$ and $[La(OH)_2]^{+}$, respectively. Note that lanthanum preference to form complexes with large coordination numbers.[25]

1.4. Zeolite modification by acidic and alkaline leaching

The zeolite structure can be modified by removing anhydrides using acidic or alkaline leaching. Both treatments develop the formation of mesopores while acidic treatment removes the extra-framework aluminum (EFAL)[26] which partially block the micropores.[27] Zeolite modification by acidic treatment influence the aluminum concentration and therefore the concentration of Brønsted acid sites is decreasing.[26] Consequently, Brønsted acid catalyzed reactions are influenced in a negative way.

Alkaline treatment using high silica materials, results in a lower Si/Al ratio whereas both atomic species are removed under formation of mesopores.[28-33] NaOH treatment removed internal Si-OH while the defects represented by SiOH in the zeolite lattice increased.[34]

Increasing pore size distribution influence diffusion properties, pore blocking decreases and the catalytic activity increases for Brønsted acid catalyzed reactions.[28,29,35] In general alkali treated materials show preserved Brønsted acidity.[26,28]

1.5. Activation of saturated hydrocarbons

In the following short subchapters different possibilities of alkane activation are described.

1.5.1. Protolytic cracking

At high temperatures alkane activation on zeolites involves the formation of a pentavalent carbonium ion as the transition state. The carbonium ions are very unstable resulting in a transformation into a carbenium ion and an alkane (Scheme 1.4 b) or into a carbenium ion and hydrogen (Scheme 1.4 c).[2]

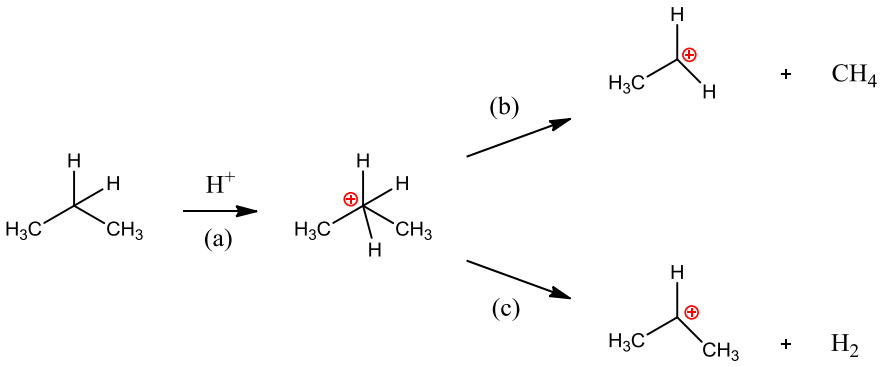

Scheme 1.4: Protolytic activation of propane: (a) carbonium ion formation, (b) protolytic cracking, (c) protolytic dehydrogenation

The intrinsic activation energy for the alkane activation is approximately 200 kJ/mol independent of the structure of the zeolitic material and hydrocarbon used.[36] Due to the high activation energy, the protolytic cracking is only observed at high temperatures.[2]

1.5.2. Hydride abstraction and hydride transfer reaction

Alkane activation can also occur by hydride abstraction on sufficiently strong Lewis acid sites. Markovnikov et al. showed, that liquid acids activate an alkene by formation of the equivalent ester. In this case, the acid add to the highest substituted carbon atom.[37] Hydride abstraction by Brønsted acid site (245 kJ/mol)[38] or extra-framework aluminum (193 kJ/mol)[39] in theoretical studies are comparable to activation energies in protolytic cracking.[2]

Hydride transfer is a fundamental step in carbenium ion based reactions like isomerization, catalytic cracking and alkylation. In hydride transfer reactions, the hydride is abstracted by a carbenium ion located on the catalyst surface.[2]

Hydride transfer reactions are strongly dependent by the nature of carbenium ions. Hydride transfer was subject of many theoretical[40-46] as well as experimental studies.[47-51] In general tertiary carbenium ions are most stable while the stability is decreasing from tertiary > secondary > primary > methyl, respectively.[48]

1.6. Reactions initialized by carbenium ions

Carbenium ion based reactions, like isomerization, catalytic cracking, alkylation as well as hydro processing like hydroisomerization are important reactions in refining industry. In this thesis all of these reactions are presented in detail.

1.6.1. Catalytic cracking

Fluid catalytic cracking (FCC) is one of the largest industrial refining processes to convert crude oil into lighter hydrocarbons. The FCC products are used as blending products as well for further reactions like alkylation.

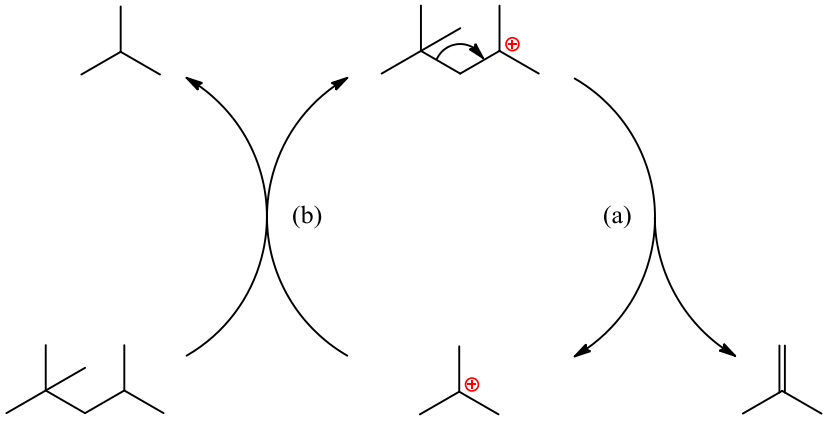

Scheme 1.5: Catalytic cracking mechanism including (a) β scission and (b) hydride transfer reaction

The key step in fluid catalytic cracking reaction is the cleavage of a C-C bond in β-position.[52] This results in the formation of an alkene and a smaller carbenium ion. The stability of the remaining carbenium ion on the catalyst surface also determines the β-scission. The chain propagation occurs via hydride transfer.[1,2]

1.6.2. Isomerization reaction

Branched hydrocarbons containing a higher octane number compared to their n-alkanes. Consequently, isomerization of hydrocarbons into their branched isomers is an important

refining process. All n-alkanes as well as branched isomers used in this thesis are shown in Table 1.1.

Table 1.1: Octane numbers of C_5 and C_8 hydrocarbons used in this thesis

Hydrocarbon	RON
n-Pentane	62
Isopentane	93
2,2-Dimethylbutane	91.8
2,3-Dimethylbutane	104.3
2-Methylpentane	73.4
3-Methylpentane	74.5
n-Hexane	24.8
2-Methylhexane	42.4
3-Methylhexane	52.0
n-Heptane	0
2,2-Dimethylpentane	92.8
2,3-Dimethylpentane	91.1
2,4-Dimethylpentane	83.1
3,3-Dimethylpentane	80.8
2,2,3-Trimethylbutane	112.1
2,2-Dimethylhexane	72.5
2,3-Dimethylhexane	71.3
2,4-Dimethylhexane	65.2
2,5-Dimethylhexane	55.5
2-Methylheptane	21.7
3-Methylheptane	36.8
4-Methylheptane	26.7
2,2,4-Trimethylpentane	100
2,3,3-Trimethylpentane	106.1
2,2,3-Trimethylpentane	109.6
2,3,4-Trimethylpentane	102.7
Octenes	>90
C_{9+}	≈ 80-85

Isomerization reaction can occur in alkyl or hydride shift isomerization (Scheme 1.6 (a)) as well as skeleton isomerization (Scheme 1.6 (b)). Skeleton isomerization occurs in a cyclopropane transition state and has higher activation energy compared to hydride shift isomerization reaction.[53-57] Because of the rather low activation energy of hydride shift isomerization this is relatively fast and occurs often as side reaction.[2,57]

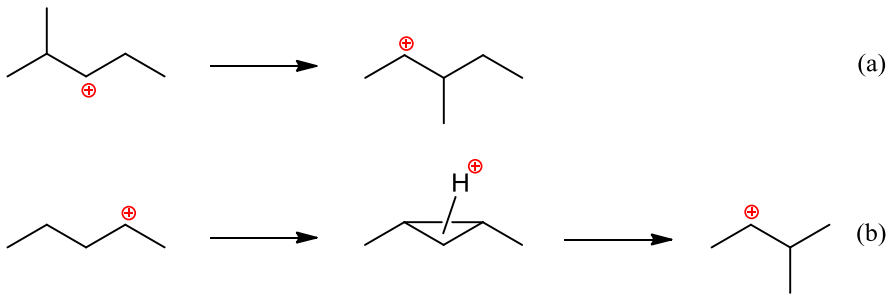

Scheme 1.6: Alkyl or hydride shift isomerization (a) as well as skeleton isomerization mechanism (b)

1.6.3. Hydroisomerization

The global refinery catalyst market accounts for about 24 % of the world catalyst market today. A variety of 800 refinery catalysts is available in markets and among them zeolites play an important role. For isomerization processes, zeolites represent a good alternative to aluminum chloride systems, but especially platinum promoted sulfated zirconium oxide draws more and more attention due to its high selectivity and activity.[58-62]

As the equilibrium of n-pentane and iso-pentane is in favor of iso-pentane at low temperatures catalysts which are active for hydroisomerization at low temperatures are preferred.

It is well known that the hydroisomerization of alkanes is catalyzed by Brønsted acid sites.[63] In the early fifties, the isomerization of light alkanes was performed on hydrogen chloride/aluminum chloride systems.[64] At this, hydrogen chloride functions as a promoter and is introduced to the system solved in the feed. The catalyst itself, aluminum chloride, is present in melted form and is kept in liquid phase by constant stirring.[65] It is generally accepted that in this system, in a first step, a hydride is abstracted from the hydrocarbon and thus a secondary carbenium ion is generated. After isomerization into a tertiary carbenium ion, with a carbenium ion as intermediate, a subsequent hydride transfer leads to the isomerization product.[66,67] An improvement of this catalytic system was the introduction of platinum, loaded

on aluminum chloride. This bifunctional catalyst showed improved properties, especially against deactivation.[68]

Hydroisomerization over platinum containing catalysts follows a different mechanism. In a first step, dehydrogenation of the n-alkane over platinum takes place and an n-alkene is generated. Subsequently a secondary carbenium ion is formed over acid sites via hydride abstraction, following the rearrangement into a more stable ternary carbenium ion. Finally the iso-alkene is formed via hydride transfer and is re-hydrogenated over platinum.[69] Scheme 1.7 illustrates the mechanism over these bifunctional catalysts.

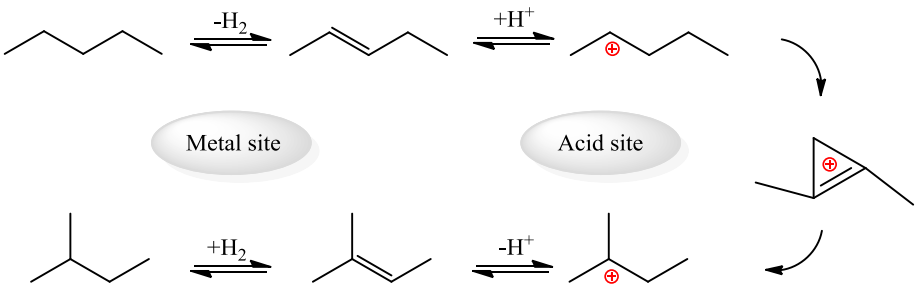

Scheme 1.7: Bifunctional hydroisomerization mechanism over platinum promoted acid catalysts

In the early seventies, a new type of catalyst for hydroisomerization of n-alkanes was introduced, zeolites were first industrially applied.

The applied catalysts are mainly based on platinum promoted H-Mordenite and are, compared to the aluminum chloride system, more stable. Even traces of water and sulfur are tolerated, thus a permanent dosing of the active components is not necessary. Another advantage of the application of zeolites is the absence of hydrogen chloride and the omitted post processing related to hydrogen chloride.[70]

The complexity of possible reactions of n-alkanes leads to a wide product range. Along with the isomerization, reactions like cracking, dehydrogenation and as a consequence of dehydrogenation reactions, oligomerization can occur. Reaction parameters like temperature, total pressure and the hydrogen to n-alkane ratio have a great impact on the product distribution. Therefore many studies are investigated on this reaction and reaction parameters.[71-74]

1.6.4. Isobutane / 2-butene alkylation

Alkylation is an ideal refining process to convert C_4 components produced in catalytic cracking units.[75] Isobutane/2-butene alkylation produces a mixture of branched C_5 - C_{9+} alkanes, called alkylate, that is an ideal blending component for gasoline. It is nearly free of alkenes, aromatics and sulfur and the octane numbers close to 100. Those attributes and the fact that fluid cracking units (FCC) produce a significant amount of C_3 – C_5 paraffins and olefins make the alkylation an important section in modern refineries.[1,2]

1.6.4.1. Initializing step

Alkylation is a carbenium ion based reaction that proceeds in a catalytic cycle shown in Scheme 1.9. The first carbenium ion initializing the alkylation cycle is generated by protonation of a 2-butene molecule (Scheme 1.8 a). A *sec*-butyl carbenium ion occurs. Then the *sec*-butyl carbenium ion abstracts a hydride from an isobutane molecule forming a *tert*-butyl carbenium ion and n-butane (Scheme 1.8 b).[76]

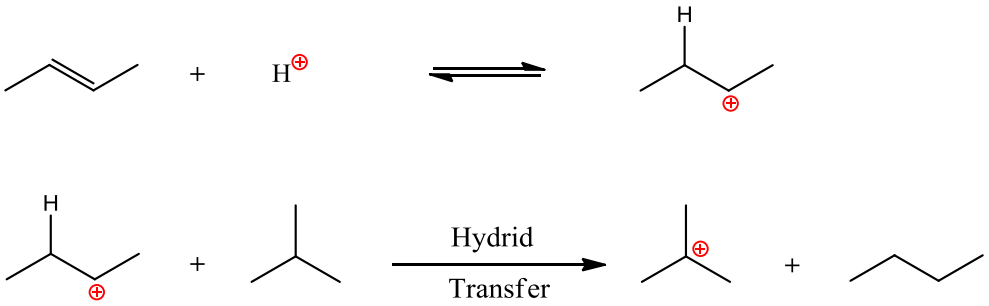

Scheme 1.8: Initializing steps in the isobutane/2-butene alkylation cycle: (a) protonation of 2-butene and hydride transfer to a *tert*-butyl carbenium ion (b)

1.6.4.2. Mechanism of isobutane and 2-butene alkylation reaction

Tert-butyl carbenium ion enters the catalytic cycle and alkene addition to a 2-butene molecule takes place. Thus the primary alkylation product of isobutane/2-butene alkylation, the 2,2,3-trimethylpentyl carbenium ion is formed. Afterwards the 2,2,3-trimethylpentyl carbenium ion can isomerize into another octyl carbenium ion or directly undergo hydride transfer reaction from isobutane to the octyl carbenium ion. Consequently, the product selectivity to 2,2,3-trimethylpentane (2,2,3-TMP), 2,2,4-TMP, 2,3,3-TMP and 2,3,4-TMP give information about

the hydride transfer capability. The originated octane is released and the *tert*-butyl carbenium ion undergoes the catalytic cycle anew.[1,2]

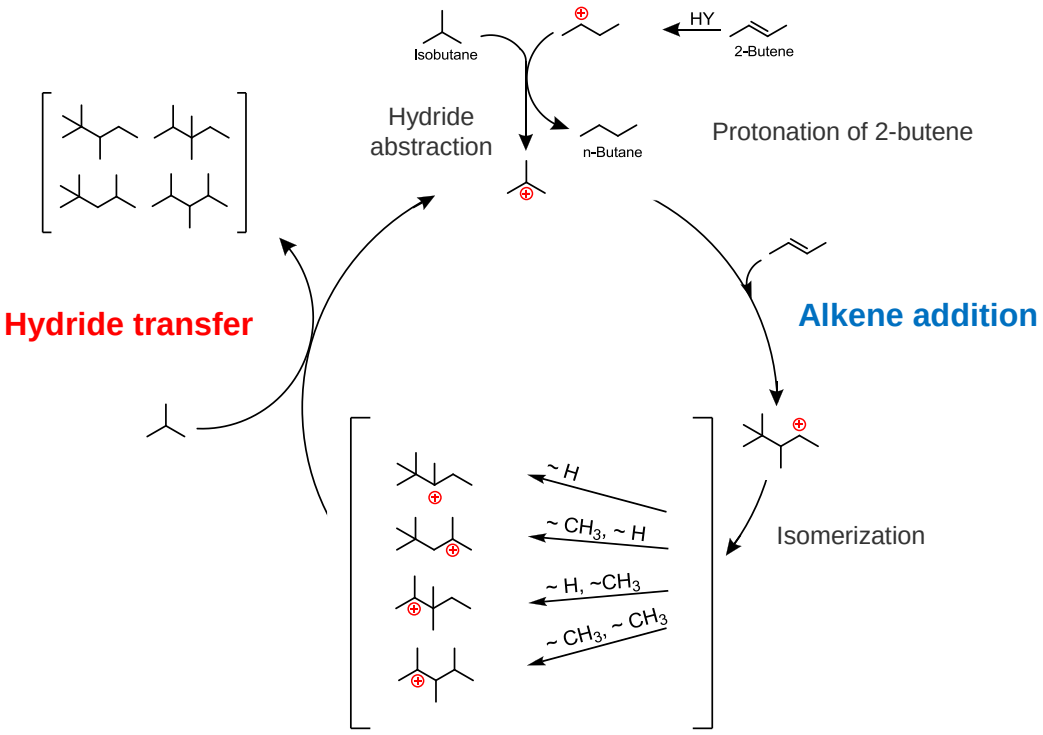

Scheme 1.9: Alkylation cycle of isobutane and 2-butene including the protonation of 2-butene, hydride abstraction, alkene addition, isomerization and hydride transfer

The ratio of hydride transfer to alkene addition controls the selectivity to octane isomers. 2,2,4-TMP can also be formed by a self-alkylation pathway. The deprotonation of a *tert*-butyl carbenium ion leads to the formation of an isobutene molecule. On the free BAS a butene molecule is protonated as it is described for the initializing step. The formed isobutene molecule adds a *tert*-butyl carbenium ion by formation of a 2,2,4-trimethylpentyl carbenium ion. This octyl carbenium ion forms a 2,2,4 TMP by hydride transfer reaction if no isomerization reaction occurs before.[1,2,5,77-79]

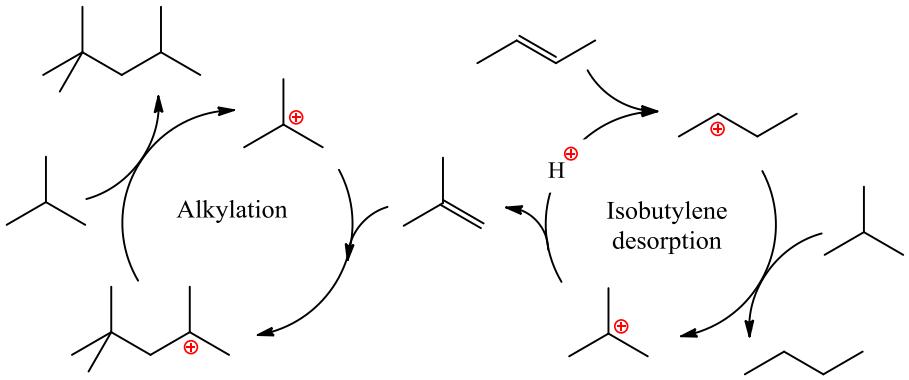

Scheme 1.10: Self-alkylation mechanism including the desorption of isobutene and addition to a *tert*-butyl carbenium ion[5]

The product fraction of oligomerization (C_{9+}) formed by alkene addition (Scheme 1.11)[77] is responsible for catalyst deactivation by blocking active acid sites.[22]

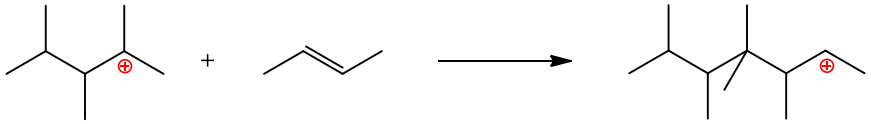

Scheme 1.11: Formation of long chained hydrocarbons by olefin addition

Catalyst deactivation and therefore regeneration is very costive thus studies on this topic are from major interest. Here the catalyst deactivation will be introduced in Section 1.7.

1.7. Catalyst deactivation

Zeolite deactivation is still one of the biggest problems in refining industry while regeneration is very costive. In general pore mouth plugging[80,81] and poisoning[82] are possible deactivation mechanisms. In pore blocking, generated large hydrocarbons block the entrance of the catalyst pore. Consequently, they cannot diffuse out of the pore, because of their size. Poisoning of active sites or active site blocking occurs if hydrocarbons directly undergo a strong chemical bond with the active sites. Moreover, some studies also suggested a combination of both mechanisms.[1,2,22,83,84]

With decreasing hydride transfer ability the lifetime of the trimethylpentyl carbenium ion generated via alkylation of isobutane and 2-butene increases. According to this further

nucleophilic attacks from 2-butene become more likely and compounds containing more than eight carbon atoms are formed (Scheme 1.11).[1,2,85,86]

Noble metal containing zeolitic catalysts can be regenerated by hydrogenative regeneration.[1,2,83,87]

1.8. Scope of the thesis

Large pore faujasite type zeolites possess great potential for acid catalyzed fluid catalytic cracking. Rare earth exchanged zeolites, especially lanthanum exchanged faujasite type zeolites draw great attention in refining industry. Recently, the alkylation of isobutane and 2-butene[22,23] and isomerization reactions has been reported under mild reaction conditions over lanthanum containing faujasites.[1,2,88] Since hydride transfer, isomerization and cracking are main elemental steps in alkylation, understanding these reactions is of great interest in order to develop new catalysts with improved catalytic performance.

In chapter 2, the adsorption / desorption properties of different lanthanum species containing faujasite type zeolites were investigated. Based on detailed NMR study and DFT calculations the impact of different lanthanum species located in supercage and sodalite cages of selected zeolites on the catalytic performance of these materials was discussed. Especially, the accessibility of La^{3+} extra-framework cations stabilized insight the zeolite lattice was of great interest.

The influence of accessible lanthanum cations incorporated into the FAU supercage onto the alkylation reaction of isobutane and 2-butene was investigated in chapter 3. 2,2,4-trimethylpentane low temperature cracking using a plug flow reactor was used to discuss secondary reactions of formed octanes during alkylation reaction.

In chapter 4 the hydroisomerization of n-pentane using lanthanum as well as platinum containing faujasite materials was investigated using a plug flow reactor. Here the reaction mechanisms using different metal sites incorporated was discussed. Therefore acid site characterization, before and after hydroisomerization of n-pentane was used to discuss the influence of active sites to the reaction mechanism.

Chapter 5 investigates the influence of alkaline treatment onto ultrastable FAU to isobutane/2-butene alkylation reaction. Before lanthanum incorporation, the material was alkaline treated using different concentrations of NaOH and time of treatment. Here especially the accessibility of active sites and the impact of structural changes in the studied zeolitic materials are discussed.

In chapter 6 most important results are summarized and conclusions are done.

1.9. References

(1) Feller, A. PhD thesis, TU München (München), 2003.

(2) Sievers, C. PhD thesis, TU München (München), 2006.

(3) Yoo, K.; Smirniotis, P. G. *Appl. Catal. A-Gen.* **2002**, *227*, 171.

(4) de la Puente, G.; Souza-Aguiar, E. F.; Zotin, F. M. Z.; Camorim, V. L. D.; Sedran, U. *Appl. Catal. A-Gen.* **2000**, *197*, 41.

(5) Feller, A.; Guzman, A.; Zuazo, I.; Lercher, J. A. *J. Catal.* **2004**, *224*, 80.

(6) Corma, A.; Gomez, V.; Martinez, A. *Appl. Catal. A* **1994**, *119*, 83.

(7) Mortier, W. J.; Sauer, J.; Lercher, J. A.; Noller, H. *J. Phys. Chem.* **1984**, *88*, 905.

(8) Reitmeier, S. PhD thesis, TU München (München), 2009.

(9) Maier, S. PhD Thesis, TU München (München), 2011.

(10) van Bokhoven, J. A.; Koningsberger, D. C.; Kunkeler, P.; van Bekkum, H.; Kentgens, A. P. M. *J. Am. Chem. Soc.* **2000**, *122*, 12842.

(11) Kawakami, H.; Yoshida, S.; Yonezawa, T. *J. Chem. Soc., Faraday Trans. II* **1984**, *80*, 205.

(12) Loewenstein, W. *Am. Miner.* **1954**, *39*, 92.

(13) Carvajal, R.; Chu, P.-J.; Lunsford, J. H. *J. Catal.* **1990**, *125*, 123.

(14) Huang, J.; Jiang, Y.; Reddy Marthala, V. R.; Ooi, Y. S.; Weitkamp, J.; Hunger, M. *Micropor. Mesopor. Mater.* **2007**, *104*, 129.

(15) Guzman, A.; Zuazo, I.; Feller, A.; Olindo, R.; Sievers, C.; Lercher, J. A. *Micropor. Mesopor. Mater.* **2005**, *83*, 309.

(16) Venuto, P. B.; Hamilton, L. A.; Landis, P. S. *J. Catal.* **1966**, *5*, 484.

(17) Bolton, A. P. *J. Catal.* **1971**, *22*, 9.

(18) Klein, H.; Fuess, H.; Hunger, M. *J. Chem. Soc., Faraday Trans.* **1995**, *91*, 1813.

(19) Eder, F.; Lercher, J. A. *Zeolites* **1997**, *18*, 75.

(20) Sievers, C.; Onda, A.; Olindo, R.; Lercher, J. A. *J. Phys. Chem. C* **2007**, *111*, 5454.

(21) Cumming, K. A.; Wojciechowski, B. W. *Catal. Rev. Sci. Eng.* **1996**, *38*, 101.

(22) Feller, A.; Barth, J.-O.; Guzman, A.; Zuazo, I.; Lercher, J. A. *J. Catal.* **2003**, *220*, 192.

(23) Feller, A.; Zuazo, I.; Guzman, A.; Barth, J.-O.; Lercher, J. A. *J. Catal.* **2003**, *216*, 313.

(24) Sievers, C.; Onda, A.; Guzman, A.; Otillinger, K. S.; Olindo, R.; Lercher, J. A.

J. Phys. Chem. C **2007**, *111*, 210.

(25) Cotton, S. Scandium, Yttrium, and the Lanthanides. In *Comprehensive Coordination Chemistry II*; Pergamon, 2003; pp 93.

(26) Corma, A.; Martínez, A.; Arroyo, P. A.; Monteiro, J. L. F.; Sousa-Aguiar, E. F. *Appl. Catal. A-Gen.* **1996**, *142*, 139.

(27) Stockenhuber, M.; Lercher, J. A. *Micropor. Mater.* **1995**, *3*, 457.

(28) Groen, J. C.; Sano, T.; Moulijn, J. A.; Pérez-Ramírez, J. *J. Catal.* **2007**, *251*, 21.

(29) Melián-Cabrera, I.; Espinosa, S.; Groen, J. C.; v/d Linden, B.; Kapteijn, F.; Moulijn, J. A. *J. Catal.* **2006**, *238*, 250.

(30) Li, X.; Prins, R.; van Bokhoven, J. A. *J. Catal.* **2009**, *262*, 257.

(31) Abelló, S.; Bonilla, A.; Pérez-Ramírez, J. *Appl. Catal. A-Gen.* **2009**, *364*, 191.

(32) Bonilla, A.; Baudouin, D.; Pérez-Ramírez, J. *J. Catal.* **2009**, *265*, 170.

(33) Groen, J. C.; Peffer, L. A. A.; Moulijn, J. A.; Pérez-Ramírez, J. *Micropor. Mesopor. Mater.* **2004**, *69*, 29.

(34) Spangsberg Holm, M.; Svelle, S.; Joensen, F.; Beato, P.; Christensen, C. H.; Bordiga, S.; Bjørgen, M. *Appl. Catal. A-Gen.* **2009**, *356*, 23.

(35) Li, Y.; Liu, S.; Zhang, Z.; Xie, S.; Zhu, X.; Xu, L. *Appl. Catal. A-Gen.* **2008**, *338*, 100.

(36) Narbeshuber, T. F.; Vinek, H.; Lercher, J. A. *J. Catal.* **1995**, *157*, 388.

(37) Marczewski, M. *J. Chem. Soc., Faraday Trans.* **1986**, *82*, 1687.

(38) Zheng, X. B.; Blowers, P. *J. Phys. Chem. A* **2006**, *110*, 2455.

(39) Mota, C. J. A.; Bhering, D. L.; Ramirez-Solis, A. *Int. J. Quantum Chem.* **2005**, *105*, 174.

(40) Boronat, M.; Zicovich-Wilson, C. M.; Corma, A.; Viruelab, P. *Phys. Chem. Chem. Phys.* **1999**, *1*, 537.

(41) Boronat, M.; Viruela, P.; Corma, A. *Phys. Chem. Chem. Phys.* **2000**, *2*, 3327.

(42) Boronat, M.; Viruela, P.; Corma, A. *J. Phys. Chem. B* **1999**, *103*, 7809.

(43) Boronat, M.; Viruela, P.; Corma, A. *J. Phys. Chem. B* **1997**, *101*, 10069.

(44) Kazansky, V. B.; Frash, M. V.; van Santen, R. A. *Catal. Lett.* **1997**, *48*, 61.

(45) Frash, M. V.; Solkan, V. N.; Kazansky, V. B. *J. Chem. Soc., Faraday Trans.* **1997**, *93*, 515.

(46) Mota, C. J. A.; Esteves, P. M.; de Amorim, M. B. *J. Phys. Chem.* **1996**, *100*, 12418.

(47) Cardona, F.; Gnep, N. S.; Guisnet, M.; Szabo, G.; Nascimento, P. *Appl. Catal. A-Gen.* **1995**, *128*, 243.

(48) Weitkamp, J.; Jacobs, P. A.; Martens, J. A. *Appl. Catal.* **1983**, *8*, 123.

(49) Platon, A.; Thomson, W. J. *Appl. Catal. A-Gen.* **2005**, *282*, 93.

(50) Platon, A.; Thomson, W. J. *Catal. Lett.* **2005**, *101*, 15.

(51) Lukyanov, D. B. *J. Catal.* **1994**, *145*, 54.

(52) Greensfelder, B. S.; Voge, H. H.; Good, G. M. *Ind. Eng. Chem.* **1949**, *41*, 2573.

(53) Sassi, A.; Sommer, J. *Appl. Catal. A-Gen.* **1999**, *188*, 155.

(54) Vansina, H.; Baltanas, M.; Froment, G. F. *IEC Prod. Res. Dev.* **1983**, *22*, 526.

(55) Blomsma, E.; Martens, J. A.; Jacobs, P. A. *J. Catal.* **1996**, *159*, 323.

(56) Boronat, M.; Viruela, P.; Corma, A. *Appl. Catal. A-Gen.* **1996**, *146*, 207.

(57) Saunders, M.; Budiansky, S. P. *Tetrahedron* **1979**, *35*, 929.

(58) Song, X.; Sayari, A. *Catal. Rev. Sci. Eng.* **1996**, *38*, 329

(59) Liu, H.; Lei, G. D.; Sachtler, W. M. H. *Appl. Catal. A-Gen.* **1996**, *146*, 165.

(60) Haase, F.; Sauer, J. *J. Am. Chem. Soc.* **1998**, *120*, 13503.

(61) Kwak, B. S.; Sachtler, W. M. H. *J. Catal.* **1994**, *145*, 456.

(62) Ono, Y. *Catal. Today* **2003**, *81*, 3.

(63) Gray, J. A.; Cobb, J. T. *J. Catal.* **1975**, *36*, 125.

(64) Pines, H.; Frankenburg, W. G.; Komarewsky, V. I.; Rideal, E. K. *Adv. Catal.* **1948**, *1*, 201.

(65) Schmeling, F. *Erdöl und Kohle* **1958**, *11*, 569.

(66) Sinfelt, J. H. *AIChE Journal* **1973**, *19*, 673.

(67) Condon, F. E. *Catalysis (P. H. Emmett, ed.)* **1958**, *6*, 43.

(68) Burbidge, B. W.; Rolfe, J. R. K. *Hydrocarbon Processing and Petroleum Refiner* **1966**, *45*, 168.

(69) Weisz, P. B.; Swegler, E. W. *Science* **1957**, *126*, 887.

(70) Guisnet, M.; Fouche, V.; Belloum, M.; Bournonville, J. P.; Travers, C. *Appl. Catal.* **1991**, *71*, 283.

(71) Chica, A.; Corma, A. *J. Catal.* **1999**, *187*, 167.

(72) Sie, S. T. *Ind. Eng. Chem. Res.* **1993**, *32*, 403.

(73) Chao, K.-J.; Wu, H.-C.; Leu, L.-J. *Appl. Catal. A-Gen.* **1996**, *143*, 223.

(74) Fujimoto, K.; Maeda, K.; Aimoto, K. *Appl. Catal. A-Gen.* **1992**, *91*, 81.

(75) Weitkamp, J.; Traa, Y. *Catal. Today* **1999**, *49*, 193.

(76) Stocker, M. *Micropor. Mesopor. Mater.* **2005**, *82*, 257.

(77) Simpson, M. F.; Wei, J.; Sundaresan, S. *Ind. Eng. Chem. Res.* **1996**, *35*, 3861.

(78) Pater, J.; Cardona, F.; Canaff, C.; Gnep, N. S.; Szabo, G.; Guisnet, M. *Ind. Eng. Chem. Res.* **1999**, *38*, 3822.

(79) Sievers, C.; Liebert, J. S.; Stratmann, M. M.; Olindo, R.; Lercher, J. A. *Appl. Catal. A-Gen.* **2008**, *336*, 89.

(80) Querini, C. A.; Roa, E. *Appl. Catal. A-Gen.* **1997**, *163*, 199.

(81) Sahebdelfar, S.; Kazemeini, M.; Khorasheh, F.; Badakhshan, A. *Chem. Eng. Sci.* **2002**, *57*, 3611.

(82) Flego, C.; Kiricsi, I.; Parker, J., W. O.; Clerici, M. G. *Appl. Catal. A-Gen.* **1995**, *124*, 107.

(83) Klingmann, R.; Josl, R.; Traa, Y.; Gläser, R.; Weitkamp, J. *Appl. Catal. A-Gen.* **2005**, *281*, 215.

(84) Diaz-Mendoza, F. A.; Pernett-Bolano, L.; Cardona-Martínez, N. *Thermochim. Acta* **1998**, *312*, 47.

(85) Weitkamp, J.; Maixner, S. *Zeolites* **1987**, *7*, 6.

(86) Stöcker, M.; Mostad, H.; Rørvik, T. *Catal. Lett.* **1994**, *28*, 203.

(87) Josl, R.; Klingmann, R.; Traa, Y.; Gläser, R.; Weitkamp, J. *Catal. Commun.* **2004**, *5*, 239.

(88) Xiao, S.; Le Van Mao, R.; Denes, G. *J. Mater. Chem.* **1995**, *5*, 1251.

Chapter 2

Nature and location of cationic lanthanum species in high alumina containing faujasite type zeolites

The nature, concentration, and location of cationic lanthanum species in faujasite-type zeolites (zeolite X, Y and ultrastabilized Y) have been studied in order to understand better their role in hydrocarbon activation. By combining detailed physicochemical characterization and DFT calculations, we demonstrated that lanthanum cations are predominantly stabilized within sodalite cages in the form of multinuclear OH-bridged lanthanum clusters or as monomeric La^{3+} at the SI sites. In high-silica faujasites (Si/Al=4), monomeric $[La(OH)]^{2+}$ and $[La(OH)_2]^{+}$ species were only found in low concentrations at SII sites in the supercages, whereas the dominant part of La^{3+} is present as multinuclear OH-bridged cationic aggregates within the sodalite cages. Similarly, in the low-silica (Si/Al=1.2) La-X zeolite, the SI' sites were populated by hydroxylated La species in the form of OH-bridged bi- and trinuclear clusters. In this case, the substantial repulsion between the La^{3+} cations confined within the small sodalite cages induces the migration of La^{3+} cations into the supercage SII sites. The uniquely strong polarization of hydrocarbon molecules sorbed in La-X zeolites is caused solely by the interaction with the accessible isolated La^{3+} cations.

2.1. Introduction

Faujasite type zeolites modified with rare earth elements such as lanthanum show remarkable catalytic activity in several industrially relevant processes such as fluid catalytic cracking,[1,2] alkylation,[3-5] and hydroisomerization.[6] In addition to stabilizing the zeolite framework during steaming,[7,8] the presence of La cations has been claimed frequently to increase the strength of the Brønsted acid sites by additional polarization of the bridging OH group.[9] While the effect of framework stabilization by La^{3+} is reasonable well understood,[10] the potential role of ion exchanged La^{3+} in the claimed increase of the acid strength and, related, the cause for the high catalytic activity are not unequivocally understood. Part of the difficulty is related to the fact that different hydrocarbon reactions require different functions of the exchanged zeolite, and the role of acid sites may be interpreted in more than one way. In this respect it should be mentioned that increasing the La^{3+} concentration in FCC catalysts has been reported to lead to higher rates of hydride transfer.[11] This observation has been attributed solely to the increased concentration of Brønsted acid sites. If hydrocarbon cracking is performed under conditions under which hydride transfer does not play a major role, the catalytic activity will scale with the concentration of accessible Brønsted acid sites.[11] On the other hand, we have previously demonstrated that the effect of La^{3+} was drastically different between X and Y type zeolites. This is probably associated with the differences in the properties of La species confined within the faujasites with different framework composition.

A representative structure of the selected faujasite materials showing the potential exchange sites is depicted in Figure 2.1 (a). Figure 2.1 (b) shows the unit cell considered for DFT calculations.

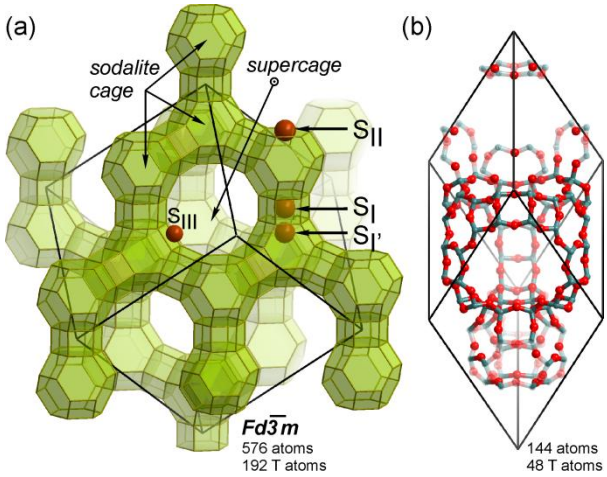

Figure 2.1: (a) Faujasite and main extra-framework sites; (b) rhombohedral faujasite unit cell considered for DFT calculations

During the ion-exchange lanthanum is introduced first in the supercages as $[La(H_2O)_n]^{3+}$.[7,12] The size of the hydrated lanthanum cation of 0.79 nm does not allow passing directly through the six-membered ring-openings (d = 0.25 nm) into the sodalite cages. Between 323 and 363 K the hydration shell of the lanthanum cations is sufficiently decreased in size to be able to principally access the sodalite cage, allowing better stabilization.[12-15] With increasing La^{3+} concentration some also remain in the supercages.[16,17] At high temperature (543 K) Na^+ cation migration from sodalite cage to SII sites in the supercage (Figure 2.1 (a)) becomes favorable.[12] Besides the migration of the La^{3+} cations during calcination, the formation of Brønsted acid sites by dissociation of water (1) of the hydrated La^{3+} cations takes place.[7,18,19]

$$[La(H_2O)_n]^{3+} \rightleftharpoons [La(OH)(H_2O)_{n-1}]^{2+} + H^+ \qquad (1)$$

It is usually assumed that La^{3+} cations are present as $[La(OH)_n]^{(3-n)+}$ cations as compiled in Table 2.1. The variation in the charge allows for an energetically more favorable incorporation of the exchangeable cation, which in itself stabilizes the lattice aluminum. Furthermore, lanthanum clusters, in particular dimers with bridging oxygen, are markedly contributing to the stabilization of the zeolitic lattice, while allowing also to generate Brønsted acid sites.[20] In addition, the hydroxylated cationic La species can self-organize in the low-silica zeolites

resulting in various multinuclear oxygen and hydroxyl-bridged clusters. Such process is driven by the high basicity of the terminal OH ligands and coordination unsaturation of the metal centers and is particularly favored for the materials with higher density of extra-framework cations.[21]

Table 2.1: Monomeric extra-framework La^{3+} species

	Monomeric extra-framework lanthanum species
La^{3+}	La^{3+} cation coordinated to three framework oxygen atoms
$[La(OH)]^{2+}$	La^{3+} cation coordinated to one hydroxyl ligand and to two framework oxygen atoms
$[La(OH)_2]^{+}$	La^{3+} cation coordinated to two hydroxyl ligand and one framework oxygen atom

In addition to stabilizing the zeolite lattice, it has been proposed that La^{3+} increases the intrinsic strength of Brønsted acid sites by increasing the Si-O-T (T = Si, Al) bond angles[10,12,22] and/or via electron-withdrawal by the exchanged cationic species.[10] In a moderate way, the strength of Brønsted acid sites may also influence the Gibbs free energy of alkane adsorption/desorption.[23]

Upon ion exchange with La^{3+} (acting as Lewis acid sites) the concentration of Brønsted acid sites decreases.[5] Although this variation in the concentration of Brønsted acid sites did not significantly influence the adsorption enthalpy,[24] Sievers et al. reported that the heat of adsorption of alkanes was significantly higher on the La^{3+} exchanged FAU than on the protonic form of the zeolite.[25,26] This has been attributed to the polarization of the C-H bonds of the sorbed alkanes by La^{3+} cations.[2,27,28] Hydroxyl ligands in the lanthanum coordination sphere are sterically hindering the polarization. Therefore, monomeric La^{3+} species have been speculated to possess the highest activity toward C-H bond polarization and activation. It was speculated that the facile activation of branched octanes over La-X is related to the strong polarization of adsorbed alkanes that enhances the formation of carbocations and promotes dehydrogenation and hydride transfer as the key step in hydrocarbon activation and conversion.[2]

Hydride transfer is also the key elementary step differentiating low and high-silica zeolites with sufficiently large pores to permit this bimolecular reaction shifting the product distribution in processes, such as cracking[1,29] and alkylation.[5,30] It takes place between the surface ester, i.e., the alkoxy group, or the carbenium ion in the excited state and an alkane hydride donor. During the reaction the former species is released as an alkane and the latter is converted into a carbenium ion. Conceptually, hydride transfer can be promoted either by weakening of the R-O bond of the alkoxy precursor,[31] or by stabilizing the transition state, or by stabilizing the final state of the hydrogen donor as alkoxy group. If the first step is important, hydride transfer is enhanced by strengthening the Brønsted acid sites (leading to sites that have a weaker R-O bond and facilitate the formation of carbenium ions), while the latter effect is enhanced by weaker acid sites stabilizing the forming of the new alkoxy group in the hydride transfer process.

La^{3+} cations are more electronegative than Mg^{2+} or Na^{+} for example but have a lower electronegativity that Si^{4+} or Al^{3+} leading to a decrease in the average electronegativity of the formed material.[32,33] The fact that La^{3+} ion exchange leads to materials with enhanced hydride transfer abilities, suggests that the promotion of hydride transfer is not induced by weakening of the alkoxy group R-O bond, but rather by stabilizing the transition state and/or of reaction products of the hydride donor.

Therefore, the understanding of the nature, concentration, and location of exchanged La^{3+} cations as well as the correlation between their structure and the stabilization of the zeolite matrix are crucial to explain and utilize the unique catalytic activity of lanthanum exchanged X zeolites. Thus, we report here on the location and structure of the ion-exchanged La^{3+} cations in zeolites USY, Y and X explored by solid state NMR, IR spectroscopy of adsorbed pyridine, as well as microcalorimetry and IR spectroscopy of adsorbed isobutane. The experimental studies are complemented by density functional theory (DFT) calculations.

2.2. Experimental

2.2.1. Materials

Three parent materials, i.e., ultra stable zeolite Y (H-USY, Si/Al = 3.1, Na = 0.18 mmol g^{-1}) obtained from Grace Davison, Na-Y from Akzo Nobel (Si/Al = 2.5), and Na-X (Si/Al = 1.2, Chemische Werke, Bad Köstritz) were used for ion-exchange with a $La(NO_3)_3$ solution.

Ultra stable zeolite Y (H-USY, Si/Al = 3.1, Na = 0.18 mmol g^{-1}) was first ion-exchanged with 0.5 M $La(NO_3)_3$ solution at a solution to zeolite ratio of 7 ml/g. The ion-exchange was carried out at 373 K for 4 h. After washing and drying for 6 h at 373 K, the resulting material was calcined in synthetic air for 4 h at 823 K. After calcination, the material was rehydrated. For higher La^{3+} concentrations, this material was exchanged in three additional steps following the identical procedure.

In order to prepare La-Y, Na-Y from Akzo Nobel was exchanged twice with a 0.2 M $La(NO_3)_3$ solution for 2 h at 353 K. Afterwards, two exchange steps using 0.5 M NH_4NO_3 solution were carried out followed by one exchange step using $La(NO_3)_3$. Higher concentrations of La^{3+} (La-Y II) were achieved by repeating the exchange procedure described above for several times. Following the ion-exchange step, the material was washed with bidistilled water, dried at room temperature and calcined using a slow temperature ramp up to 723 K. Afterwards, the obtained material was rehydrated at 343 K.

La-X was prepared by contacting Na-X (Si/Al = 1.2, Chemische Werke, Bad Köstritz) with 0.2 M $La(NO_3)_3$ solution at 353 K for 2 h. The parent material was ion-exchanged twice with a liquid-to-solid ratio of 11 ml/g, washed with bidistilled water, dried at room temperature, calcined at 723 K for 1 h in air flow and finally rehydrated. To prepare La-X with a higher lanthanum concentration (La-X II), three additional ion-exchange steps were performed following the procedure described above.

2.2.2. Physicochemical characterization

The concentrations of Si and Al were determined by atomic adsorption spectroscopy (ThermoFisher). The lanthanum concentration was determined by inductively coupled plasma-optical emission spectrometry with an FTMOA81A ICP-OES-Spectrometer from Spectro-Analytical Instruments.

Nitrogen physisorption isotherms were measured using a PMI automated sorptometer. The apparent surface area was calculated using the Brunauer-Emmett-Teller (BET) theory.[34] The micropore volumes were evaluated using the t-plot method according to Halsey.[35]

The crystallinity of the synthesized and modified materials were analyzed by powder X-ray diffraction using a Philips X'Pert Pro system equipped with an X'celerator module using CuKα radiation. Diffractograms were obtained from 5 to 75° 2Θ with a step size of 0.033°. The cell size parameters were calculated from the X-ray diffraction pattern of the zeolite material mixed with 5 % of silicon using the silicon reflections as reference following the ASTM method.[36]

The MAS NMR measurements were performed on a Bruker AV500 spectrometer (B_0 = 11.7 T) with a spinning rate of 12 kHz. For ^{1}H MAS NMR measurements the samples were activated in vacuum at 723 K for 15 h and afterwards packed in a 4 mm ZrO_2 rotor under nitrogen atmosphere. For the ^{1}H MAS NMR measurements a 90° excitation pulse was applied (3.8 µs) by a recycle time of 40 s. The chemical shift of an external highly symmetric cycloalkane, adamantane ($C_{10}H_{16}$) standard was used (δ = 1.78 ppm) for calibration. For quantification, an external MFI zeolite containing 0.360 mmol H^+/g was selected as standard. As the concentration of bridging hydroxyl groups might be overestimated due to the rapid proton exchange with adsorbed water,[37] the samples were activated following the procedure described above prior to analysis.

For ^{27}Al MAS NMR measurements, the samples were fully hydrated before packing them into a 4 mm ZrO_2 rotor. For a single pulse ^{27}Al MAS NMR measurement 2400 scans were recorded by a recycle time of 0.25 s. The excitation pulse had a length of 0.46 µs, which corresponds to a π/12-pulse. The chemical shifts are reported relative to an external standard of solid $Al(NO_3)_3$ (δ = -0.54 ppm). For a single ^{27}Al MQ MAS NMR spectrum 2400 scans were co-added. Here, the recycle time was 250 ms using a pulse sequence (pulse lengths: 3.0, 1.1 and 20.0 µs) including a typical 3 Q filter.

Infrared spectra of adsorbed pyridine were measured using a *Thermo Nicolet 5700 FT-IR* spectrometer in the transmission-absorption mode between 400 and 4000 cm^{-1} with a resolution of 4 cm^{-1} to determine the concentration of Lewis and Brønsted acid sites. The total concentration of Brønsted acid sites (BAS) and Lewis acid sites (LAS) was determined at 423 K after evacuating for 1 h to remove physisorbed pyridine. Strong Lewis and Brønsted acid sites (SLAS and SBAS) are defined to retain pyridine for 0.5 h at 723 K. For quantification, the molar extinction coefficients of 0.73 for Brønsted acid sites and 0.96 for Lewis acid sites determined by a combination of microgravimetric and IR spectroscopic analysis of adsorbed pyridine, was used.

The change in intrinsic strength of the acidic sites of the used materials was investigated by temperature programmed desorption (TPD) of adsorbed ammonia. For this, all samples were pressed into pellets with a specific particle size in the range of 0.5 and 0.71 mm. After activation in vacuum (p = 10^{-3} mbar) at 723 K for 1 h (heating rate of 10 K min^{-1}), ammonia was adsorbed (p = 1 mbar) at 373 K for 1 h. The physisorbed ammonia was removed by outgassing the materials for 2 h at 373 K. The signal m/z^+ = 16 of desorbing ammonia was monitored from 373 K up to 1043 K (heating rate of 10 K min^{-1}) using a Pfeiffer QMS 200 mass spectrometer.

2.2.3. Computational methods

Quantum chemical calculations were performed using density functional theory (DFT), the Vienna ab initio simulation package (VASP).[38] The gradient-corrected PBE exchange-correlation functional was used.[39] Electron-ion interactions were described with the projected-augmented wave (PAW) method[40,41] and for valence electrons a plane wave basis set was applied. The energy cut-off was set to 400 eV. The Brillouin zone sampling was restricted to Γ point.[42] Such computational settings were previously shown to be adequate for an accurate description of relevant properties of zeolites.[21,43,44] Similar to our previous studies[43,44] the periodic faujasite models were represented by a rhombohedral faujasite unit cell ($Si_{48}O_{96}$, Figure 2.1 (b)). Lower- and higher-silica La^{3+}-exchanged faujasite were constructed based on the experimentally determined chemical composition of the respective La-X and La-Y zeolites. The corresponding periodic models are denoted as LaFAU-1.2 and LaFAU-2.7, respectively. The LaFAU-1.2 unit cell contained 26 Si, 22 Al, 100 O, 7 La, 8 H and 1 Na atoms (Si/Al=1.18). Initially, 3 monomeric La^{3+} and 4 $[La(OH)]^{2+}$ cations were introduced. The unit cell of the higher-silica LaFAU-2.7 was constructed from 35 Si, 13 Al, 103 O, 6 La and 9 H atoms (Si/Al=2.69) with La represented as 2

$[La(OH)_2]^+$, 3 $[La(OH)]^{2+}$ and 1 La^{3+}. Prior to optimization of the atomic positions, the cell parameters of LaFAU-1.2 and LaFAU-2.7 both accommodating all La^{3+} species within the sodalite structural units were relaxed. The optimized cell parameters for LaFAU-1.2 were a=b=c=1.7691 nm with α=β=γ=60.00° and for LaFAU-2.7 a=b=c=1.7468 nm with α=β=γ=60.00°. Subsequently, full geometry optimization was performed for all La distributions with these fixed cell parameters using a conjugated gradient algorithm. The system was assumed to be converged, when the energy difference between subsequent optimization steps was below 10^{-4} eV.

2.2.4. Adsorption of isobutane

The gravimetric sorption capacities of isobutane were measured on a Setaram TG-DSC 111 instrument. In order to avoid bed depth and thermal effects a low amount of powder sample (approximately 10 mg) was used. Activation was performed at 723 K for 1 h with a heating rate of 10 K min^{-1} under vacuum ($p < 10^{-7}$ mbar). The weight increase and the thermal flux were measured during equilibration with isobutane at 348 K using small pressure steps up to 500 mbar. The heats of adsorption were directly obtained by integration of the observed heat signal.

To compare the extinction coefficients of the used materials infrared measurements at 348 K up to 10 mbar were carried out. Therefore, the same activation procedure as for the gravimetric measurements was used. Isobutane was adsorbed at same pressure as used in gravimetric measurements. The extinction coefficient was determined plotting the uptake (gravimetric measurements) against the absorbance (IR spectroscopic measurements).

2.3. Results

2.3.1. Influence of lanthanum on physicochemical properties

The results of the physicochemical characterization are summarized in Table 2.2. It should be noted that the residual Na^+ concentration and the La^{3+} ion-exchange degree were determined considering only the overall aluminum concentrations. The presence of extra-lattice aluminum is however limited to less than 20 % in all samples.

Table 2.2: Physicochemical properties of investigated zeolites

	La-USY I	La-USY II	La-Y I	La-Y II	La-X I	La-X II
Si [mmol/g]	10.45	7.97	6.54	6.31	5.48	4.84
Al [mmol/g]	2.61	2.62	2.49	2.45	5.03	3.96
Na [mmol/g]	0.04	0.05	0.20	0.02	0.34	0.01
La [mmol/g]	0.19	0.47	0.83	1.05	1.29	1.25
Si/Al[mol/mol]	4.0	3.0	2.6	2.6	1.1	1.2
Na/Al[mol/mol]	0.02	0.02	0.08	0.01	0.07	0.00
La/Al[mol/mol]	0.07	0.18	0.33	0.43	0.26	0.32
La^{3+} exch. degree [%]	21	54	99	129	78	96
BET surf. area [m^2/g]	712	726	737	646	645	648
Microp. vol. [cm^3/g]	0.26	0.26	0.28	0.25	0.22	0.26
Mesop. vol. [cm^3/g]	0.12	0.06	0.05	0.08	0.16	0.05
Unit cell size [nm]	2.45	2.45	2.47	2.47	2.50	2.49

The table shows clearly that only in the aluminum rich zeolites the significant concentration of La^{3+} could be exchanged, in USY samples at best 50 % of the ion-exchange capacity could be reached. This indicates that isolated framework Al sites are unable to exchange La^{3+} cations under the conditions used. Even extended ion-exchange did not influence the Si/Al ratio in La-Y and La-X materials, while it caused minor desilication in USY. Similarly, the micropore volume was hardly influenced by the exchange procedure.

To better understand the type and local environment of aluminum atoms ^{27}Al MAS NMR and ^{27}Al MQ MAS NMR were used.[45] ^{27}Al MAS NMR spectra showed tetrahedrally (60 - 40 ppm) as well as octahedrally coordinated aluminum (at about 0 ppm). The concentrations of the aluminum species are summarized in Table 2.3. The corresponding ^{27}Al MAS NMR and ^{27}Al MQ MAS NMR spectra are shown in Figure 2.2.

Table 2.3: Concentration of incorporated tetrahedral framework and octahedral extra-framework aluminum species determined by ^{27}Al MAS NMR and ^{27}Al MQ MAS NMR measurements

Catalyst	La-USY I		La-USY II	
	δ [ppm]	Conc. [mmol/g] [a]	δ [ppm]	Conc. [mmol/g] [a]
Td Al^{3+} close to H^+ or Na^+	60	0.55	60	0.64
Td Al^{3+} weakly distorted by La^{3+}	58	0.48	57	0.67
Td Al^{3+} strongly distorted by La^{3+}	54	1.08	51	1.07
Mobile EFAl	0	0.20	4	0.17
Separate EFAl phase	-3.7	0.29	-3.7	0.07

Catalyst	La-Y I		La-Y II	
	δ [ppm]	Conc. [mmol/g] [a]	δ [ppm]	Conc. [mmol/g] [a]
Td Al^{3+} close to H^+ or Na^+	60	0.78	59	0.39
Td Al^{3+} weakly distorted by La^{3+}	55	0.71	55	0.89
Td Al^{3+} strongly distorted by La^{3+}	49	0.96	49	1.17
Mobile EFAl	-0.5	0.04	-	-
Separate EFAl phase	-	-	-	-

Catalyst	La-X I		La-X II	
	δ [ppm]	Conc. [mmol/g] [a]	δ [ppm]	Conc. [mmol/g] [a]
Td Al^{3+} close to H^+ or Na^+	59	1.04	59	0.99
Td Al^{3+} weakly distorted by La^{3+}	-	-	-	-
Td Al^{3+} strongly distorted by La^{3+}	55	3.71	56	2.69
Mobile EFAl	0	0.28	2	0.14
Separate EFAl phase	-	-	-7.7	0.14

[a] Based on the total aluminum concentration determined by AAS

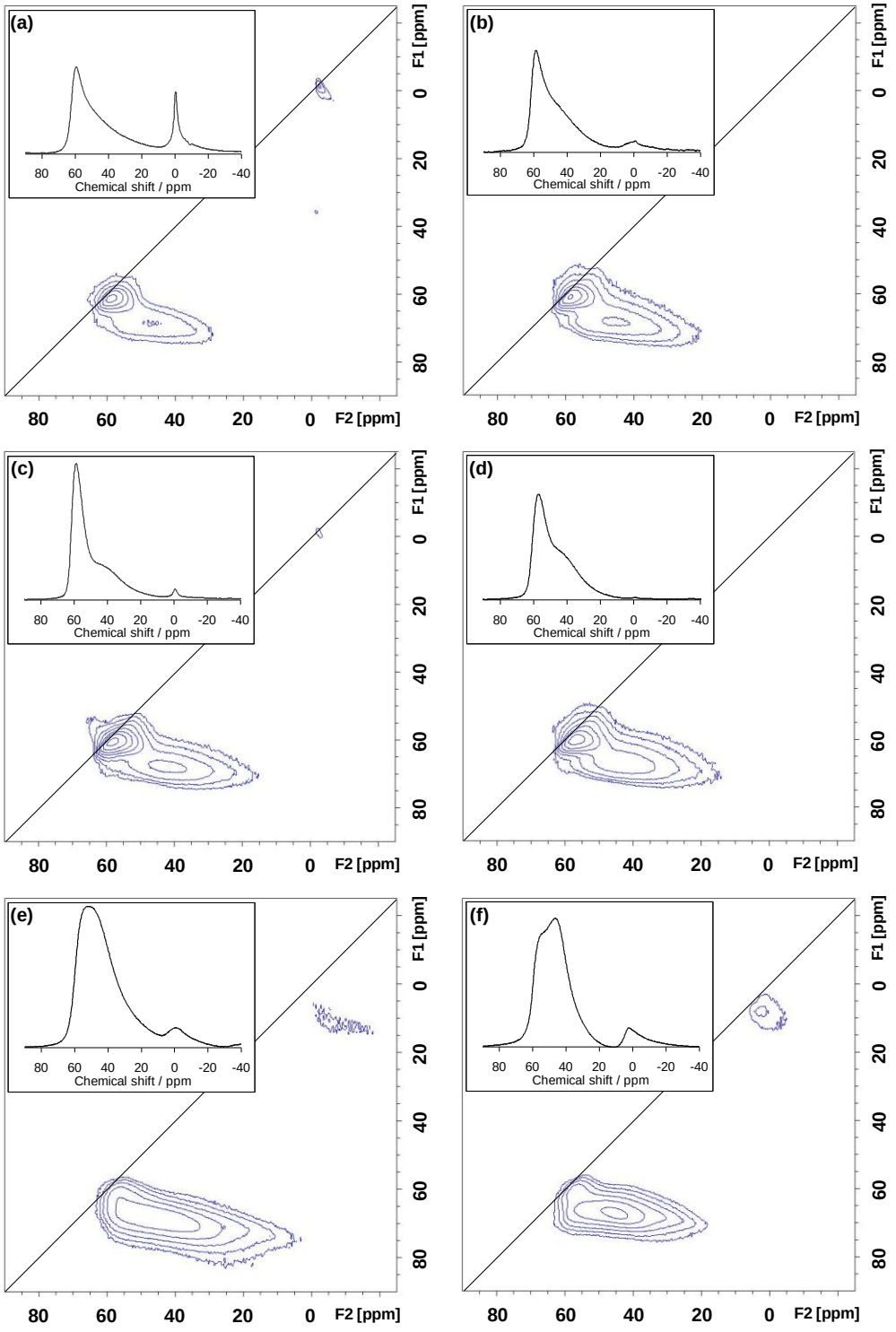

Figure 2.2: ^{27}Al MAS NMR and ^{27}Al MQ MAS NMR of La-USY I (a) and La-USY II (b), La-Y I (c) and La-Y II (d), La-X I (e) and La-X II (f). Procedure: 2400 scans, 12 kHz

Tetrahedral aluminum species in the zeolitic lattice are equivalent to framework aluminum. Octahedral aluminum as well as non-framework tetrahedral aluminum with a corresponding signal at 0 ppm and 60 ppm are corresponding to the extra-framework aluminum (EFAl) species.[46]

It should be noted that the peak corresponding to octahedral aluminum in the spectra of La-USY and La-Y was sharp and almost symmetric and the respective signal in ^{27}Al MQ MAS NMR is located close to the diagonal indicating only a minor distortion by the local environment. Thus, we ascribe the signal to aluminum cations with a high flexibility[47] and speculate that the corresponding EFAl species form charge compensating cations. While all samples have been treated similarly, the concentration of EFAl in La-Y samples was minimal, while reaching up to 20 % of the total aluminum for the other materials. Ion-exchange steps reduced the EFAl concentrations. Interestingly, the repeated La^{3+} exchange induced the partial insertion of EFAl into the lattice, as indicated by the increasing concentration of tetrahedrally coordinated aluminum determined by the NMR experiments for the two USY materials remained constant, the second ion-exchange step led to a substantial decrease of the octahedral aluminum concentration in La-USY II sample, most probably due to the reinsertion of the octahedrally coordinated Al into the zeolite framework.[47] The peak corresponding to octahedral aluminum in La-X showed a tailing indicating the presence of a second EFAl species located outside the zeolite pores, having a more pronounced quadrupolar interaction.

The chemical shift of tetrahedrally coordinated framework aluminum is influenced by the nature of its charge compensating cation.[20] If the framework charge from an aluminum atom is compensated by a La^{3+} cation, the coordination sphere of the framework aluminum atom is distorted, resulting in a substantial quadrupolar induced shift to higher field. As the concentration of the lanthanum increased, the signal of Al^{3+} species influenced by the presence of H^+ and Na^+ cations decreased. The intensity of the peak at 42 ppm corresponding to tetrahedral aluminum species distorted by La^{3+} cations in ultra-stable zeolite USY and zeolite Y, increased with increasing La^{3+} concentrations. Similarly, the peaks in ^{27}Al MQ MAS NMR assigned to the weakly distorted Al^{3+} species in La-USY II (δ_{F1}= 57 ppm) and La-Y II (δ_{F1}= 55 ppm) became more intense with increasing La^{3+} concentration in the zeolitic materials. The concentration of weakly distorted Al^{3+} increased significantly with increasing aluminum concentration in the studied zeolite Y and ultra-stable zeolite Y, (see Table 2.3). The concentration of strongly distorted Al^{3+} species in USY II (δ_{F1}= 51 ppm) remained constant with

increasing La^{3+} concentration, while it was slightly increased for La-Y II (δ_{F1}= 49 ppm). The peak corresponding to the strongly La^{3+}distorted tetrahedral aluminum in La-X I (δ_{F1}= 55 ppm) as well as La-X II (δ_{F1}= 56 ppm) was very intense due to the higher aluminum concentration compared to the USY and Y materials. Tetrahedral Al^{3+} weakly distorted by La^{3+} (as observed for La-USY and La-Y) was not observed.

In the ^{27}Al MQ MAS NMR spectra of La-USY and La-Y materials, two signals corresponding to two different aluminum species, one weakly distorted by hydroxylated $[La(OH)_2]^+$ and one strongly distorted by hydroxylated $[La(OH)]^{2+}$ and La^{3+} were distinguished. La-X only showed a single strongly distorted aluminum, indicating that lanthanum cations were incorporated such that lattice aluminum interacted with bare La^{3+} and $[La(OH)]^{2+}$ cations.

To illustrate better the details of the hydroxyl groups of the explored samples, the simulated peaks of ^{1}H MAS NMR are compiled together with the original spectra in Figure 2.3. Table 2.4 summarizes the results of the analysis of the corresponding ^{1}H MAS NMR spectra.

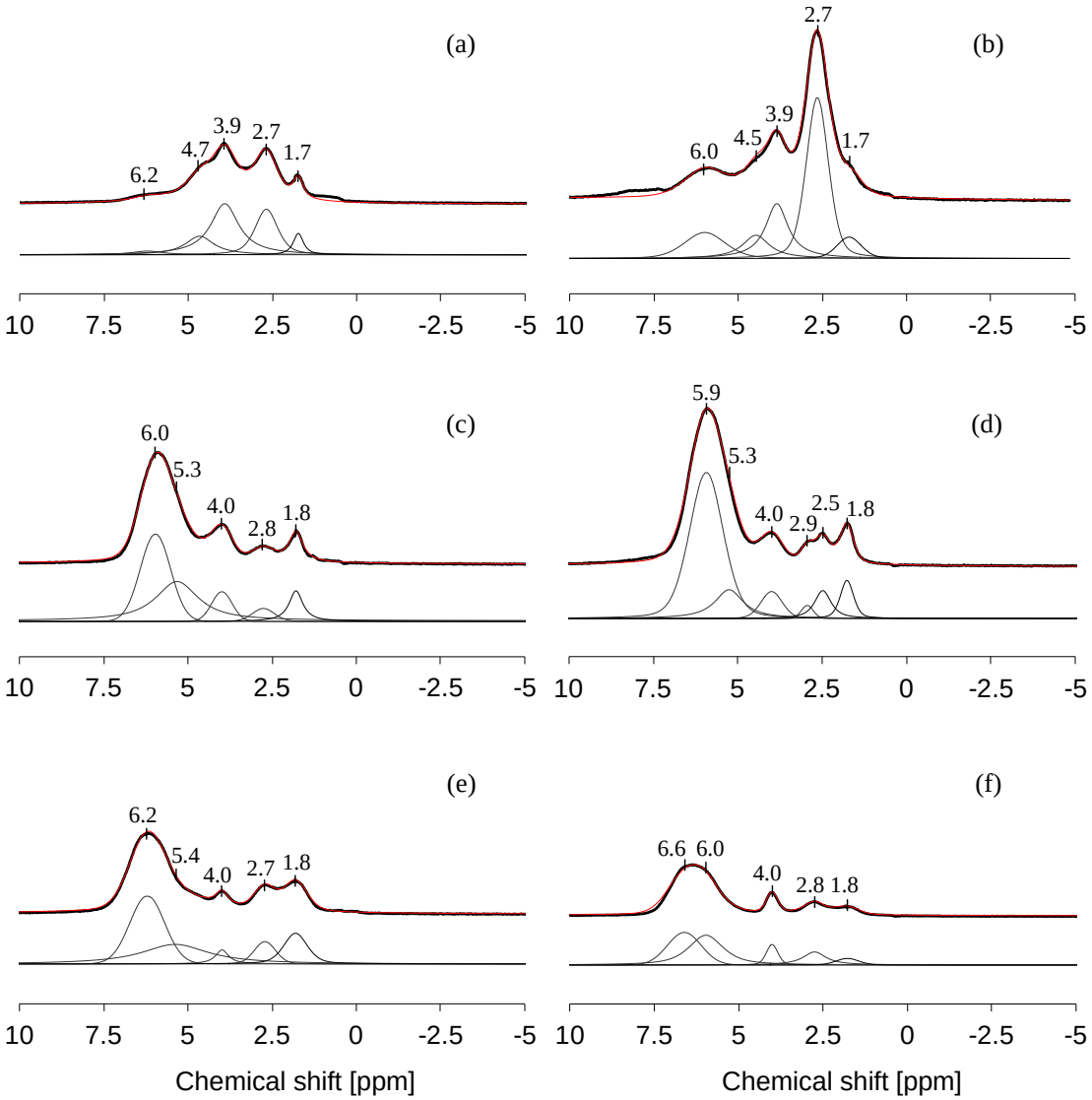

Figure 2.3: Recorded and simulated ^{1}H MAS NMR spectra of La-USY I (a) and La-USY II (b), La-Y I (c) and La-Y II (d), La-X I (e) and La-X II (f) materials. Experimental conditions: 4 mm rotor, 12 kHz, 100 scans

Table 2.4: Concentration of hydroxyl groups present in zeolite materials determined by ^{1}H MAS NMR measurements

Catalyst	$La(OH)_X$		Bridging OH				AlOH		SiOH	
			Small cavities		Large cavities					
	[ppm]	[mmol/g]	[ppm]	[mmol/g]	[ppm]	[mmol/g]	[ppm]	[mmol/g]	[ppm]	[mmol/g]
La-USY I	6.2	0.05	4.7	0.19	3.9	0.50	2.7	0.30	1.7	0.07
La-USY II	6.0	0.29	4.5	0.21	3.9	0.43	2.7	0.96	1.7	0.14
La-Y I	6.0	0.62	5.3	0.55	4.0	0.14	2.8	0.07	1.8	0.15
La-Y II	5.9	1.27	5.3	0.27	4.0	0.14	2.9/2.5	0.19	1.8	0.14
La-X I	6.2	0.56	5.4	0.45	4.0	0.06	2.7	0.12	1.8	0.20
La-X II	6.6	0.26	6.0	0.32	4.0	0.06	2.8	0.11	1.8	0.04

The zeolites contained four different OH groups, i.e., silanol groups (SiOH) at the external surface or at lattice defects, OH groups on extra-framework aluminum species (AlOH), OH groups associated with La^{3+} cations (LaOH) and bridging OH groups (SiOHAl).[37,48,49] The ^{1}H MAS NMR chemical shifts of the OH groups were linearly correlated to the wavenumber of the corresponding IR bands of the OH groups. The large chemical shift of the LaOH group[9] is attributed to hydrogen bonding of the LaOH group to basic framework oxygen atoms.[49] Increasing the La^{3+} concentration caused a downfield shift of the corresponding peak for the LaOH group in the ^{1}H MAS NMR spectra. For La-USY and La-Y, the LaOH peak was found at about 6 ppm, whereas the peak shifted to 6.2 ppm and 6.6 ppm, for La-X I and La-X II, respectively. La-USY I also showed a downfield shift of the corresponding LaOH peak to 6.2 ppm. This downfield shift was more pronounced with increasing framework aluminum concentration in dealing with the increasing base strength of the lattice oxygen.

The charge-compensation of a multiply charged extra-framework cation requires an appropriate number of framework Al atoms to be present. In the limiting case, a La^{3+} without partial charge compensation by OH groups requires the presence of three framework Al^{3+} in the vicinity. The statistical probability of three aluminum atoms in one 6-membered ring in FAU can be estimated following Mikovsky et al.[50] A first approximation of the ratio between different hydroxylated La^{3+} species can be made so assuming that La^{3+} is present as isolated

species. Three formal types of La species are considered, i.e., La^{3+}, $[La(OH)]^{2+}$, and $[La(OH)_2]^{+}$ (see Table 2.1). The concentration of various lanthanum species was determined by combining the information about the concentration of La^{3+} in the zeolite and the ^{1}H MAS NMR spectra. At lower lanthanum concentrations La^{3+} will be first incorporated in the form of monomeric La^{3+} inside the sodalite cages. Consequently, with very low lanthanum concentration in La-USY I the percentage of occupied La^{3+} sites was highest. With increasing lanthanum content the location at energetically less favored sites, i.e., the formation of $[La(OH)]^{2+}$ and $[La(OH)_2]^{+}$ in the sodalite cages is assumed. Table 2.5 summarizes the results of this estimation for different faujasite materials.

Table 2.5: Estimation of the potential distribution of La species from the statistical distribution of Al in the zeolite lattice

Catalyst	La^{3+}_{total} (AAS) [mmol/g]	$[La(OH)_2]^{+}$ theor. [mmol/g]	$[La(OH)]^{2+}$ theor. [mmol/g]	La^{3+} [mmol/g]
La-USY I	0.19	0.02	0.01	0.16
La-USY II	0.47	0.09	0.11	0.27
La-Y I	0.83	0.17	0.28	0.38
La-Y II	1.05	0.35	0.57	0.13
La-X I	1.29	0.00	0.56	0.73
La-X II	1.25	0.00	0.26	0.99

Given the low concentration of aluminum higher La^{3+} exchange degree in La-USY and La-Y favored the formation of $[La(OH)]^{2+}$ and $[La(OH)_2]^{+}$ species. For La-X , in contrast, a maximum of 0.73 and 0.99 mmol/g of La^{3+} are estimated to be bare La^{3+} (see Table 2.5). It should be emphasized that such an estimate is based solely on the statistical distribution of aluminum in the zeolite lattice.

Nature and concentration of acid sites characterized qualitatively and quantitatively by IR spectroscopy of adsorbed pyridine are compiled in Table 2.6. The concentrations of the

Brønsted acidic SiOHAl groups in La-Y and La-X determined were in excellent agreement with the concentrations determined by ^{1}H MAS NMR. The concentrations of SiOHAl groups in La-USY showed a larger deviation (see Tables 2.4 and 2.6). This is speculated to be caused by the different coordinations of incorporated La^{3+} species and requires further investigations.

Table 2.6: Brønsted (BAS) as well as Lewis (LAS) acid site concentration determined by infrared spectroscopy of adsorbed pyridine. Activation at 723 K for 1 h in vacuum. Adsorption at 0.1 mbar, outgassing for 1 h, all measurements were performed at 423 K. SBAS and SLAS are defined to retain pyridine at 723 K for 0.5 h

Acid sites [mmol/g]	La-USY I	La-USY II	La-Y I	La-Y II	La-X I	La-X II
BAS	0.917	0.779	0.789	0.435	0.565	0.369
LAS	0.417	0.518	0.239	0.201	0.405	0.545
SBAS	0.557	0.501	0.021	0.009	0.055	0.062
SLAS	0.282	0.270	0.056	0.056	0.083	0.064

With increasing La^{3+} concentration, the concentration of Brønsted acid sites (BAS) decreased while that of Lewis acid site (LAS) increased for La-USY and La-X and remained constant in La-Y materials. Note that La-Y and La-X materials contain a much lower concentrations of strong Brønsted acid sites (SBAS), usually associated with isolated aluminum atoms in the lattice, as well as strong Lewis acid sites (SLAS) compared to La-USY. Most importantly, the concentration of strong acid sites in La-USY was approximately one order of magnitude higher than in the other materials. A significant decrease in the intensity of the IR band corresponding to La-OH stretching vibrations was observed with increasing pyridine adsorption in USY materials (Figure A 2 a), whereas it stayed almost unchanged in the case of zeolite Y and X (Figure A 2 b and c).
In order to experimentally determine the influence of various incorporated La^{3+} species on the intrinsic acid strengths of the studied materials, TPD of adsorbed ammonia was performed. As shown in Figure A 1, the temperature of ammonia desorption peak mainly remained unchanged for all investigated samples suggesting that the incorporation of various lanthanum intermediates has almost no influence on the intrinsic acidic strength. A certain uncertainty of

this method originates from the lower heat of adsorption of NH_3 compared to pyridine (caused primarily the smaller size of ammonia and the resulting weaker physisorptive interaction with the zeolite pore) and the consequential weaker interaction with acidic sites. Therefore, we observed an overall lower thermal stability of ammonia with all investigated samples compared to the stability of adsorbed pyridine measured by the IR spectra of the adsorbate.

2.3.2. DFT calculations

To probe stability and structural properties of La^{3+} cations in faujasite zeolites, periodic DFT calculations were performed on two faujasite models (LaFAU-2.7 and LaFAU-1.2) with different unit cell compositions mimicking, the La-Y and La-X samples. Table 2.7 summarizes the calculated relative stabilities (ΔE values) and provides information on the nature of the La species in the selected zeolites.

Table 2.7: Calculated relative stabilities (ΔE) and approximated La species formed in different structural units of the most stable optimized structures of LaFAU-2.7 and LaFAU-1.2 models[a]

	Dominant species				Occupation [La per U.C.]			ΔE [kJ/mol]
	SOD-1	SOD-2	D6R	SC	SI	SI'	SII	
LaFAU-2.7^{SOD}	$La_3(\mu\text{-}OH)_2$	$HOLa_3$ $(\mu\text{-}OH)_3$ $(\mu^3\text{-}OH)$	–	–	0	6	0	0
LaFAU-2.7^{SII}	$La_3(\mu\text{-}OH)_2$	$HOLa_2$ $(\mu\text{-}OH)_2$	–	La $(OH)_2$	0	5	2	+33
LaFAU-1.2$^{SOD\text{-}1}$	$La_3(\mu\text{-}OH)$ $(\mu^3\text{-}OH)$	$La_3(\mu\text{-}OH)$ $(\mu^3\text{-}OH)$	La	–	1	6	0	0
LaFAU-1.2$^{SOD\text{-}2}$	$La_3(\mu^3\text{-}OH)$	$La_3(\mu\text{-}OH)_3$	La	–	1	6	0	+2
LaFAU-1.2^{SII}	$La_3(\mu^3\text{-}OH)_2La^{SII}$	$HOLa_2(\mu\text{-}OH)$	La	La	1	5	1	+40

[a] SOD: Sodalite cage, D6R: Hexagonal prism, SC: Supercage

2.3.2.1. Nature of lanthanum cations in La-Y

Ten configurations with different distributions of the charge-compensating La^{3+} species were compared for the high-silica containing LaFAU-2.7 model by means of DFT calculations. All structures initially included two $[La(OH)_2]^+$, three $[La(OH)]^{2+}$ and one La^{3+} species, as well as two Brønsted acid sites as charge-compensating species per cell unit. Geometry optimization calculations showed that the distribution of the charge-compensating species has a strong influence on the relative stability of the zeolite. The least favorable configuration contained predominantly exchangeable lanthanum species at the supercage SII sites. This configuration was 300 kJ/mol less stable than the configuration (LaFAU-2.7^{SOD}, Figure 2.4 and Table 2.7), where all the La^{3+} species were accommodated within the sodalite cages. Note that the initial distribution of La in the proposed structure involved the presence of La^{3+} at the SI site, whereas all other hydroxylated La^{3+} species were situated at the SI' positions. Upon geometry optimization calculations, this initial configuration was substantially altered. The La^{3+} cations migrated from the SI to the SI' position. Moreover the aggregation of the hydroxylated $La(OH)_n$ species resulting in the formation of $[La_3(\mu\text{-}OH)_2]^{7+}$ and $[HOLa_3(\mu\text{-}OH)_3(\mu^3\text{-}OH)]^{4+}$ clusters was observed for the proposed structures. The driving force for the formation of such multinuclear aggregates is the pronounced basicity of terminal La-OH groups and the presence of numerous anionic framework sites within the sodalite cages of faujasite.

The trinuclear $[HOLa_3(\mu\text{-}OH)_3(\mu^3\text{-}OH)]^{4+}$ species can undergo dissociation resulting in the formation of a binuclear $[HOLa_2(\mu\text{-}OH)_2]^{3+}$ cluster, which further remains stabilized within the sodalite cage, whereas the monomeric $[La(OH)_2]^+$ species migrates to the SII site resulting in the second most stable (LaFAU-2.7^{SII}, Figure 2.5) configuration. This configuration is 33 kJ/mol less favorable compared to the LaFAU-2.7^{SOD} as shown in Table 2.7. The high basicity of the terminal OH groups in $[La(OH)_2]^+$ led to severe distortions of the neighboring framework Al sites. One of the OH groups formed a La-(μ-OH)-Al bridge resulting in a trigonal pyramidal coordination of the framework Al (see Figure 2.5).

Subsequent decomposition of the intra-sodalite La^{3+} clusters substantially destabilizes the system. Migration of one of the La^{3+} cations from the $[La_3(\mu\text{-}OH)_2]^{7+}$ (Figures 2.4 and 2.5, left panels) into the adjacent D6R site decreases the total energy by 50 kJ/mol. The formation of additional monomeric $[La(OH)_2]^+$ or La^{3+} species in any of the faujasite structural unit increases the total energy of the system by more than 250 kJ/mol, compared to the LaFAU-2.7^{SOD} structure.

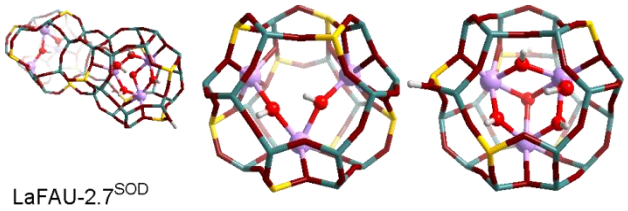

Figure 2.4: Optimized structure of LaFAU-2.7 model with all La^{3+} cations accommodated within sodalite cages and D6R units (LaFAU-2.7^{SOD}). From left to right the general view of the sodalite cages interconnected by a D6R unit and the magnified views of the individual sodalite cages containing La sites are shown

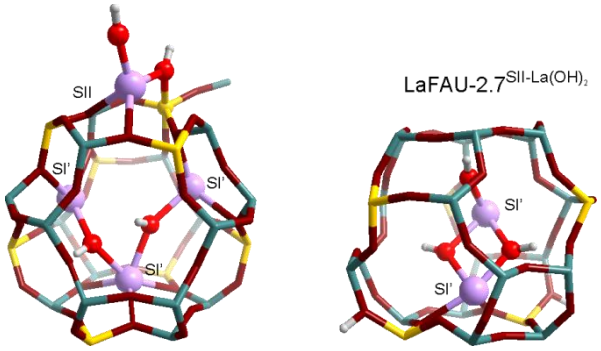

Figure 2.5: Optimized structure of LaFAU-2.7 model with $[La(OH)_2]^+$ species located at the SII position in the faujasite supercage (LaFAU-2.7^{SII}). From left to right the SII site with the adjacent sodalite cage and another sodalite cage accommodating all La species are shown

Despite the anticipated more efficient charge-compensation of La^{3+} cations at SI positions of D6R units, these sites are not populated in the stable LaFAU-2.7 configurations. Indeed, when a simplified model of La-modified faujasite with Si/Al ratio of 3 (La^{3+}/FAU-3) and accommodating solely La^{3+} cations is considered, the configuration with all La^{3+} cations at SI sites were found to be most stable. Migration of La^{3+} from the SI positions, in which La^{3+} cations are provided with efficient charge-compensation and favorable coordination environment, to the open SII site destabilizes the system by 300 kJ/mol. In the more realistic

LaFAU-2.7 model, the presence of the additional OH ligands substantially modifies this picture. The high basicity and polarity of the $[La(OH)]^{2+}$ species results in clustering of the hydroxylated La^{3+} cations occupying SI' sites. Because of the lower formal charge and partial coordinative saturation of these hydroxylated La species, their migration into the open SII positions becomes feasible.

In the case of higher-silica LaFAU-2.7, La^{3+} species predominantly occupy SI' positions as multinuclear hydroxylated cationic clusters, although a notable amount of lanthanum may still be present at the accessible SII sites in the faujasite supercages as monomeric hydroxylated lanthanum cations. It is plausible that the degree of hydroxylation of these species depends on the framework Al concentration within the zeolitic site.

2.3.2.2. Nature of lanthanum cations in La-X

In the case of the low-silica containing LaFAU-1.2 faujasite model, the stability of 25 possible configurations that differ in the relative location of the extra-framework species were examined. At the initial stage, the LaFAU-1.2 models were constructed by introducing 3 La^{3+}, 4 $[La(OH)]^{2+}$, 4 H^{+} and 1 Na^{+} extra-framework cations at different cation sites of the faujasite structure to compensate for the negative lattice charge. The geometries of the so constructed models were subsequently optimized. In this case, the stability of 25 possible configurations was examined. Similar to the LaFAU-2.7 model, the locations of all La^{3+} species within the sodalite cages and D6R structural unit were energetically more favorable (Figure 2.6, Table 2.7). Two distinct configurations (LaFAU-1.2^{SOD-1} and LaFAU-2.7^{SOD-2}) with very close total energies were determined. In both cases, a single monomeric La^{3+} cation was situated at the SI site, whereas all other La^{3+} species formed trinuclear lanthanum clusters in the SI' position of the sodalite cages. In LaFAU-1.2^{SOD-1} (Figure 2.6, top panel) both distinguishable sodalite cages contained $[La_3(\mu\text{-}OH)(\mu^3\text{-}OH)]^{7+}$ species, whereas $[La_3(\mu\text{-}OH)]^{8+}$ and asymmetric $[La_3(\mu\text{-}OH)_3]^{6+}$ clusters were predominantly observed in the FAU-1.2^{SOD-2} model. The higher formal charge of the clustered La^{3+} species formed in the lower-silica containing faujasite model is due to the higher Al density, and hence higher density of framework anionic sites, required for the direct charge-compensation of the multiple-charged extra-framework cations.

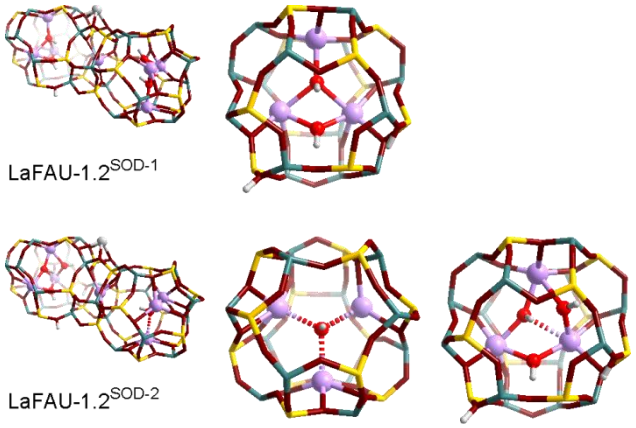

Figure 2.6: Optimized structure of LaFAU-1.2 model with all La cations accommodated within the sodalite cages and D6R units (LaFAU-1.2^{SOD-1} and LaFAU-1.2^{SOD-2}). From left to right the general view of the sodalite cages interconnected by a D6R unit and the magnified views of the individual sodalite cages containing the La sites are shown (in the case of LaFAU-1.2^{SOD-1} both sodalite cages accommodate similar La species)

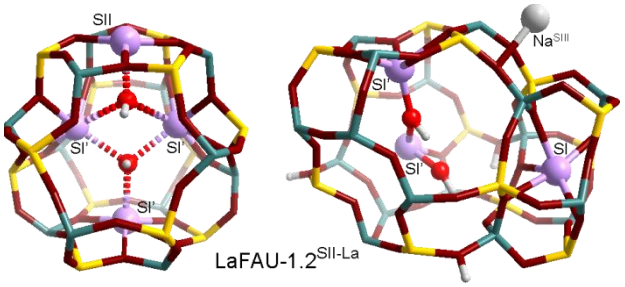

Figure 2.7: Optimized structure of the lower-silica containing LaFAU-1.2 model with a single La^{3+} cation at the SII position of the faujasite supercage (LaFAU-1.2^{SII}). From left to right the magnified views of the sodalite cage with the corresponding supercage La species at the SII sites and another sodalite cage with the adjacent D6R unit accommodating all La species in the models are shown

The second most stable configuration (LaFAU-1.2^{SII}) results from the migration of one of the La^{3+} cations from the sodalite cage of LaFAU-1.2^{SOD-1} to the SII position. The relative energy of the respective structure is 40 kJ/mol higher than determined for LaFAU-1.2^{SOD-1} (Table 2.7). Interestingly, a similar migration of a hydroxylated $[La(OH)]^{2+}$ species destabilized the system by more than 120 kJ/mol. Besides the higher Al^{3+} concentration in the lower-silica faujasite, additional interactions with the OH groups of the clustered lanthanum species within the adjacent sodalite cage led to the stabilization of the formally La^{3+} species at the open SII sites in the supercage (Figure 2.7, left panel).

The possible stabilization of cationic species with higher formal charge at the open SII sites of lower-silica faujasite was shown by DFT calculations performed on a simplified model of low-silica faujasite with a Si/Al ratio equal to 1 containing solely La^{3+} cations. Note that the uniform cation distribution in such a model results in a complete occupation of all SI' positions. Because of the strong repulsion between the densely arranged cationic species with rather high formal positive charge, a clear tendency for the redistribution of La^{3+} species was observed in this simplified model. Indeed, the concerted migration of two La^{3+} from SI' to the accessible SII and the shielding of the SI positions stabilizes the structure by 290 kJ/mol. Similar to the higher-silica faujasite model discussed above, the quantitative differences between this simplified model and the realistic LaFAU-1.2 are related to the tendency of the hydroxylated cationic lanthanum species to form aggregates within the sodalite cages.

The DFT calculations indicate that the increased framework Al concentration allows the stabilization of extra-framework lanthanum species bearing a higher formal positive charge. Similar to the case of the higher-silica faujasite model, hydroxylated La^{3+} cations self-organize within the sodalite cages to form clustered OH-bridged species. Accessible SII positions within the supercage can be occupied only by monomeric La^{3+} cations by additional stabilization with OH groups from lanthanum clusters within the sodalite cages.

2.3.3. Adsorption of isobutane

Having explored up to now the nature of La^{3+} cationic species, we use isobutane as a probe to understand the effects of the La^{3+} distribution in the three materials has upon reacting molecules. The combination of information on the thermodynamic parameters associated with isobutane adsorption and the impact on the bonds in the sorbed molecule (measured by

microcalorimetry, thermogravimetry and IR spectroscopy) will allow to draw conclusions on the interaction of isobutane with various active sites (see Table 2.8).

Table 2.8: Thermodynamic equilibrium constants of isobutane adsorption determined by microgravimetric and IR measurements[a]

	La-USY I	**La-USY II**	**La-Y I**	**La-Y II**	**La-X I**	**La-X II**
SP_{BAS}[mmol/g]	0.028	0.028	0.017	0.021	0.038	0.055
K [-]	0.110	0.131	0.105	0.087	0.255	0.261
ΔS^o[J/(K mol)]	-90.9	-97.2	-82.4	-77.3	-111.4	-107.3
ΔH^o [kJ/mol]	-38	-39	-35	-34	-43	-41
Extinction coefficient						
Low uptake [mmol/g]	25	26	28	30	100	102
High uptake [mmol/g]	20	20	22	21	59	50

[a] SP_{BAS} : Point of changing the regime

The adsorption capacity of the La-containing zeolites was between 1.34 mmol/g (La-X I) and 2.0 mmol/g (La-USY II), indicating that the mesopore volume of the strongly dealuminated materials provide some adsorption sites. The heat of adsorption of isobutane was between 43 (La-X I) and 35 kJ/mol (La-Y I and La-Y II). Subtle, but significant differences between the thermodynamic properties were observed between the studied materials. With USY and Y, the sorption enthalpy and entropy values were the highest (least entropy loss and least negative enthalpy). The slightly lower enthalpy and entropy with La-USY compared to La-Y is tentatively attributed to the slightly higher concentration of BAS in the latter material. The lowest entropy loss was observed with La-X (having also the highest concentration of accessible La^{3+} inside the supercages). It is interesting to note that a perfect compensation between the entropy and enthalpy of adsorption was found for all samples studied (see the appendix) indicating that all samples provide the same geometric environment for the sorbate.[25]

The selective polarization of adsorbed isobutane was also probed through the molar extinction coefficient of the C-H bonds.[51,52] The sensitivity is related to fact that the intensity of IR active vibrations is proportional to the dynamic change of the dipole moment. For stretching vibrations, this change is usually the larger the more polar a dipole is. Thus, an increase of the polarity of the -H, e.g., by elongation of the bond or the induction of charge by polarization, will lead to a higher molar extinction coefficient for a particular C-H stretching vibration. Because of the overlap between the bands for the C-H stretching vibrations an attribution of the molar extinction coefficient to individual vibrations was not possible and, therefore, the integral intensities of the C-H stretching bands are plotted as a function of the uptake in Figure 2.8.

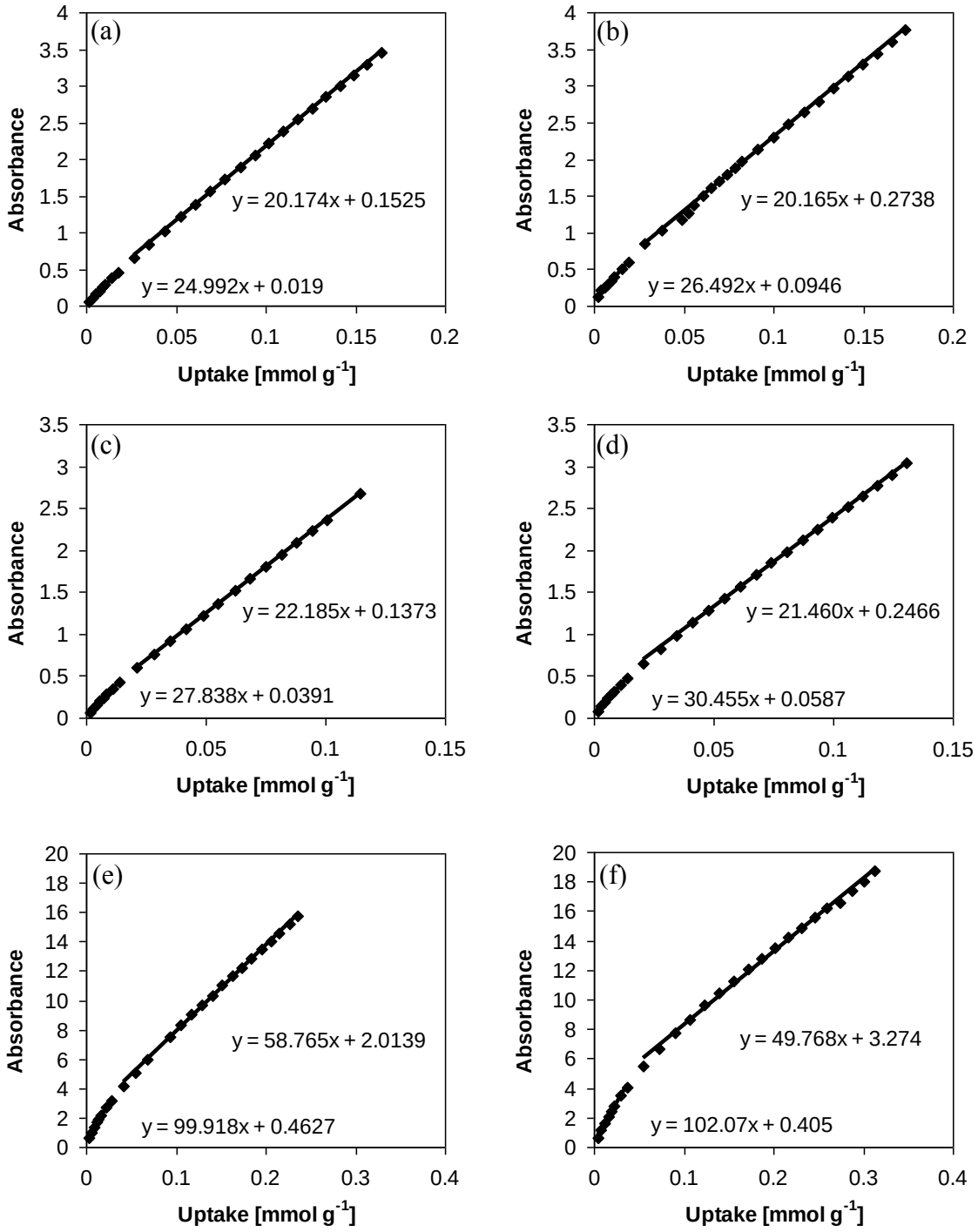

Figure 2.8: Isobutane absorbance at 2900 cm^{-1} at different uptakes on La-USY I (a) and La-USY II (b), La-Y I (c) and La-Y II (d) and on La-X I (e) and La-X II (f) materials

Two different stoichiometric adsorption regimes are observed for all studied zeolites. At low coverage, the polarization of the adsorbed isobutane was stronger than at high coverage. With La-USY and La-Y, the change of these regimes was observed at rather low isobutane loadings (La-Y I = 0.017 mmol/g, La-USY II = 0.028 mmol/g) and was less pronounced than with La-X. The higher integral intensity, i.e., the higher extinction coefficient, of isobutane on La-X II after adsorption was in contrast observed until the loading reached 0.055 mmol/g. Note that in this regime more isobutane was adsorbed than on La-USY and La-Y, i.e., more sites were available, in which isobutane was highly polarized compared to the zeolites containing less aluminum. The extinction coefficient of adsorbed isobutane on the low-silica La-X zeolites was four times higher than with the higher-silica Y and USY-based materials. So, while the extinction coefficients at higher uptakes were similar for La-USY (La-USY I = 20.2, La-USY II = 20.2) and La-Y (La-Y I = 22.2, La-Y II = 21.5) materials, it was much higher for La-X materials (La-X I = 58.8, La-X II = 49.8).

It is important to emphasize that at low isobutane loadings (at which the high molar extinction coefficient is observed) interactions of adsorbed isobutane with OH groups were not observed in the studied materials (see Figures A 3 a-f). As presence of one compensation effect for all zeolites shows that the materials have identical available pore geometries, this indicates that specific differences between the states of adsorbed isobutane must be related to the presence of accessible La^{3+} cations. At higher isobutane loadings (1-10 mbar isobutane) isobutane interacted with Si-OH (stretching band at 3726 – 3733 cm^{-1}) beside the La-OH (3521 – 3548 cm^{-1}) groups. Furthermore, the perturbation of a small fraction of the bridging OH groups was observed at high isobutane loadings for La-USY and La-X (see Figure A 3).

2.4. Discussion

2.4.1. Nature and location of La^{3+} cations

In slightly acidic aqueous solution (pH 6) a variety of hydrated La^{3+} cations ($[La(H_2O)_n]^{3+}$, $n \leq 8$) exist at ambient temperature.[53] The large size of these hydrated La^{3+} cations (0.79 nm) sterically limits the exchange positions for La^{3+} cations. Thus, during the liquid ion-exchange, lanthanum is first predominantly exchanged in the faujasite supercages. When such an exchanged zeolites is heated, the hydration shell of the La^{3+} cation decreases, allowing the migration of La^{3+} through the six-membered ring windows (0.25 nm) of faujasite into the sodalite cages. Because of the better stabilization, La^{3+} cations are mainly located inside the sodalite cage after thermal treatment, being coordinated to framework oxygen atoms close to the 6-membered ring window of the hexagonal prism (sites I and I') or in the supercage (site II). If required by lower framework aluminum concentrations La^{3+} cations are able to dissociate water and form cations of the type $[La(OH)_n]^{(3-n)+}$ as well as the corresponding balancing protons. Only at higher La concentrations, the location in the supercages close to the 4-membered ring at the position III and III', slightly inside the supercage and close to the 6-membered ring window of the sodalite cage at position II as well as shifted towards the center of supercage at position II* become favorable. A large part of this redistribution is also caused by the repulsion of cations in the constraints of the double six rings and the sodalite cage.

The formation of multinuclear OH-bridged lanthanum clusters is another way of compensating for the mutual repulsion of the La^{3+} cations and is chemically feasible because of the pronounced basicity of the terminal La-OH groups and the presence of numerous anionic framework sites within the sodalite cages as shown by the DFT calculations with two model faujasites (LaFAU-1.2 and LaFAU-2.7). Consistent with previous suggestions[54,55] the computational results indicate that oxygen bridged La^{3+} clusters are stable within the sodalite cages.

In zeolites with low aluminum concentrations (La-USY I and La-Y I) monomeric La^{3+} cations are mainly stabilized within the sodalite cages. Charge compensation, derived from the total negative charge of the framework aluminum (shown in Table 2.3) and the concentration of monomeric La^{3+} species (summarized in Table 2.5), in La-USY materials (La-USY I, 84 %, and La-USY II, 57 %) increased with increasing La^{3+} concentration inside the sodalite cages. Increasing concentrations of La^{3+} in La-Y I led to an increased fraction of hydroxylated lanthanum cations

and concomitantly in the decrease of the concentration of initially monomeric La^{3+} species (La-Y I, 46 %, and La-Y II, 12 %), most probably due to the migration of further La^{3+} cations during the second calcination leading eventually to the formation of multinuclear OH-bridged lanthanum clusters.

The computational studies for the high-silica LaFAU-2.7 model (several configurations differing in the distribution of the charge compensating La^{3+} species were explored) show that the charge compensating La^{3+} cations tend to aggregate with the hydroxylated lanthanum cations to form multinuclear aggregates inside the sodalite cage. Various clustered OH-bridged lanthanum species ($[La_3(\mu\text{-}OH)_2]^{7+}$ and $[HOLa_3(\mu\text{-}OH)_3(\mu^3\text{-}OH)]^{4+}$) within the sodalite cage were shown to be more stable than individual hydroxylated La^{3+} cations (see Figure 2.4 and 2.5), which have been speculated to exist.[54,55]

The major fraction of lanthanum in high alumina La-X is similarly introduced in the form of hydroxylated OH-bridging clusters ($[La_3(\mu\text{-}OH)(\mu^3\text{-}OH)]^{7+}$, $[La_3(\mu\text{-}OH)]^{8+}$, and $[La_3(\mu\text{-}OH)_3]^{6+}$) within the sodalite cages (see Figure 2.6). Also in this material the location of La^{3+} within the sodalite cages and D6R structural unit is energetically most favorable. The increased concentration and the associated repulsion between the cationic La species confined in the sodalite cages of lower-silica zeolites leads to the population of the supercage SII exchange sites by La^{3+} cations. The coordination unsaturation of the La^{3+} at these sites is partially compensated by the formation of additional coordination bonds with the OH moieties of the multinuclear clusters in the sodalite cage. Interestingly, additional La^{3+} exchange followed by a second thermal treatment step did not result in an increase of the overall La^{3+} concentration in La-X II materials, however, the concentration of monomeric La^{3+} species increased (La-X I = 57 %; La-X II = 79 % of monomeric La^{3+}). This shows that the increased duration of thermal treatment allows a better distribution across all sites.

Based on evidence from solid state MAS NMR and theoretical calculations indicate that higher framework aluminum concentrations stabilize the coordination of isolated, bare La^{3+} cations at ion-exchange sites, this also induces severe distortions of the zeolitic lattice. In contrast, hydroxylated La^{3+} cations cause only weak distortions on the neighboring aluminum, most probably via the formation of hydrogen bonds. Thus, the aluminum distribution indirectly changes the properties and the impact of La^{3+} cations in faujasite type materials.

Although we note that in addition to stabilizing the zeolitic framework, incorporated La^{3+} influences the local coordination of the tetrahedral framework and the extra-framework

aluminum, we do not have evidence that the exchange and the related lattice distortion leads to strengthening of Brønsted acid sites. The IR spectra of adsorbed pyridine showed that La^{3+} exchange decreased the concentration of BAS. However, just marginal changes in the intrinsic acidic and basic properties of the La-FAU were shown by TPD of ammonia (see Figure A 1) indicating that the Brønsted acid site strength is not influenced by the La^{3+} cations. The IR spectra of adsorbed pyridine show that in La-USY and La-Y La^{3+} cations in the supercages are stabilized in the hydroxylated (La-OH stretching vibration at 3500 - 3550 cm^{-1}) form, whereas in X zeolites they are mainly stabilized in the non-hydroxylated form (see Figure A 2). This is in excellent agreement with the DFT results (see Figure 2.5 and 2.7 for visualization).

As a side note, we would like to mention here that solid state MAS NMR (see Figure 2.2) and the chemical composition (Table 2.2), suggests that repeated exchange surprisingly aids reinsertion of the octahedrally coordinated aluminum into tetrahedral lattice positions. This unique reinsertion chemistry is normally related to the presence of bases such ammonia. We speculate at present that basic hydroxylated La^{3+} cations fulfill that role in the present case.

2.4.2. Influence of different lanthanum species on alkane activation

Some of the La exchanged zeolites considered here showed remarkable catalytic activity in dehydrogenation of alkanes at low temperatures and in facilitating hydride transfer.[2,26] In our previous studies, it has been established that this ability is related to an unusually strong polarization of alkane C-H bonds.[26] This polarization apparently depends drastically on the concentration of aluminum, decreasing in severity with decreasing concentration of aluminum. The fraction of isobutane that is strongly polarized decreases markedly with decreasing concentration of aluminum in the lattice (change on the molar extinction coefficient) indicating that only the fraction of La^{3+} incorporated as bare and accessible cations contributes to the strong polarization. The strong interaction induced by La^{3+} is best illustrated overall by the fact that the heat of adsorption of isobutane increased in the presence of La^{3+} by 10 kJ/mol compared to a zeolite containing only Brønsted acid sites and 16 kJ/mol compared to an aluminum free zeolite.[25,56,57]

The increase of total La^{3+} concentration within the same zeolite influenced the thermodynamic properties of adsorbed isobutane only, if the concentration of the accessible La^{3+} in the supercage varied. IR spectra of adsorbed isobutane showed that the strong Brønsted acid sites (bridging SiOHAl groups, see Fig. A 3) had only a marginal effect on the extinction coefficient.

The high extinction coefficient of isobutane adsorbed at accessible La^{3+} sites is a clear sign of the strong polarization of the C-H bond (see Fig. 2.8 and Table 2.8). It is important to emphasize that the presence of hydroxyl groups at La^{3+} drastically reduces the strength of interaction and hence also the polarization of the C-H bond.

The similar changing points of the regime (SP_{BAS}) for zeolites with primarily $[La(OH)]^{2+}$ and $[La(OH)_2]^{+}$ as well as the lower but equal extinction coefficients show that both cations interact identically with isobutane and have also a finite, but very low concentration in the accessible supercage. The high extinction coefficient (i.e., the highest isobutane polarization) show that only La-X has bare La^{3+} cations in SII positions (see Table 2.2 and 2.5). Once these sites are covered the remaining sorption sites only moderately increase the molar extinction coefficient of the C-H stretching vibration indicating a much weaker interaction with isobutane. Note that only with La-X, the change to the second regime with lower extinction coefficients occurs at a substantial isobutane coverage indicating that only with this material sufficiently strong La^{3+} cations can induce C-H bond polarization.

Thus, we conclude that only the monomeric non-hydroxylated La^{3+} species in supercages cause the strong polarization and that the fraction of molecules strongly polarized strictly correlates with the concentration of this La^{3+} cationic species. On the basis of the detailed ^{13}C MAS NMR studies, Sievers et al. demonstrated that a stronger positive partial charge is induced to secondary and tertiary carbon atoms, whereas primary carbons are less polarized.[26] Therefore, we assume that accessible La^{3+} interacts primarily with the hydrogen at the tertiary carbon atom of isobutane leading to the polarization of this C-H bond, as sketched in Figure 2.9.

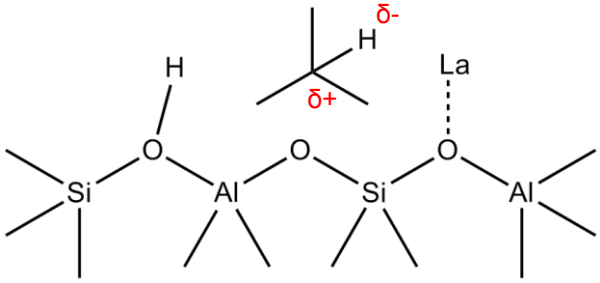

Figure 2.9: Alkane polarization on monomeric La^{3+} extra-framework cations located in accessible position in supercages

2.5. Conclusions

We have shown that the chemical composition of the zeolite determines the location and structural properties of La-containing extra-framework species. Only after exposing the zeolites to higher temperatures La^{3+} is able to be accommodated in the double six-rings and the sodalite cages. The predominant part of the introduced La is present in the zeolites as multinuclear hydroxylated species. Low concentrations of aluminum caused the cations to partially dissociate water and to form hydroxylated La^{3+} cations and bridging SiOHAl groups in a distance to these sites. The distant location of such isolated La species in low-Al zeolite matrices hampers their self-organization into more stable multinuclear aggregates. With the increased lattice Al concentration in faujasite, the La content also increases as well as the formal positive charge of the extra-framework species. Due to the higher concentration and, therefore, more pronounced repulsion between the La^{3+} cations in the small sodalite cages, some of the La^{3+} cations migrate into the accessible supercage SII cation sites. The higher negative charge of the lattice of Al rich faujasites allows a more efficient stabilization of such accessible bare La^{3+} species at SII positions in the supercage. Furthermore, the close proximity of the hydroxylated extra-framework La clusters within the adjacent sodalite cage allows the formation of an additional stabilizing coordination bond between the OH ligands in these aggregates and the La^{3+} at the SII site.

Only the isolated La^{3+} cations stabilized at the supercage cation sites are able to exert the unique polarization of secondary and tertiary C-H bonds and activate alkanes through polarization of the C-H bond. This polarization appears also to be the key feature for hydride transfer and allows the stable and repetitive generation of carbenium ions from di-branched alkanes at ambient conditions, which will be subject of further investigations.

2.6. Acknowledgements

The authors would like to thank Dr. Gabriele Raudaschl-Sieber for supporting the NMR experiment and Prof. Gary Haller for in depth discussion. We also gratefully acknowledge the financial support in the framework of IDECAT for exchange visits between collaborating partners. NWO-NCF (SH-170-11) is acknowledged for providing access to the computational facilities.

2.7. References

(1) Cumming, K. A.; Wojciechowski, B. W. *Catal. Rev. Sci. Eng.* **1996**, *38*, 101.

(2) Sievers, C.; Onda, A.; Guzman, A.; Otillinger, K. S.; Olindo, R.; Lercher, J. A. *J. Phys. Chem. C* **2007**, *111*, 210.

(3) Feller, A.; Barth, J.-O.; Guzman, A.; Zuazo, I.; Lercher, J. A. *J. Catal.* **2003**, *220*, 192.

(4) Feller, A.; Zuazo, I.; Guzman, A.; Barth, J.-O.; Lercher, J. A. *J. Catal.* **2003**, *216*, 313.

(5) Feller, A.; Lercher, J. A. *Adv. Catal.* **2004**, *48*, 229.

(6) Xiao, S.; Le Van Mao, R.; Denes, G. *J. Mater. Chem.* **1995**, *5*, 1251.

(7) Guzman, A.; Zuazo, I.; Feller, A.; Olindo, R.; Sievers, C.; Lercher, J. A. *Micropor. Mesopor. Mater.* **2005**, *83*, 309.

(8) Guzman, A.; Zuazo, I.; Feller, A.; Olindo, R.; Sievers, C.; Lercher, J. A. *Micropor. Mesopor. Mater.* **2006**, *97*, 49.

(9) Huang, J.; Jiang, Y.; Reddy Marthala, V. R.; Ooi, Y. S.; Weitkamp, J.; Hunger, M. *Micropor. Mesopor. Mater.* **2007**, *104*, 129.

(10) van Bokhoven, J. A.; Roest, A. L.; Konigsberger, D. C.; Miller, J. T.; Nachtegaal, G. H.; Kentgens, A. P. M. *J. Phys. Chem. B* **2000**, *104*, 6743.

(11) Sanchez-Castillo, M. A.; Madon, R. J.; Dumesic, J. A. *J. Phys. Chem. B* **2005**, *109*, 2164.

(12) Klein, H.; Fuess, H.; Hunger, M. *J. Chem. Soc. Faraday Trans.* **1995**, *91*, 1813.

(13) Lee, E. F. T.; Rees, L. V. C. *Zeolites* **1987**, *7*, 143.

(14) Bennett, J. M.; Smith, J. V. *Mater. Res. Bull.* **1969**, *4*, 343.

(15) Olson, D. H.; Kokotailo, G. T.; Charnell, J. F. *J. Colloid Interface Sci.* **1968**, *28*, 305.

(16) Herreros, B.; Man, P. P.; Manoli, J. M.; Fraissard, J. *J. Chem. Soc.-Chem. Commun.* **1992**, 464.

(17) Hunger, M.; Engelhardt, G.; Weitkamp, J. *Micropor. Mater.* **1995**, *3*, 497.

(18) Venuto, P. B.; Hamilton, L. A.; Landis, P. S. *J. Catal.* **1966**, *5*, 484.

(19) Ward, J. W. *J. Catal.* **1969**, *14*, 365.

(20) Sievers, C.; Liebert, J. S.; Stratmann, M. M.; Olindo, R.; Lercher, J. A. *Appl. Catal. A-Gen.* **2008**, *336*, 89.

(21) Pidko, E. A.; van Santen, R. A.; Hensen, E. J. M. *Phys. Chem. Chem. Phys.* **2009**, *11*, 2893.

(22) Gaare, K.; Akporiaye, D. *J. Phys. Chem. B* **1997**, *101*, 48.

(23) Eder, F.; Stockenhuber, M.; Lercher, J. A. *Stud. Surf. Sci. Catal.* **1995**, *97*, 495.

(24) Miyamoto, Y.; Katada, N.; Niwa, M. *Micropor. Mesopor. Mater.* **2000**, *40*, 271.

(25) Eder, F.; Lercher, J. A. *Zeolites* **1997**, *18*, 75.

(26) Sievers, C.; Onda, A.; Olindo, R.; Lercher, J. A. *J. Phys. Chem. C* **2007**, *111*, 5454.

(27) Pidko, E. A.; Xu, J.; Mojet, B. L.; Lefferts, L.; Subbotina, I. R.; Kazansky, V. B.; van Santen, R. A. *J. Phys. Chem. B* **2006**, *110*, 22618.

(28) Pidko, E. A.; van Santen, R. A. *ChemPhysChem* **2006**, *7*, 1657.

(29) García, P.; Lima, E.; Aguilar, J.; Lara, V. *Catal. Lett.* **2009**, *128*, 385.

(30) Feller, A.; Guzman, A.; Zuazo, I.; Lercher, J. A. *J. Catal.* **2004**, *224*, 80.

(31) Kazansky, V. B. *Catal. Today* **1999**, *51*, 419.

(32) Sanderson, R. T. *J. Chem. Educ.* **1964**, *41*, 187.

(33) Sanderson, R. T. *J. Chem. Educ.* **1956**, *33*, 443.

(34) Lippens, B. C.; Linsen, B. G.; De Boer, J. H. *J. Catal.* **1963**, *3*, 32.

(35) Halsey, G. *Chem. Phys.* **1948**, *16*, 931.

(36) ASTM. Standard Test Method for Determination of the Unit Cell Dimension of a Faujasite-Type Zeolite. In *Annual Book of ASTM Standards*, 1985; Vol. D3942-85.

(37) Hunger, M.; Freude, D.; Pfeifer, H. *J. Chem. Soc. Faraday Trans.* **1991**, *87*, 657.

(38) Kresse, G.; Furthmuller, J. *Phys. Rev. B* **1996**, *54*, 11169.

(39) Perdew, J. P.; Burke, K.; Ernzerhof, M. *Phys. Rev. Lett.* **1996**, *17*, 3865.

(40) Kresse, G.; Joubert, D. *Phys. Rev. B* **1999**, *59*, 1758.

(41) Blöchl, P. E. *Phys. Rev. B* **1994**, *50*, 17953.

(42) Monkhorst, H. J.; Pack, J. D. *Phys. Rev. B* **1976**, *13*, 5188.

(43) Pidko, E. A.; Mignon, P.; Geerlings, P.; Schoonheydt, R. A.; van Santen, R. A. *J. Phys. Chem. C* **2008**, *112*, 5510.

(44) Stavitski, E.; Pidko, E. A.; Kox, M. H. F.; Hensen, E. J. M.; van Santen, R. A.; Weckhuysen, B. M. *Chem. Eur. J.* **2010**, *16*, 9340.

(45) Millot, Y.; Man, P. P. *Solid State Nucl. Magn. Reson.* **2002**, *21*, 21.

(46) Samoson, A.; Lippmaa, E.; Engelhardt, G.; Lohse, U.; Jerschkewitz, H. G. *Chem. Phys. Lett.* **1987**, *134*, 589.

(47) Omegna, A.; van Bokhoven, J. A.; Prins, R. *J. Phys. Chem. B* **2003**, *107*, 8854.

(48) Weihe, M.; Hunger, M.; Breuninger, M.; Karge, H. G.; Weitkamp, J. *J. Catal.* **2001**, *198*, 256.

(49) Hunger, M. *Catal. Rev. Sci. Eng.* **1997**, *39*, 345.

(50) Mikovsky, R. J.; Marshall, J. F.; Burgess, W. P. *J. Catal.* **1979**, *58*, 489.

(51) Kazansky, V. B.; Pidko, E. A. *J. Phys. Chem. B* **2005**, *109*, 2103.

(52) Kazansky, V. B.; Subbotina, I. R.; Jentoft, F. C.; Schlögl, R. *J. Phys. Chem. B* **2006**, *110*, 17468.

(53) Riedel, E. *Anorganische Chemie 6. Auflage*; Walter de Gruyter GmbH & Co.KG: Berlin, 2004.

(54) Aguilar-Pérez, F.; Gómez-Tagle, P.; Collado-Fregoso, E.; Yatsimirsky, A. K. *Inorg. Chem.* **2006**, *45*, 9502.

(55) Carvajal, R.; Chu, P.-J.; Lunsford, J. H. *J. Catal.* **1990**, *125*, 123.

(56) Eder, F.; Lercher, J. A. *J. Phys. Chem. B* **1997**, *101*, 1273.

(57) Eder, F.; Stockenhuber, M.; Lercher, J. A. *J. Phys. Chem. B* **1997**, *101*, 5414.

This chapter is based on:

Schüßler, F.; Pidko, E. A.; Kolvenbach, R.; Sievers, C.; Hensen, E. J. M.; van Santen, R. A.; Lercher, J. A. *J. Phys. Chem. C* **2011**, 115, 21763

Chapter 3

Influence of La^{3+} cations in zeolites for acid catalyzed alkane reactions

La^{3+} cations exchanged into ultra-stable zeolite Y and zeolite X uniquely influence catalytic isomerization, cracking and alkylation of alkanes. La^{3+} cations not only stabilize zeolite lattice, they polarize alkane C-H bonds and enhancing so the rates of cracking, dehydrogenation, and isomerization. This is achieved by a tighter transition state than observed with La^{3+} free zeolites. The presence of La^{3+} cations also enhances drastically the hydride transfer rates observed with the zeolites for alkylation leading to high catalyst stability in isobutane alkylation. Solid state NMR shows that the positive effects are drastically enhanced, if non-hydroxylated La^{3+} cations are accessible for the reacting molecules. Reactive alkanes with adjacent tertiary or quaternary carbon atoms crack and isomerize over these catalysts already close to ambient temperatures.

3.1. Introduction

Rare earth exchanged zeolites are widely used in refining processes to stabilize the molecular sieves against dealumination and to enhance so the acid site concentration.[1-3] The resulting catalysts show higher activities and enhanced hydride and hydrogen transfer characteristics.[4,5] As such cation exchanged zeolites show remarkable properties in polarizing and activating CH bonds of alkanes, understanding their properties is an important target.

In a preceding paper, we have shown that La^{3+} cations after ion exchange are first predominantly located in the faujasite supercages due to the large hydration sphere of the cation.[6] After thermal treatment, the cations migrate to the sodalite cage being coordinated to framework oxygen atoms close to the six ring window of the hexagonal prism, and arrange in a complex way as discussed in ref.[6]. At higher La^{3+} concentrations, the location in the FAU supercages in position III and III', slightly inside the supercage and close to the 6-membered ring window of the sodalite cage at position II as well as shifted towards the center of supercage at position II* become favorable.

The presence of La^{3+} has a marked impact upon catalytic properties. The catalyst stability in isobutane/2-butene alkylation, for example, is significantly improved, partly because La^{3+} increases better maintains the concentration of strong Brønsted acid sites (SBAS)[5] by preventing hydrolysis and dealumination during the pretreatment cycles of the catalyst. Lewis acid sites, which are present in higher concentrations in La^{3+} free materials, facilitate the formation of highly unsaturated carbonaceous deposits causing catalyst deactivation.[7-9]

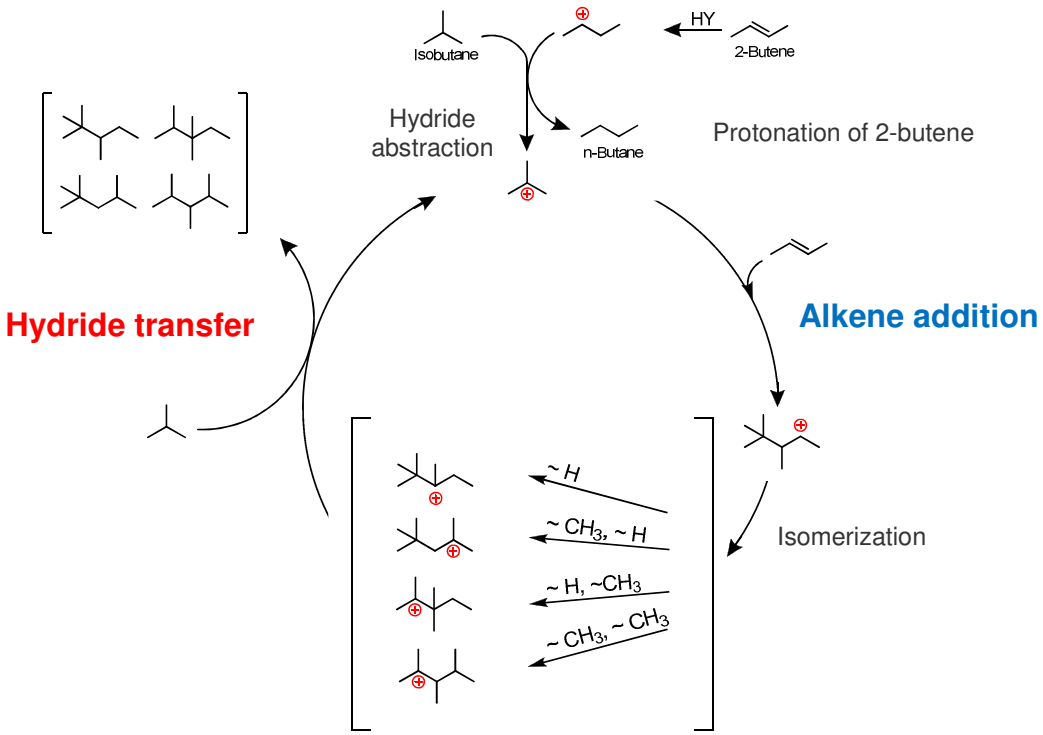

Figure 3.1: Mechanism of isobutane/2-butene alkylation involving the protonation of 2-butene, alkene addition, isomerization and hydride transfer

Let us address first the role of a high concentration of Brønsted acid sites and the specific role of the La^{3+} cations. Figure 3.1 summarizes the reaction mechanism of isobutane/2-butene alkylation. In this cycle, the alkene addition to the in situ formed *tert*-butyl carbenium ion (formed via hydride transfer from isobutane to the *sec*-butyl carbenium generated by 2-butene protonation) and the hydride transfer from isobutane to the alkylation products are the most relevant steps. The 2,2,3-trimethylpentyl carbenium ion is the primary alkylation product, which may rapidly isomerize. The cycle closes by hydride transfer from isobutane to the trimethylpentyl carbenium ion forming trimethylpentane (TMP) and a *tert*-butyl carbenium ion. A high concentration of catalytically active Brønsted acid sites favors a high ratio of carbenium ions to 2-butene and suppresses multiple alkylations. La^{3+} drastically enhances hydride transfer and reduces the residence time of the reactive intermediates. Both measures reduce multiple alkylation and reduce so the formation of carbonaceous deposits that deactivate the catalysts.

It has been shown, however, that La^{3+} cations influence the catalytic activity very differently, depending on the zeolite structure and the specific location in the framework.[6] Therefore, we

explore in this paper, the impact of the concentration, the location and the specific nature of the La^{3+} cations on the catalytic activity of USY and X type zeolites by comparing H-USY, La-USY and La-X samples. To better understand the relation between the acid-base and catalytic properties, the alkylation of isobutane with 2-butene is compared to propane and n-pentane cracking, as well as to 2,2,4-TMP isomerization and cracking.

3.2. Experimental

3.2.1. Materials

La-exchanged zeolite X (La-X) was prepared from Na-X (Si/Al = 1.2), provided by Chemische Werke, Bad Köstritz. The parent material was ion exchanged twice with 0.2 M $La(NO_3)_3$ solution at 353 K for 2 h with a liquid-to-solid ratio of 11 ml/g. The material was washed subsequently with bidistilled water and dried at room temperature. Afterwards, the sample was calcined in flowing synthetic air at 723 K for 1 h. After rehydration, three additional ion exchange steps were carried out (for details of preparation see refs.[1,10]). For the synthesis of La-USY a parent H-USY (Si/Al = 3.1, Na = 0.18 mmol g^{-1}) from Grace Davison was used. Firstly, the sample was ion-exchanged with 0.5 M $La(NO_3)_3$ and a liquid-to-solid ratio of 7 ml/g at 373 K for 4 h. After washing and drying at 373 K for 6 h, the resulting material was calcined in synthetic air at 823 K for 4 h. In order to remove remaining Na^+ cations from the zeolite, the material was exchanged with 5 M NH_4NO_3 solution over 4 h at 373 K. After filtration the same drying and calcination procedure as described above was applied. The catalysts compared here are equivalent to La-USY I and La-X II described in ref.[6].

3.2.2. Physicochemical characterization

The concentrations of aluminum, silicon and sodium were determined by atomic absorption spectroscopy (AAS) using a Solaar M5 absorption spectrometer (ThermoFisher). The La^{3+} concentration was determined by ICP-OES (SpectroFlame Typ FTMOA81A from Spectro Analytical Instruments). The pore size distribution and BET surface area were measured by nitrogen physisorption using a PMI automated BET sorptometer.

The nature and concentration of acid sites was analyzed by infrared spectroscopy of adsorbed pyridine. The samples were pressed into self-supporting wafers and activated in vacuum (10^{-6} mbar) at 723 K for 1 h with a heating rate of 10 K min^{-1}. Pyridine was then adsorbed at 423 K at

a pressure of 0.1 mbar until no further changes were observed. In order to remove all of the physisorbed pyridine, the system was outgassed for 1 h at 423 K. The concentration of strong acid sites was probed by increasing the temperature to 723 K for 0.5 h. Acid sites that retained pyridine under these conditions were classified as strong Brønsted acid sites (SBAS) and strong Lewis acid sites (SLAS). The concentration of Brønsted and Lewis acid sites was determined based on the integrals of the IR bands at 1540 cm^{-1} and 1450 cm^{-1}, respectively. For quantification, the molar extinction coefficient of 0.73 for Brønsted acid sites and 0.96 for Lewis acid sites was used. These extinction coefficients were determined for a standard material using a combination of microgravimetric measurements of the thermal stability of pyridine and infrared spectroscopy of adsorbed pyridine.

For ^{27}Al MAS NMR measurements the samples were fully hydrated. The samples were packed into a 4 mm ZrO_2 rotor and measured on a Bruker AV500 spectrometer (B_0 = 11.7 T) with a spinning rate of 12 kHz. For ^{27}Al MAS NMR single pulse experiment 2400 scans were recorded using a recycle time of 0.25 s. In this case an excitation pulse of 0.46 µs corresponding to a π/12-pulse was used. The chemical shifts of all spectra are reported relative to an external standard of solid $Al(NO_3)_3$ (δ = -0.5427 ppm). For ^{29}Si MAS NMR spectra 10000 scans were recorded at a resonance frequency of 99.3308 MHz and a recycle time of 50 s. The spectrum was referenced against $Si(SiMe_3)_4$ at the position of -9.843 ppm.

^{139}La NMR was measured in static mode. The resonance frequency was 70.6 MHz and 1 x 10^6 scans were used for La-X and La-USY, respectively. A Hahn echo pulse sequence was applied.[11] The pulse lengths for p_1 and p_2 were 0.8 µs and the pulse delay was 10 µs. The recycle rate was 200 ms. The peak position was referenced against a saturated solution of $LaCl_3$ (0 ppm). All samples for ^{139}La NMR spectroscopic measurements were prepared and measured according the literature published procedure.[12,13]

Powder X-ray diffraction (XRD) patterns were measured on a Philips X'pert diffractometer equipped with an X'celerator module using CuKα radiation. Diffractograms were recorded from 5 to 75° 2Θ using a step size of 0.033°. The unit cell dimension was calculated from the X-ray diffraction pattern of the zeolite material mixed with 5 % of silicon using the silicon reflections as reference.[14]

3.2.3. Isobutane/2-butene alkylation reaction

The alkylation of isobutane/2-butene was performed in a 50 ml CSTR reactor (Autoclave Engineers) at 348 K and 25 bar.[10,15] The olefin space velocity used was 0.2 $g_{butene}g^{-1}_{catalyst}h^{-1}$.[10] In order to avoid multiple alkylation, an isobutane to 2-butene ratio of 10/1 and a Mahoney-Robinson spinning basket reactor (1600 rpm) were used to achieve a low concentration of 2-butene throughout the reactor. The purities of isobutane and 2-butene were 99.95 % and 99.5 %, respectively. The catalysts were activated in situ in H_2 at 393 K for 4 h and for 14 h at 453 K with a heating ramp of 2 K min^{-1} prior to use. The product distribution was measured using a 50 m HP-1 column (ID = 0.32 mm, film = 0.52 µm) in a HP6890 chromatograph equipped with a FID detector.

3.2.4. Protolytic cracking of alkanes

The protolytic cracking of propane and n-pentane was performed in a plug flow reactor (length = 350 mm; inner diameter = 6 mm, quartz) at atmospheric pressure. The catalysts (pellet size: 250 – 325 µm) were activated in situ at 803 K with a heating ramp of 2 K min^{-1} for 2 h in synthetic air (flow rate: 20 ml min^{-1}). Before introducing the reactant (3.0 vol.% for propane and 2 vol.% for n-pentane in helium), the reactor was flushed for 30 minutes with pure helium. The catalytic reaction was performed between 753 and 793 K. The conversion was kept below 1.5 % in order to avoid the contributions from products of the bimolecular or secondary reactions pathways, the absence of which was confirmed by the equimolar ratio of ethylene to methane. Reactant and products were separated and analyzed by on-line chromatographic measurements (HP 5890, capillary column: HP-Al_2O_3/KCl, 50 m × 0.32 mm × 8.0 µm) using an FID detector. The apparent activation energies for the protolytic cracking of propane and n-pentane were determined from the slopes of the Arrhenius plots in a temperature range of 753–783 K. The corresponding activation entropies were obtained using transition state theory.

3.2.5. Isomerization and cracking of 2,2,4-TMP

The conversion of 2,2,4-TMP was studied in the same reactor as used for the protolytic cracking of propane. The catalysts (pellet size: 150 – 250 µm) were first activated in situ at 393 K for 4 h and at 453 K for 12 h in hydrogen atmosphere (flow rate 30 ml min^{-1}). Catalyst

stability studies were performed at 368 K using 5.0 mol% of 2,2,4-TMP. Kinetics were measured in the range of 348–368 K. 5.0 mol% of 2,2,4-TMP was introduced into a He atmosphere (flow rate of 9.7 ml min^{-1}) using a saturator with three consecutive saturation flasks, in which the first two were filled with 2,2,4-TMP, while the last remained empty. The reactant and products were analyzed with an on-line GC (HP 5890, capillary column: HP-1 column, 50 m × 0.32 mm × 0.52 µm).

3.3. Results

3.3.1. Chemical composition and physicochemical properties

The chemical composition and the physicochemical properties of the studied materials are compiled in Table 3.1.

Table 3.1: Physicochemical properties and acid site distribution of H-USY, La-USY and La-X

	H-USY	**La-USY**	**La-X**
Chemical composition			
Si/Al	3.1	4.0	1.2
Al/unit cell in framework[a]	28.0	27.2	79.4
Unit cell size [nm]	2.45	2.45	2.49
Na/Al	0.060	0.015	0.002
La/Al	0	0.074	0.315
Micropore volume [cm^3/g]	0.28	0.26	0.26
Acidity [mmol/g]			
BAS	0.995	0.917	0.369
LAS	0.436	0.417	0.545
SBAS	0.513	0.557	0.062
SLAS	0.301	0.282	0.064

[a] Framework aluminum atoms per unit cell size calculated by ref.[16]

Not only the absolute concentration of La^{3+} cations, but also the concentration relative to Al^{3+} was much higher in La-X (0.315) than in La-USY (0.074). While conceptually the ratio of La^{3+} exchanged per Al containing tetrahedron of the zeolite should be 1/3, this value is only

reached with zeolite X suggesting that isolated Al^{3+} sites are unable to exchange La^{3+}. The micropore volumes as well as the unit cell size and the intensity of the diffractogram show that the preparation procedures did not affect the crystal structure. In both La^{3+} exchanged zeolites the Na^{+} content was low, 1.5 and 0.2 % of the maximum exchange degree, respectively. These remaining Na^{+} cations, located in the hexagonal prism or six-membered ring openings of the sodalite cages hardly influence the studied reactions, because both locations are inaccessible for the reacting molecules.

USY had a much higher concentration of total and strong Brønsted acid sites (H-USY = 0.513 $mmol_{SBAS}/g_{catalyst}$ and La-USY = 0.557 $mmol_{SBAS}/g_{catalyst}$) compared to La-X (0.062 $mmol_{SBAS}/g_{catalyst}$). The low concentration of Brønsted acid sites in the latter zeolite is related to its high ratio of La/Al leaving only a relatively small concentration of aluminum tetrahedra that are able to form a hydroxy group. The concentration of strong Lewis acid sites was much higher for the H-USY and La-USY than for the La-X samples.

The local environment of aluminum atoms in H-USY, La-USY and La-X was investigated by ^{27}Al MAS NMR and ^{29}Si MAS NMR. The corresponding ^{27}Al MAS NMR spectra are shown in Figure 3.2.

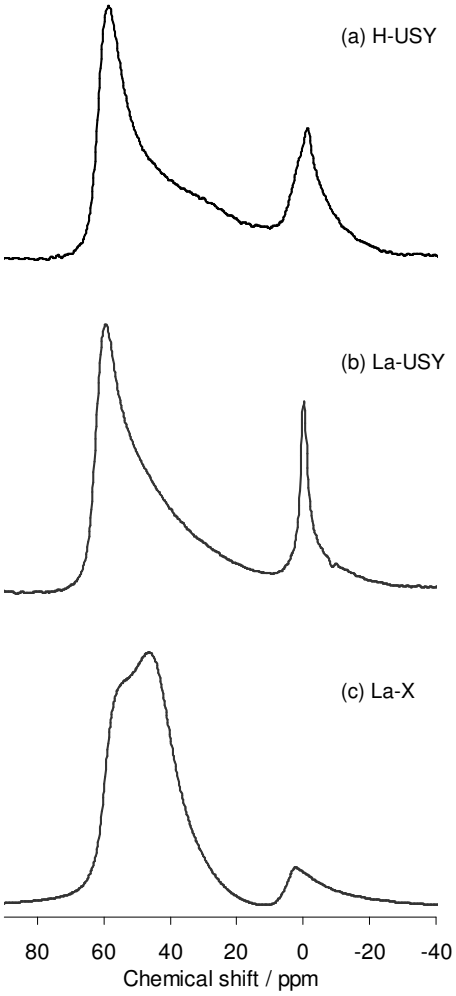

Figure 3.2: ^{27}Al MAS NMR of H-USY (a), La-USY (b) and La-X (c) partly reproduced from ref [6]

Peaks for tetrahedrally (60 – 40 ppm) as well as octahedrally coordinated aluminum (ca. 0 ppm) were observed for all samples. The concentration of octahedrally coordinated aluminum in H-USY and La-USY (24.8 and 18.8 %) were higher than in La-X (7.0 %). Aluminum causing the peak at 58 ppm is considered to be tetrahedrally coordinated and the charge of the tetrahedron is compensated by H^+ and Na^+. The strong distortion of the peak at 45 ppm in La-X is attributed to the presence of La^{3+} cations compensating the charge of three aluminum-oxygen tetrahedral.[10] With La-USY only a shoulder was observed at 45 ppm, because the much lower concentration of aluminum in the lattice makes the presence of three aluminum-oxygen tetrahedra that can be compensated by La^{3+} highly improbable.

The spectra of the corresponding ^{29}Si MAS NMR measurements and the number of aluminum neighbors are compiled in Figure 3.3 and Table 3.2, respectively.

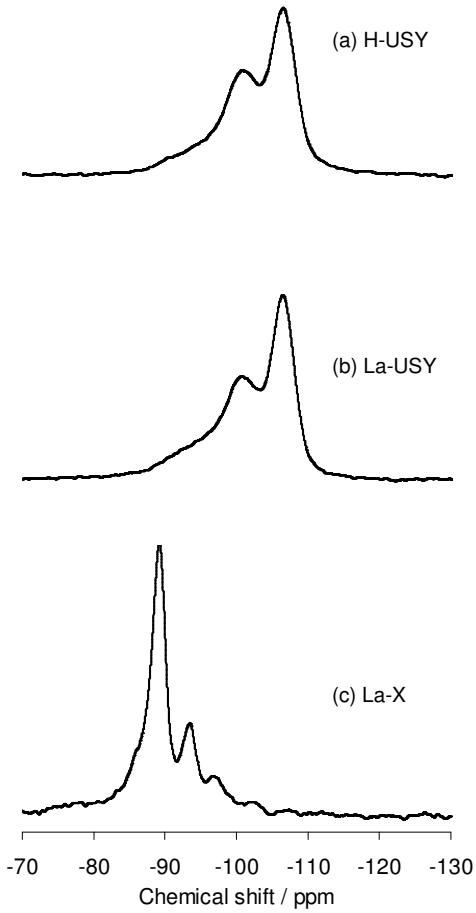

Figure 3.3: ^{29}Si MAS NMR of H-USY (a), La-USY (b) and La-X (c) materials

Table 3.2: Tetrahedral and octahedral coordinated aluminum determined by ^{27}Al MAS NMR as well as aluminum coordinated next to silicon determined by ^{29}Si MAS NMR

Catalyst	Framework Al [%]	EFAl [%]	Si(**0**Al) [%]	Si(**1**Al) [%]	Si(**2**Al) [%]	Si(**3**Al) [%]	Si(**4**Al) [%]
H-USY	75.2	24.8	38.6	57.0	4.3		
La-USY	81.2	18.8	33.4	55.2	11.4		
La-X	92.9	7.0	3.4	9.2	8.8	11.3	67.2

In the ^{29}Si MAS NMR spectra the peak positions are shifted upfield by about 4 ppm in the presence of La^{3+} cations. This is attributed to higher Al-O-Al or Al-O-Si bond angles in the six ring window of the sodalite cage in agreement with observations by Klein et al. and Gaare et al.[17,18]. Note that in line with the differences in the stabilization of the La^{3+} cations, most Si atoms of H-USY and La-USY have 0 to 1 aluminum neighbor, while in La-X most Si tetrahedra have 3 or 4 neighboring aluminum – oxygen tetrahedra (Table 3.2).

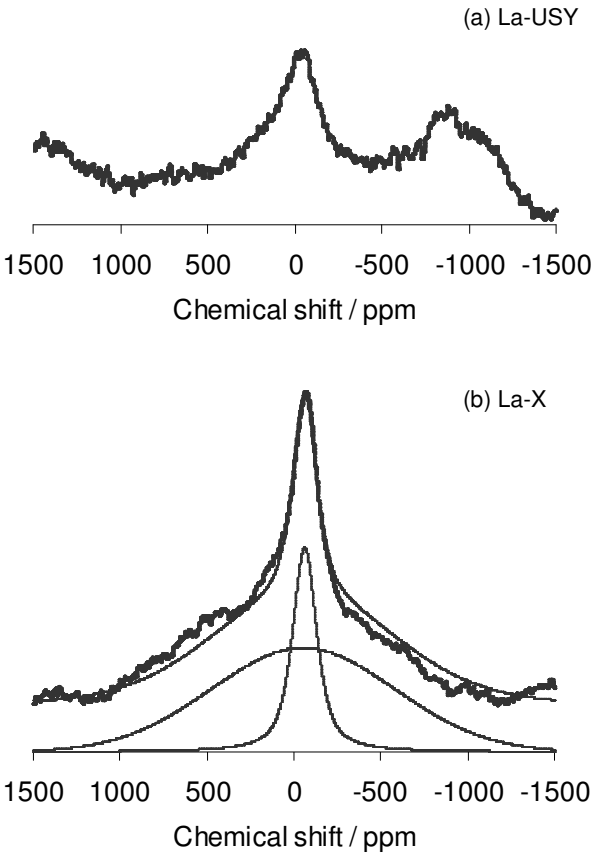

Figure 3.4: ^{139}La NMR of La-USY (a) and La-X (b): experimental data (-) and theoretical fit (-)

The location of La^{3+} cations was also directly investigated by ^{139}La NMR. The spectra of corresponding materials are shown in Figure 3.4. Through the incorporation of La^{3+} cations in the center of a 6-membered oxygen ring system inside the sodalite cages, the charge distribution caused a large quadrupolar moment. In a previously published scientific report by Hunger et all, a very broad peak with a line width of 190 ± 10 kHz is observed as a consequence

of the lanthanum incorporation.[19] La^{3+} cations in supercages are more flexible, in particular when they are in a fully hydrated state creating a smaller electric field gradient and have a smaller quadrupolar moment. In the spectrum of La-X a sharp peak at -67 ppm with a line-width of 11.7 kHz was observed (Figure 3.4 b) together with a second broad peak having the same chemical shift, but a line width of 87.6 kHz. Following Hunger et al. we attribute the former to La^{3+} cations in the FAU supercage,[19] while the latter peak is attributed to La^{3+} cations in the sodalite cage. The line width of the broad peak (87.6 kHz) was approximately half of the value published previously, suggesting an increased structural flexibility of the investigated materials. Simulations of the spectrum of La-X (Figure 3.4 b) showed that approximately 25 % of the incorporated lanthanum cations are located in the supercages.

The signal of La^{3+} cations in La-USY had a lower intensity, in line with the considerably lower La^{3+} content. Therefore, only one relatively sharp peak at -32 ppm with a line-width of 22.0 kHz was observed (Figure 3.4 a). The peaks are assigned to $[La(OH)_2]^+$ and $[La(OH)]^{2+}$. The concentration of La^{3+} in supercages was concluded to be very small.

3.3.2. Catalyzed reactions

Alkylation of isobutane/2-butene

The alkylation of isobutane with 2-butene can only be conducted in a meaningful way, if the concentration of 2-butene in the reacting mixture is so low that it is nearly fully converted. The reason for this constraint lies in the fact that the oligomerization of 2-butene, responsible for a low product quality and premature catalyst deactivation, has a substantially higher forward rate constant than hydride transfer and all other reactions associated with alkylation.[20,21] Table 3.3 compiles the analysis of individual compounds produced with TOS. Overall, the main products were C_5-C_7 hydrocarbons, various C_8 isomers and small amounts of larger alkanes (C_{9+}). The C_5-C_7 products were formed from cracking via β-scissions, whereas the C_{9+} products originated from multiple alkylation on strong Brønsted acid sites and oligomerization on the weaker Brønsted acid sites. The C_8 fraction, and in particular trimethylpentanes, which are important for the alkylate quality, constituted 68-79 wt.% of the total C_{5+} yield over the lifetime of each catalyst (Table 3.3). n-Butane was produced in substantial amounts over the entire TOS (Table 3.3). As n-butane cannot be formed directly by β-scission of a carbenium ion, the only possible reaction route for its formation involves hydride transfer from isobutane to a sec-butoxy surface species formed in the initiating reaction step by adsorption of 2-butene on

a strong Brønsted acid site (Figure 3.1).

In understanding that the primary product of isobutane/2-butene alkylation is 2,2,3-TMP, the C_8 product distribution are used here to characterize the relative rates of hydride transfer and isomerization. The formation of n-butane and 2,2,4-TMP was used as tracer for "self-alkylation", *i.e.*, for the reaction of isobutene (formed by desorption of a *tert*-butyl carbenium ion) with a *tert*-butyl carbenium ion. For each desorbing isobutene a new catalytic cycle had to start resulting in the formation of n-butane (Fig. 3.1). Overall, the products were C_5-C_7, and C_8 alkanes, as well as various larger alkanes. The fraction of C_5-C_7 was selected as indicator for the catalytic cracking during alkylation, whereas multiple alkylation is characterized by the C_{9+} fraction.

The catalyst lifetime, defined as the duration of the (near-) complete 2-butene conversion, is the most important parameter to evaluate the efficiency of the catalysts.[5,22] In the present case, the incorporation of La^{3+} in USY prolonged the catalyst lifetime from 5 to 12 h (Table 3.3). For La-X the catalyst lifetime was even further increased to more than 16 h, although the catalyst had a significantly lower concentration of strong Brønsted acid sites (0.06 mmol SBAS/$g_{catalyst}$) than the other two (0.51, 0.56 mmol SBAS/$g_{catalyst}$).

Table 3.3: Product distribution following the H-USY, La-USY and La-X catalyzed alkylation of isobutane/2-butene[a]

Catalyst	Lifetime at full conversion [h]	$C_{5\text{-}7}$ [g $g_{cat.}^{-1}$] (wt.%)	C_8 [g $g_{cat.}^{-1}$] (wt.%)	C_{9+} [g $g_{cat.}^{-1}$] (wt.%)	n-butane [g $g_{cat.}^{-1}$]
H-USY	5	0.26 (11.1)	1.68 (71.5)	0.41 (17.4)	0.05
La-USY	12	0.98 (17.8)	3.85 (68.9)	0.68 (12.3)	0.22
La-X	16	0.92 (10.9)	6.68 (78.9)	0.87 (10.2)	0.29

[a] Activation procedure: in situ activation in H_2 atmosphere, 4 h at 393 K and 14 h at 453 K, heating ramp = 2 K min^{-1}. Reaction conditions: reaction temperature = 348 K, isobutane/2-butene = 10, OSV = 0.2 $g_{butene}g_{catalyst}^{-1}h^{-1}$, stirring speed = 1600 rpm, amount produced until the begin of the deactivation

The La^{3+} reduced the relative rate of multiple alkylation (C_{9+}). The selectivity to C_{9+} decreased from H-USY through La-USY to La-X by more than 40 % despite the much increasing overall

amounts of product hydrocarbons (Table 3.3). It is important to note that the relative rate to C_{9+} was constant for H-USY over the time the catalyst was active (Figure 3.5 a), while it was negligible for the La^{3+} containing catalysts for the first 3-5 hours and increased only as the catalyst approached the end of its lifetime. This shows that La^{3+} is at least initially able to reduce the lifetime of the carbenium ions on the catalyst, thus reducing the probability to be further alkylated to heavier products.

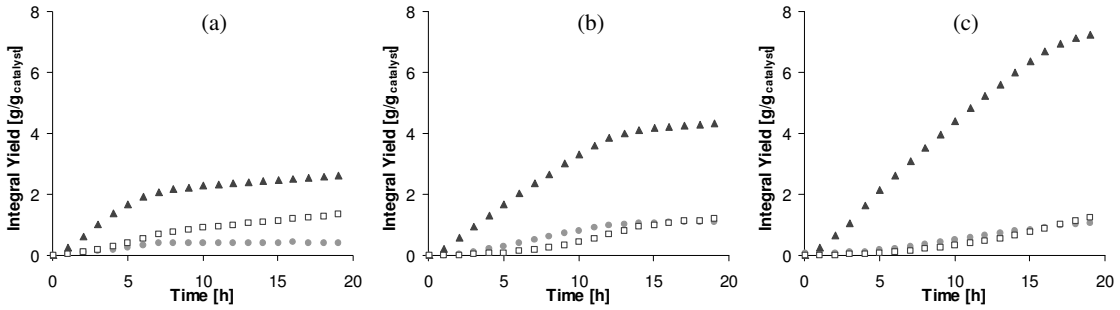

Figure 3.5: Total product yields of C_5-C_7 (●), C_8 (▲) and C_{9+} (□) in the presence of H-USY (a), La-USY (b) and La-X (c). Activation procedure: in situ in H_2, 4 h at 393 K and 14 h at 453 K, heating ramp = 2 K min^{-1}. Reaction conditions: reaction temperature = 348 K, isobutane/2-butene = 10, OSV = 0.2 $g_{butene}g_{catalyst}^{-1}h^{-1}$, stirring speed = 1600 rpm

The effect of La^{3+} incorporation on the catalyst selectivity to TMP, dimethylhexane (DMH) and methylheptanes (MHp) are compiled in Table 3.4. The selectivity in the C_8 fraction is shown in Figure 3.6 as a function of time on stream. The selectivity for each product was calculated integrally until the start of the deactivation.

Table 3.4: Detailed product distribution within the octane (C_8) fraction in solid acid catalyzed alkylation of isobutane/2-butene. Activation procedure: in situ in H_2, 4 h at 393 K and 14 h at 453 K, heating ramp = 2 K min^{-1}. Reaction conditions: reaction temperature = 348 K, isobutane/2-butene = 10, OSV = 0.2 $g_{butene}\, g_{catalyst}^{-1} h^{-1}$, stirring speed = 1600 rpm

Selectivity	H-USY [%]	La-USY [%]	La-X [%]
2,4-DMH	2.49	4.52	3.35
2,3-DMH	5.35	4.95	4.37
2-MHp	0.01	0.23	0.16
4-MHp (3,4-DMH)	0.92	0.73	0.71
3,4-DMH (4-MHp)	0.71	0.86	0.85
3-MHp	0.10	0.26	0.15
2,5-DMH/2,2,3-TMP	5.94	11.61	10.10
2,2,4-TMP	20.80	35.32	26.10
2,3,3-TMP	33.62	24.20	32.73
2,3,4-TMP	29.37	16.97	21.25
Σ TMP	89.73	88.1	90.18
Σ DMH	8.55	10.33	8.57
Σ MHp	1.03	1.22	1.02

Table 3.4 shows that TMP was the most abundant product (ca. 90 wt.% of the total C_8 fraction). The high 2,2,4-TMP selectivity suggests that self-alkylation, i.e., the intermediate generation of iso-butene via hydride transfer from n-butyl carbenium ions, has a significant influence on isobutane/2-butene alkylation.[10] The presence of La^{3+} in USY increased the selectivity to 2,2,4- and 2,2,3-TMP, indicating a faster hydride transfer rate. In contrast to La-USY, increasing La^{3+} concentration in La-X lowered the product selectivity of 2,2,4-TMP and significantly increased the selectivity towards 2,3,4-TMP and 2,3,3-TMP isomers under the same reaction conditions (Figure 3.6).

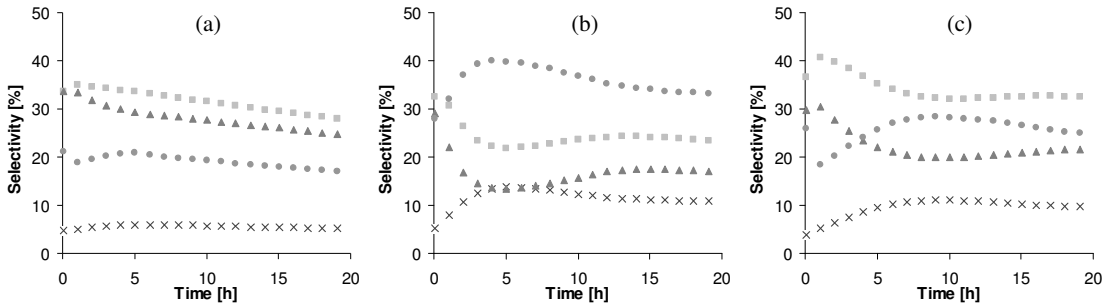

Figure 3.6: Product selectivity of 2,5-DMH/2,2,3-TMP (×), 2,2,4-TMP (●), 2,3,3-TMP (■) and 2,3,4-TMP (▲) over H-USY (a), La-USY (b) and La-X (c). Activation procedure: in situ activation in H_2 atmosphere, 4 h at 393 K and 14 h at 453 K, heating ramp = 2 K min^{-1}. Reaction conditions: reaction temperature = 348 K, isobutane/2-butene = 10, OSV = 0.2 $g_{butene}g_{catalyst}^{-1}h^{-1}$, stirring speed = 1600 rpm

The product yields of C_8 olefins and n-butane from catalytic n-butane alkylation (Fig. 3.7) showed that self-alkylation in the presence of H-USY was slow relative to the formation of unsaturated octane isomers. The absolute rates and the relative importance of self-alkylation increased drastically in the presence of La^{3+}. Note that C_8 olefins began to be formed once the level of 2-butene conversion had dropped below 99.5 %.

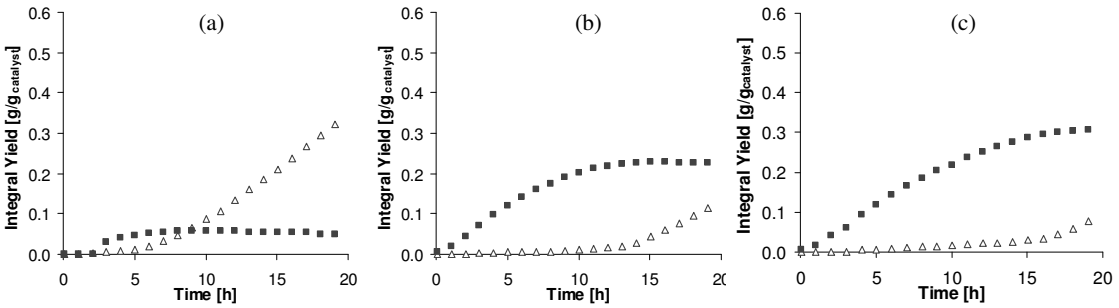

Figure 3.7: Product yield of unsaturated C_8 (Δ) and n-butane (■) as a function of TOS over H-USY (a), La-USY (b) and La-X (c). Activation procedure: in situ activation in H_2 atmosphere, 4 h at 393 K and 14 h at 453 K, heating ramp = 2 K min^{-1}. Reaction conditions: reaction temperature = 348 K, isobutane/2-butene = 10, OSV = 0.2 $g_{butene}g_{catalyst}^{-1}h^{-1}$, stirring speed = 1600 rpm

Protolytic cracking of alkanes

The rate constants, the activation energies and entropies of protolytic cracking and dehydrogenation of propane and n-pentane over modified and unmodified zeolites are compiled in Tables 3.5 and 3.6. The overall rate constant for cracking (i.e., the sum of all rate constants for the individual pathways) increased by a factor of 2 and that for dehydrogenation by a factor of 3 as the concentration of accessible La^{3+} sites in the catalysts increased. The activation energy for propane cracking on the parent ultra-stable zeolite Y was similar to that (166 kJ/mol) reported by Xu et al. for H-USY (Si/Al = 2.5) in a temperature range of 675 - 875 K and a propane partial pressure of 0.01 bar.[23] The activation energies were lower by 22-46 kJ/mol and entropies by 39-72 J/mol K for propane dehydrogenation than for cracking on all catalysts. For H-USY and La-USY (Ea_{app} = 131 kJ/mol and ΔS_{app} = -155 J/mol K), however, higher activation energy and entropies were obtained for dehydrogenation of propane compared to La-X (Ea_{app} = 104 kJ/mol and ΔS_{app} = -185 J/mol K). It should be noted on passing that La-X has a much higher fraction of isolated, non-hydroxylated La^{3+} cations (0.99 mmol/g) at SII positions in supercages, than La-USY (0.16 mmol/g), that are able to induce sufficiently strong polarization of secondary and tertiary C-H bonds.[6] The much more effective dehydrogenation is likely related to the unique capability of La^{3+} in La-X to stabilize a hydride anion, allowing therefore a better stabilization of the ionic elimination of H_2.

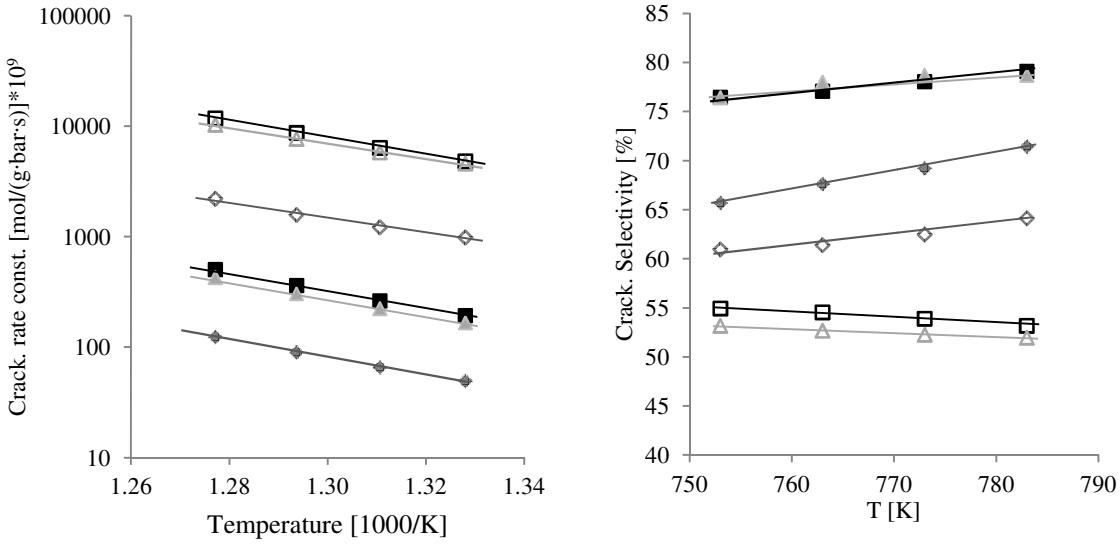

Figure 3.8: Rate constants (a) and selectivity (b) of propane (closed symbols) and n-pentane (open symbols) protolytic cracking with H-USY (■), La-USY (▲) and La-X (♦) materials. Activation: in situ in synthetic air (20 ml min^{-1}), 2 h at 803 K (2 K min^{-1}). Reaction: temperature range 753-783 K, propane (n-pentane) partial pressure of 0.03 (0.02) bar

Table 3.5: Measured rate constants (k), activation energies (Ea_{app}) and entropies (ΔS_{app}) for monomolecular propane cracking and dehydrogenation over H-USY, La-USY and La-X [a]

Catalyst	H-USY	La-USY	La-X	H-USY	La-USY	La-X	H-USY	La-USY	La-X
Pathway	k[b] [10^{-3} mol/(mol_{SBAS}·s·bar)]			Ea_{app}[c] [kJ/mol]	Ea_{app}[d] [kJ/mol]	Ea_{app}[e] [kJ/mol]	ΔS_{app}[f] [J/(mol K)]	ΔS_{app}[g] [J/(mol K)]	ΔS_{app}[h] [J/(mol K)]
$C_1 + C_2^=$	0.70	0.55	1.48	156	154	150	-111	-116	-113
$C_3^= + H_2$	0.20	0.15	0.61	131	132	104	-155	-155	-185
C/D	3.5	3.7	2.5						

[a]All the catalysts were activated in situ in synthetic air (20 ml min^{-1}) for 2 h at 803 K (2 K min^{-1}). Reactions were performed in a reaction temperature range of 753 – 783 K with 10 K intervals, propane partial pressure = 0.03 bar. Entropies were derived according to transition state theory.[24]

[b]Rate constants were determined at 773 K.

[c] ± 2 kJ/mol. [d] ± 6 kJ/mol. [e] ± 7 kJ/mol. [f] ± 4 J/(mol K). [g] ± 8 J/(mol K). [h] ± 14 J/(mol K).

The corresponding measured first order rate constants (k_{app}) at 773 K, activation energies and entropies for n-pentane conversion over the same samples are summarized in Table 3.6 and are shown in Figure 3.8. Overall, the measured rate constants for monomolecular cracking of n-pentane increased significantly (> 10 fold) compared to propane. In n-pentane two symmetric, equivalent central C-C bonds exist. Depending on the carbon being attacked by the proton, cracking at this bond can proceed via two different pathways leading to C_2 and $C_3^=$ or to C_3 and $C_2^=$. The formation of C_2 and $C_3^=$ is 4 - 11 kJ/mol favored over the formation of C_3 and $C_2^=$. For n-pentane, entropies of activation decrease from the terminal C-C bond to more inner C-C bonds. The more negative activation entropy values for the cleavage of the central bond reflect the lower configurational entropy of the more symmetric carbonium ion. For all cracking pathways, measured energies and entropies of activation decreased with increasing La^{3+} content of the zeolite, similar to the trend observed with propane. However, activation entropies stay almost unchanged with increasing La^{3+} content in the case of propane.

Table 3.6: Measured rate constants (k), activation energies (Ea_{app}) and entropies (ΔS_{app}) for monomolecular n-*pentane* cracking in terms of different pathways over H-USY, La-USY and La-X

Catalyst	H-USY	La-USY	La-X	H-USY	La-USY	La-X	H-USY	La-USY	La-X
Pathway	k^b [10^{-3} mol/(mol_{SBAS}·s·bar)]			$Ea_{app}{}^c$ [kJ/mol]	$Ea_{app}{}^d$ [kJ/mol]	$Ea_{app}{}^e$ [kJ/mol]	$\Delta S_{app}{}^f$ [J/(mol K)]	$\Delta S_{app}{}^g$ [J/(mol K)]	$\Delta S_{app}{}^h$ [J/(mol K)]
$C_1 + C_4^=$	4.4	2,0	14,9	153	147	136	-103	-113	-122
$C_2 + C_3^=$	5.3	3,7	20,0	139	134	128	-120	-128	-132
$C_3 + C_2^=$	2.5	9,4	8,5	150	142	132	-112	-125	-132
Overall cracking	12.2	15.1	43.4	147	140	131	-103	-114	-120
$C_5^= + H_2$	10.1	12.6	15.3	158	152	109	-105	-115	-169
C/D	1.2	1.2	2.8						

[a] All catalysts were activated in situ in synthetic air (20 ml min^{-1}) for 2 h at 803 K (2 K min^{-1}). Reactions were performed in a reaction temperature range of 753 – 783 K with 10 K intervals, pentane partial pressure = 0.02 bar. Entropies were derived according to transition state theory.[24]

[b]Rate constants were determined at 773 K.

[c] ± 2 kJ/mol. [d] ± 3.5 kJ/mol. [e] ± 3 kJ/mol. [f] ± 5 J/(mol K). [g] ± 3 J/(mol K). [h] ± 3 J/(mol K).

For both examined molecules, the energetic barriers for the protolytic cracking were considerably lower in the presence of isolated La^{3+} sites. For H-USY and La-USY activation energy of dehydrogenation of propane was 20 kJ/mol lower than the activation energy for total cracking, whereas, in case of n-pentane 10 kJ/mol higher activation energy was determined. For both molecules, the energy barriers for the dehydrogenation pathway were influenced in the same manner in the presence of La-X resulting in a drop of activation energy and activation entropy when compared to H-USY and La-USY.

Catalytic conversion of 2,2,4-TMP

All catalysts strongly deactivated at the beginning of 2,2,4-TMP conversion. Measured turnover rates for H-USY and La-USY under steady state conditions were similar, while that of La-X was much higher (up to factor of 6, see Table 3.7).

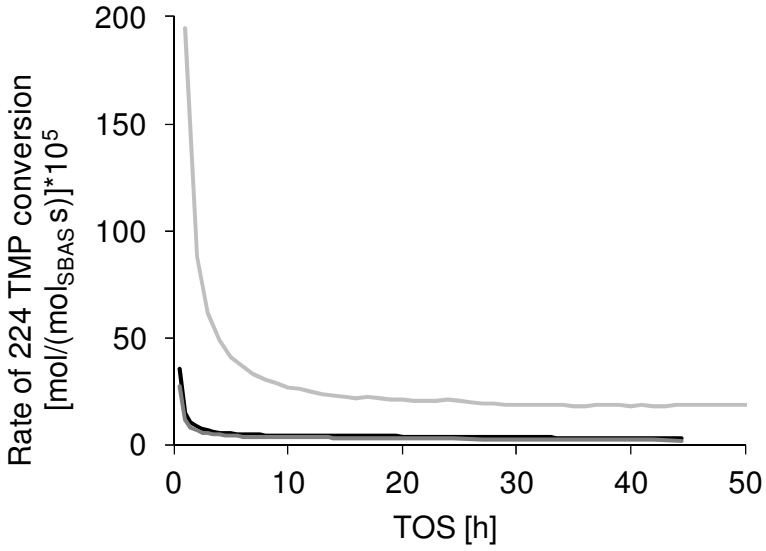

Figure 3.9: Rate of 2,2,4-TMP conversion with increasing time on stream over H-USY (black), La-USY (gray) and La-X (light gray) materials. Activation was performed in situ in H_2 flow (30 ml min^{-1}), for 4 h at 393 K and 12 h at 453 K. Reaction: 368 K, 5 mol% 2,2,4-TMP in He (9.7 ml min^{-1})

At large, the apparent activation energies increased with the concentration of La^{3+}. The presence of La^{3+} in La-USY, however, did not significantly enhance the rate constant of 2,2,4-TMP conversion (Figure 3.10 and Table 3.7). This is in good agreement with the fact that only a very small concentration of La^{3+} is accessible and it is also hydroxylated, minimizing its impact on molecules.[6,25] The dominating reaction was catalytic cracking, forming isobutane as the main product, and the selectivity to isomerization never exceeded 30 %. The selectivity towards cracking increased moderately as more La^{3+} was present in the zeolite. At 348 K, for example, 73-74 % of the converted 2,2,4-TMP was catalytically cracked on USY (H-USY= 74 %, La-USY= 73 %), while on La-X 87 % selectivity was observed.

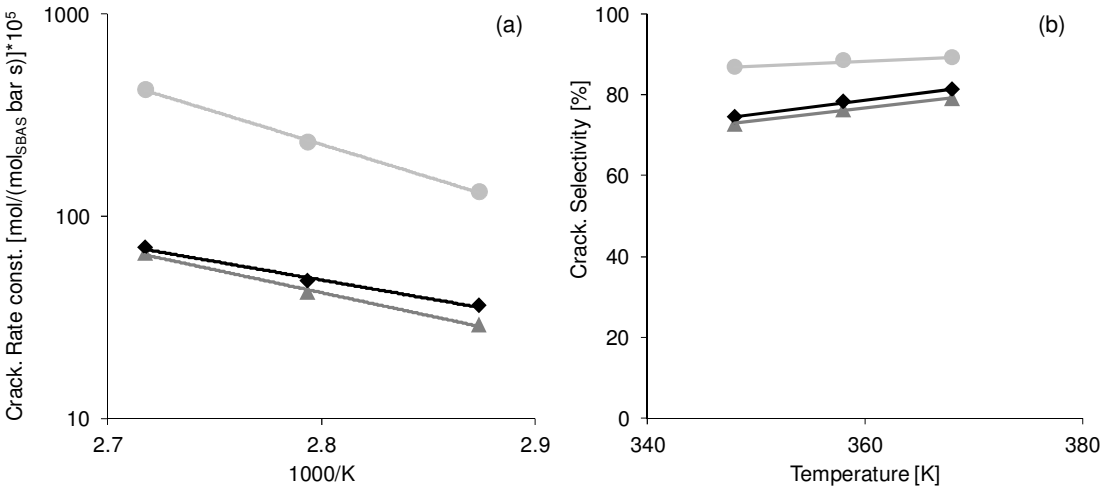

Figure 3.10: Rate constant normalized by active Brønsted acid sites (a) and cracking selectivity (b) of 2,2,4-TMP conversion at H-USY (♦), La-USY (▲) and La-X (●). Activation: in situ in H_2 atmosphere (flow rate 30 ml min^{-1}), 4 h at 393 K and 12 h at 453 K. Reaction: measurements were performed at every 10 K in a reaction temperature range of 348 to 368 K, 5 mol% 2,2,4-TMP in He atmosphere

Table 3.7: Activation energies and pre-exponential factors for cracking and isomerization of 2,2,4-TMP catalyzed by H-USY, La-USY and La-X materials[a]

Catalyst	H-USY	La-USY	La-X
$E_{A\ cracking}$ [kJ/mol]	35	43	62
$E_{A\ isomerization}$ [kJ/mol]	14	25	50
$k_{cracking}$ [10^{-5} mol/(mol$_{SBAS}$·s·bar)] at 368 K	69.8	65.3	423.0
$k_{isomerisation}$ [10^{-5} mol/(mol$_{SBAS}$·s·bar)] at 368 K	16.1	17.4	51.5
$A_{cracking}$ [mol/(g$_{catalyst}$·s·bar)]	$3.4\cdot10^{-2}$	$5.0\cdot10^{-1}$	$1.6\cdot10^{2}$
$A_{isomerization}$ [mol/(g$_{catalyst}$·s·bar)]	$7.5\cdot10^{-6}$	$3.2\cdot10^{-4}$	$3.9\cdot10^{-1}$
$A_{cracking/SBAS}$ [mol/(mol$_{SBAS}$·s·bar)]	$6.6\cdot10^{1}$	$9.0\cdot10^{2}$	$2.6\cdot10^{6}$
$A_{isomerization/SBAS}$ [mol/(mol$_{SBAS}$·s·bar)]	$1.5\cdot10^{-2}$	$5.8\cdot10^{-1}$	$6.4\cdot10^{3}$

[a] 2,2,4-TMP Cracking: the selected materials were activated in situ in H_2 atmosphere (30 ml min^{-1}), 4 h at 393 K and 12 h at 453 K. Catalytic reaction: 348 to 368 K in 10 K intervals, 5 mol% 2,2,4-TMP in He (9.7 ml min^{-1})

After 5 and 45 h on stream a lower concentration of coke was deposited on La-X (8.8 wt%) than on H-USY or La-USY (10.5 wt%). Thermogravimetric analysis indicated that H-USY was nearly fully covered with 2,2,4-TMP under the used partial pressure in line with the observed reaction order of zero. The true activation energy, which is measured under these conditions, increased for cracking and isomerization of 2,2,4-TMP with the concentration of La^{3+} (Table 3.7). The estimated reaction enthalpy for catalytic cracking of 2,2,4-TMP was 77 ± 0.1 kJ/mol at thermodynamic equilibrium.[26] The calculated reaction entropy was 168 ± 0.3 J/mol K, while the equilibrium constant was calculated to be equal to 0.75. The maximum possible conversion was, therefore, 2.4 % at 318 K and 15.9 % at 368 K. A slightly higher selectivity to isobutane was found for La-X compared to the other two catalysts.

3.4. Discussion

The role and influence of La^{3+} on the catalytic properties of faujasite type zeolites has been intensively discussed, without reaching an unequivocal conclusion in addition to the fact that the presence of La^{3+} stabilizes the zeolite lattice.[10] This lack of consensus with respect to the role of La^{3+} in catalysis is related to the fact that the investigated zeolites are highly complex and contain a wide variety of acid sites and potential catalytically active groups. In principle, this holds also true for the present study, limiting the conclusions to structure activity correlations derived from the physicochemical characterization presented here and in a preceding paper.[6] We used three materials, i.e., H-USY, La-USY and La-X, because all three have shown acceptable and stable catalytic performance for alkylation of isobutane with 2-butene, as well as for cracking of propane, n-pentane and 2,2,4-trimethylpentane. All these reactions are catalyzed by Brønsted acid sites, but depend to different extents on hydride transfer and allow in this way separating the effect of the concentration of Brønsted acid sites from indirect influences imposed by La^{3+} cations.

Let us first analyze and summarize the location and speciation of the La^{3+} cations and their potential impact on the acid base properties of the studied materials. Only for USY a direct comparison between the presence and absence of La^{3+} is possible, as the purely acidic form of zeolite X is thermally instable. On the other hand, the comparison between La-USY and La-X allows evaluating the role of different coordinations of La^{3+}, in the pore system. ^{29}Si and ^{27}Al MAS NMR show that La^{3+} exchange stabilized pairs of next nearest neighbor Al in the lattice (4.3 % Si(2Al) in H-USY and 11.4 % in La-USY), while the concentrations of isolated Al-O tetrahedra changed inversely. It is interesting to note, however, that the marked increase of Si-oxygen tetrahedra without aluminum neighbors suggests that the difference between the stability of nearest neighbor aluminum pairs and isolated aluminum must be very small. In case of a marked difference in stability, the disappearance of Si(2Al) should have been compensated by an equally large increase in the concentration of Si(1Al) (see Table 3.2).

The higher concentration of EFAl in H-USY compared to La-USY matches the lower concentration of Si(2Al). As expected, La-X has a very high concentration of Si(4Al) and Si(3Al), as well as a low concentration of EFAl. The ^{27}Al MAS NMR spectra indicate that La^{3+} causes significant distortion of the zeolite lattice at the ion-exchanged sites. Because of the much larger concentration of La^{3+}, the effect is much more visible with La-X, but clearly discernible also with La-USY. In agreement with the literature,[13,19] we assign the peak with a line width of

11.7 kHz in the ^{139}La NMR spectra to La^{3+} in the supercage. The quantification for La-X (La/Al ratio of 0.315) indicates that a quarter of the La^{3+} cations are located there. As expected, the corresponding peak for La^{3+} cations was drastically weaker for La-USY (Figure 3.4 a). The low intensity is associated with the significantly lower concentration of exchanged La^{3+}. The detailed assignment of peaks in ref[13,19] allows us to conclude that La^{3+} cations in the supercage and in the sodalite cage of La-USY mainly exist as $[La(OH)]^{2+}$ or $[La(OH)_2]^{+}$. It is interesting to note that the line width for La^{3+} cations in the sodalite cage was 87.6 kHz and is, thus, significantly smaller than reported by Hunger et al. (190 ± 10 kHz) and Herreros et al. (150 kHz),[13,19] indicating a higher mobility of these cations in the present case.

Conceptually, the exchange of La^{3+} leads on the one hand not only to a better stabilization of the zeolite framework, but also to a reduction of the concentration of Brønsted acid sites. On the other hand, La^{3+} cations result in an increase in Lewis acidity. Moreover, as visualized in Table 3.1 for USY materials, the stabilization by La^{3+} of aluminum in the lattice led to an increase of the strong Brønsted acid sites (bridging hydroxyl groups). This indicates surprisingly that not only the next nearest neighboring pairs of aluminum oxygen tetrahedra (stabilizing preferentially the exchanged La^{3+} cations), but that also isolated bridging OH groups have been stabilized by La^{3+}. It has to be emphasized that these acid sites are characterized by adsorbed pyridine, which probes only the sites accessible in the supercages.

The increase of the concentration of Brønsted acid sites and the decrease of the concentration of Lewis acid sites suggests that La^{3+} is located primarily in the sodalite cages in the form of $[La(OH)]^{2+}$ and that this stabilization also creates strong Brønsted acid sites in the supercages. The mechanism and reason for the stabilization of the aluminum-oxygen tetrahedra across such a long distance is not understood at this point, but a more in-depth analysis is beyond the scope of this contribution. The strong Lewis acid sites observed with H-USY and La-USY are caused solely by coordinatively unsaturated Al^{3+} cations. La^{3+} cations being much larger than Al^{3+} cations bind pyridine only very weakly, irrespective of the hydroxyl groups attached to them.

The larger concentration of La^{3+} exchanged and especially the higher ratio of La/Al led to a very small concentration of Brønsted acid sites in La-X. However, estimating it from the overall concentration of aluminum and the concentration of octahedral aluminum in the zeolite, the relative distribution between the accessible and inaccessible strong Lewis acid sites remained about the same for La-X and La-USY. We had shown in a preceding paper[6] that the higher

concentrations of La^{3+} lead to repulsion between the cations in the sodalite cages, causing about 25 % of the La^{3+} cations to be located at the SII sites in the supercage. The higher concentration of negative charge of the lattice oxygen allows the stabilization at such positions.

Having established the location and nature of the Brønsted and Lewis acid sites, as well as of the La^{3+} cations, let us turn to discussing the catalytic chemistry of the Brønsted acid catalyzed reactions. It should be mentioned at this point that it has been well established by preceding contributions that accessible La^{3+} cations are able to polarize C-H bonds strongly[6] and that they are even able to generate reactive carbenium ions with alkanes having two adjacent tertiary or quaternary carbon atoms. Two of the investigated reactions, *i.e.*, the alkylation of isobutane with 2-butene and the conversion of 2,2,4-trimethylpentane imply such alkanes, while in the cracking of propane only primary and secondary carbon atoms are involved.

Starting with the protolytic cracking of propane, one notes that on first sight the catalytic activity sympathetically increases with the concentration of Brønsted acid sites for all three zeolites investigated. Normalization of the rates to the strong Brønsted acid sites (SBAS) showed, however, an increase in the propane cracking rate by factor of two and slightly more than a factor of three for the propane dehydrogenation rate with increasing concentration of La^{3+} (Table 3.1, 3.5). The fact that protolytic dehydrogenation of propane is more favored than protolytic cracking by isolated La^{3+} cations close to SBAS, as it is the case in La-X, clearly indicates the unique ability of those sites to polarize C–H bonds facilitating at the same time the addition of a proton to the negatively charged secondary hydrogen in the activated alkane molecule. This is reflected also in the significantly decreased activation energies for dehydrogenation over La-X (104 kJ/mol) compared to the other two materials (130 kJ/mol).

The fact that the catalyst with the highest activity has the lowest concentration of extra-lattice alumina leads us to conclude that only the specific polarization of the C-H bond induced by fully accessible La^{3+} (which is much stronger than that induced by Al^{3+}) is able to significantly influence protonation of alkanes via C-H bond polarization. This agrees well with the fact that the concentration of octahedrally coordinated, Lewis acidic extra-framework aluminum sites do not influence the rate of protolytic cracking.[27] In comparison, the polarization of La^{3+} on the C–C bond was less marked, as evidenced from the slight decrease in activation energies and entropies on La-X compared to USY catalysts. Therefore, kinetic differences between cracking and dehydrogenation mainly reflect entropic effects of the transition state confinement. As

the measured activation entropies were lower on all catalysts by 39 – 72 J/(mol K) for the protolytic dehydrogenation of propane than for cracking, a more tightly bound transition state is indicated in presence of La^{3+}.

Principally, the protolytic cracking of n-pentane can take place on different pathways. These different pathways will be analyzed carefully in the successive section. For all investigated catalysts, cleavage of the terminal bond (leading to C_1 and $C_4^=$) is energetically more demanding than the cleavage of internal C-C bonds. Depending on the carbon atom protonated the latter route results either in C_2 and $C_3^=$ or in C_3 and $C_2^=$. The pathway resulting in C_2 and $C_3^=$ is 11 kJ/mol energetically more favored over the alternative pathway on H-USY. If the transition state of cracking was early, resembling the reactants, an energetic difference between those two alternative pathways could not be explained. Therefore, we conclude that the transition state is late and resembles the products. The formation of the energetically more stable larger alkenes is consequently favored. However, the differences in the activation energies are consequentially decreased with increasing content of accessible La^{3+} sites in the zeolitic structure reflecting a better stabilization of the activated transition state species. The higher activation entropy for cracking at the terminal C-C bond shows a higher degree of rotational and vibrational freedom of this transition state compared to cracking at internal C-C bonds. For all catalysts, measured activation entropies at the central C-C bond were comparable for both pathways indicating the similarity between the two transition state structures.

When comparing the activation energies between the three different catalysts, one needs to consider enthalpic and entropic differences between the two adsorbed molecules. For n-pentane, the heat of adsorption increases by 10 kJ/mol when going from H-USY (46 kJ/mol) to La-X (56 kJ/mol).[4,28] The apparent activation energy for cracking drops by 16 kJ/mol and by 49 kJ/mol for dehydrogenation. This indicates a decrease in the intrinsic energetic barriers (not a solely adsorption effect) due to the polarization effect of isolated La^{3+} present in La-USY and in La-X. Entropies of adsorption decrease by 17 J/mol K when going from H-USY (-88 J/mol K) to La-X (-105 J/mol K).[4,28] Consequently, true activation entropies are comparable for H-USY and La-X for the cracking pathways. The difference in measured activation entropies seems, therefore, to reflect only the entropic difference between the gas phase and the adsorbed

state. A more accentuated decrease of the true activation entropy was observed for the dehydrogenation pathway. Interaction of isolated La-X with C-H restricts strongly the vibrational and rotational freedom of n-pentane and lowers the enthalpic barrier.

The enhancement of specific catalytic rates was even more pronounced with larger molecules. With La-USY, the La^{3+} cations hardly influenced the catalytic cracking of 2,2,4-TMP compared to USY. This is consistent with the data from IR spectroscopy of adsorbed pyridine and ^{139}La NMR spectroscopy. The predominant stabilization of La^{3+} in the form of monomeric $[La(OH)_n]^{3-n}$ species limits the interaction of hydrocarbons with the cation. Only the accessible lanthanum cations in La-X are able to significantly polarize the branched hydrocarbons and increase so the rate of 2,2,4-TMP dehydrogenation. Isobutane is the major product formed under these reaction conditions indicating the cracking of 2,2,4-TMP in β-position producing isobutene, which must be followed by hydride transfer to generate the alkane. Thus, the initial activation produces two carbenium ions (see the mechanism in Figure 3.11 adapted from ref.[29]). The true activation energy of 2,2,4-TMP cracking increased in the presence of La^{3+} from 35 via 43 to 62 kJ/mol (Table 3.7). Because the absolute values and their increase is similar to the heat of adsorption of isobutane on the respective zeolites[4] it is suggested that a step closely associated to the desorption of the products is rate determining. Note that also the pre-exponential factor increased when normalized to the concentration of protons, exhibiting that more entropy is generated in the release of the product, a similar compensating behavior as found in the thermodynamic data of adsorption.

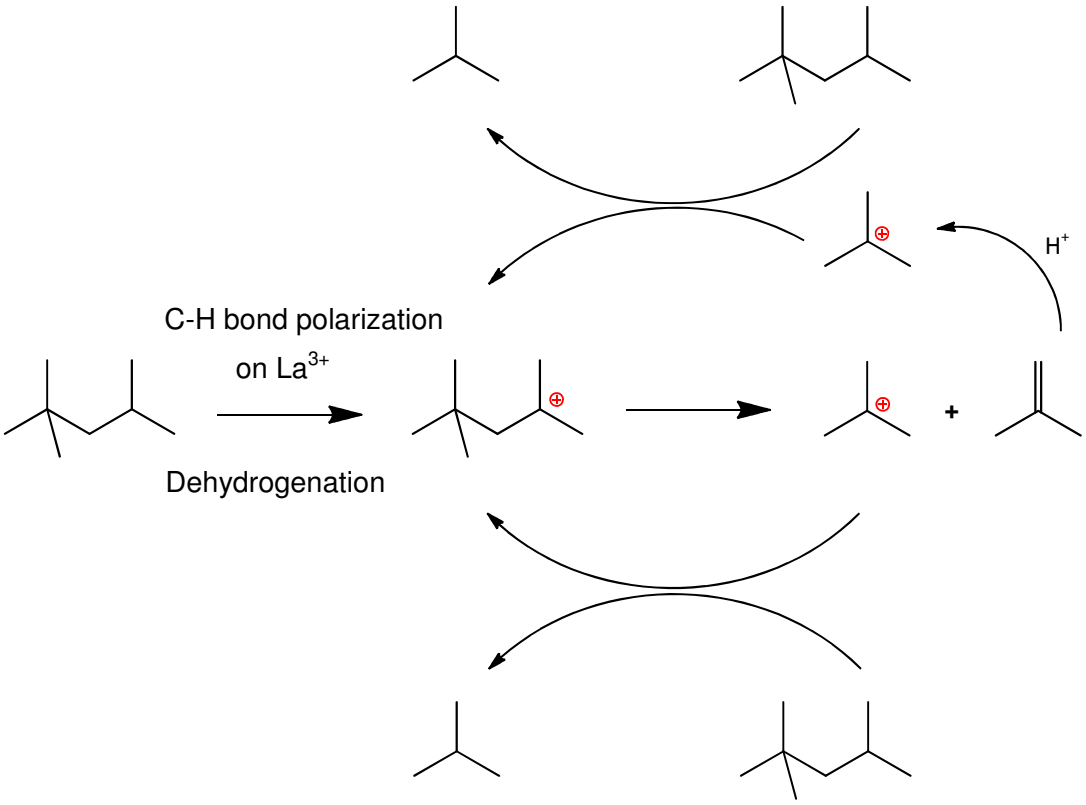

Figure 3.11: Proposed reaction mechanism for the catalytic cracking of in-situ formed iso-octanes in the presence of accessible La^{3+} cations incorporated inside the supercages of zeolitic materials

For alkylation La^{3+} acts via enhancing hydride transfer. The overall alkylation of isobutane with 2-butene utilizes the unique hydride transfer capabilities of La^{3+}. At steady-state the reaction is controlled by two steps, the addition of 2-butene and the hydride transfer from isobutane to the surface bound alkyl. As the former reaction is much easier, all alkylation catalysts tend to build up over time a hydrocarbon deposit that eventually deactivates the zeolite. For a given space velocity of olefins, the higher the concentration of Brønsted acid sites is, the lower the tendency of this reaction will be. The presence of La^{3+} enhances the selectivity to the second reaction by polarizing the hydride donating isobutane. Especially with La-X the enhanced cracking rates of highly branched alkanes would further stabilize the catalyst by breaking down surface bound hydrocarbons during reaction. In consequence, the productivity of La-X was about four times as high as that of H-USY.

3.5. Conclusions

H-USY, La-USY and La-X materials with comparable pore structure but different Si/Al ratios and La^{3+} concentrations were used to study the impact of accessible lanthanum cations for Brønsted acid site catalyzed reactions. Overall, accessible La^{3+} cations strongly polarize C-H bonds in alkanes and stabilize hydrides as well as hydride transfer. The impact of the La^{3+} cations depends on their coordination, *i.e.*, the more accessible the cation is (the less hydroxylated) the stronger its impact on catalysis becomes.

With respect to protolytic cracking of propane and n-pentane, the main role of non-hydroxylated La^{3+} cations present in La-X is to facilitate the polarization of C–H bonds, thus, resulting in enhanced dehydrogenation. This is supported by the unusually low energy of activation for dehydrogenation catalyzed by La-X. These variations in the energy of activation are related to the stronger polarization of the secondary C–H bond, with commensurate increase in the confinement of the transition states indicated by the greater entropy loss for alkane dehydrogenation on La-X.

Cracking of 2,2,4-trimethylpentane showed that the polarization of the tertiary C-H bond and the subsequent dehydrogenation may be an important, but not the decisive step for maintaining cracking activity at such low temperatures. Increasing concentrations of La^{3+} led to higher rates. The very low values of activation energies observed suggest that the rate determining step is not associated with the cleavage of the C-C bond, but rather with the hydride transfer of the primarily formed alkenes or the associated desorption.[30,31] Note in that context that the observed energies of activation are close to the heats of adsorption of isobutane in La-X.[4,6] The increase in the true energy of activation for the overall process is, thus, attributed to the stronger interaction of the products with the catalyst.

Finally, the drastic improvement of the catalytic properties for isobutane alkylation with 2-butene is clearly related with the drastically improved hydride transfer ability and in part cracking induced by the presence of La^{3+}. This led to drastically increased productivity before deactivation through a longer lifetime. Improved cracking and hydride transfer controlled the accretion of oligomers that eventually deactivate the catalyst by encapsulation. It is unclear at present, whether the superior hydride transfer abilities are related to a greater polarization of the C-H bonds and hence a more active hydride transfer or whether the transition state itself is stabilized in a unique way.

The present study shows clearly that accessible polarizable cations such as La^{3+} are able to generate a unique environment for hydrocarbon reactions. The fact that only La-X showed such drastically enhanced catalytic properties emphasizes the importance of the coordination of La^{3+} in such an environment and guides the development for new generations of highly active catalysts.

3.6. Acknowledgements

The authors thank Prof. Cornelia Breitkopf for fruitful discussions in the network of IDECAT. Support of Dr. Gerhard Althoff-Ospelt with respect to the ^{139}La NMR measurements is gratefully acknowledged.

3.7. References

(1) Guzman, A.; Zuazo, I.; Feller, A.; Olindo, R.; Sievers, C.; Lercher, J. A. *Micropor. Mesopor. Mater.* **2005**, *83*, 309.

(2) Venuto, P. B.; Hamilton, L. A.; Landis, P. S. *J. Catal.* **1966**, *5*, 484.

(3) Bolton, A. P. *J. Catal.* **1971**, *22*, 9.

(4) Sievers, C.; Onda, A.; Olindo, R.; Lercher, J. A. *J. Phys. Chem. C* **2007**, *111*, 5454.

(5) Feller, A.; Guzman, A.; Zuazo, I.; Lercher, J. A. *J. Catal.* **2004**, *224*, 80.

(6) Schüßler, F.; Pidko, E. A.; Kolvenbach, R.; Sievers, C.; Hensen, E. J. M.; van Santen, R. A.; Lercher, J. A. *J. Phys. Chem. C* **2011**, *115*, 21763.

(7) Sievers, C.; Zuazo, I.; Guzman, A.; Olindo, R.; Syska, H.; Lercher, J. A. *J. Catal.* **2007**, *246*, 315.

(8) Flego, C.; Kiricsi, I.; Parker, J., W. O.; Clerici, M. G. *Appl. Catal. A-Gen.* **1995**, *124*, 107.

(9) Diaz-Mendoza, F. A.; Pernett-Bolano, L.; Cardona-Martínez, N. *Thermochim. Acta* **1998**, *312*, 47.

(10) Sievers, C.; Liebert, J. S.; Stratmann, M. M.; Olindo, R.; Lercher, J. A. *Appl. Catal. A-Gen.* **2008**, *336*, 89.

(11) Kunwar, A. C.; Turner, G. L.; Oldfield, E. *J. Magn. Reson.* **1986**, *69*, 124.

(12) Weihe, M.; Hunger, M.; Breuninger, M.; Karge, H. G.; Weitkamp, J. *J. Catal.* **2001**, *198*, 256.

(13) Herreros, B.; Man, P. P.; Manoli, J. M.; Fraissard, J. *J. Chem. Soc.-Chem. Commun.* **1992**, 464.

(14) ASTM. Standard Test Method for Determination of the Unit Cell Dimension of a Faujasite-Type Zeolite. In *Annual Book of ASTM Standards*, 1985; Vol. D3942-85.

(15) Feller, A.; Barth, J.-O.; Guzman, A.; Zuazo, I.; Lercher, J. A. *J. Catal.* **2003**, *220*, 192.

(16) Fichtner-Schmittler, H.; Lohse, U.; Miessner, H.; Maneck, H.-E. *Z. Phys. Chem.* **1990**, *271*, 69.

(17) Klein, H.; Fuess, H.; Hunger, M. *J. Chem. Soc. Faraday Trans.* **1995**, *91*, 1813.

(18) Gaare, K.; Akporiaye, D. *J. Phys. Chem. B* **1997**, *101*, 48.

(19) Hunger, M.; Engelhardt, G.; Weitkamp, J. *Micropor. Mater.* **1995**, *3*, 497.

(20) de Jong, K. P.; Mesters, C. M. A. M.; Peferoen, D. G. R.; van Brugge, P. T. M.; de Groot, C. *Chem. Eng. Sci.* **1996**, *51*, 2053.

(21) Simpson, M. F.; Wei, J.; Sundaresan, S. *Ind. Eng. Chem. Res.* **1996**, *35*, 3861.

(22) Feller, A.; Lercher, J. A. *Adv. Catal.* **2004**, *48*, 229.

(23) Xu, B.; Bordiga, S.; Prins, R.; van Bokhoven, J. A. *Appl. Catal. A-Gen.* **2007**, *333*, 245.

(24) Gounder, R.; Iglesia, E. *J. Am. Chem. Soc.* **2009**, *131*, 1958.

(25) Pidko, E. A.; van Santen, R. A.; Hensen, E. J. M. *Phys. Chem. Chem. Phys.* **2009**, *11*, 2893.

(26) Wang, P.; Wang, D.; Xu, C.; Gao, J. *Appl. Catal. A-Gen.* **2007**, *332*, 22.

(27) Narbeshuber, T. F.; Brait, A.; Seshan, K.; Lercher, J. A. *Appl. Catal. A-Gen.* **1996**, *146*, 119.

(28) Eder, F.; Stockenhuber, M.; Lercher, J. A. *J. Phys. Chem. B* **1997**, *101*, 5414.

(29) Sievers, C.; Onda, A.; Guzman, A.; Otillinger, K. S.; Olindo, R.; Lercher, J. A. *J. Phys. Chem. C* **2007**, *111*, 210.

(30) Blaszkowski, S. R.; Nascimento, M. A. C.; van Santen, R. A. *J. Phys. Chem.* **1996**, *100*, 3463.

(31) Corma, A. *J. Catal.* **2003**, *216*, 298.

Chapter 4

Mechanistic studies on the hydro-isomerization of n-pentane over lanthanum and platinum ion exchanged faujasites and platinum promoted sulfated zirconium oxide

The catalytic performance for the hydroisomerization of n-pentane on a set of lanthanum and platinum containing catalysts was studied at 5 – 25 bar and temperatures of 483 – 533 K. The promotion effect of lanthanum and platinum, when ultra-stable zeolite Y serves as a support, is demonstrated. For comparison platinum promoted sulfated zirconium oxide was prepared by impregnation. The catalytic reaction results showed a considerable improvement of the initial conversion activity of n-pentane when lanthanum containing bimetallic catalysts were used. Sulfated zirconium oxide promoted by platinum exhibit the highest catalytic activity and selectivity for the acid catalyzed hydroisomerization of n-pentane. Through the analysis of the product distribution, the hydroisomerization mechanism on the synthesized model catalysts is proposed. By analyzing the measured kinetic data it was possible to determine the activation energy of the elementary isomerization step and the corresponding pre-exponential factors. The activation over non-modified ultra-stable zeolite Y proceeds via hydride abstraction forming alkoxy groups, which consequently isomerize. Lanthanum exchanged solid acid catalysts favor the C-H bond polarization which may be regarded as intermediate to hydride abstraction. Platinum containing catalysts favor the isomer formation according to a bifunctional mechanism. In the presence of mixed lanthanum and platinum containing USY both mechanistic pathways are accounting for the isomer formation.

4.1. Introduction

Because iso-pentane and branched paraffins are valuable high-octane components for high performance fuels, which are produced via hydroisomerization of n-alkanes over solid acid catalyst, the design of effective catalysts is an important goal of research. The hydroconversion activities and selectivities of isomerization of n-paraffins over solid acid catalysts have been extensively studied in the past decades in an attempt to correlate the structural properties with the activity in the hydroisomerization process.[1,2] Extensive work has been devoted to the preparation and characterization of solid acid catalysts for the hydroisomerization of saturated hydrocarbons.[2,3] Hydroisomerization catalysts are dual functional catalysts containing a metal dispersed on a solid acid and can combine the high catalytic activity of transition metals with the shape selective constrains unique to zeolite structures. The catalytic activation of alkanes proceeds via hydride transfer from the initial n-alkanes with the formation of adsorbed branched carbenium ions. In principle, there are two main mechanistic pathways postulated for the isomer formation involving the intramolecular (monomolecular) and intermolecular (bimolecular) rearrangement. The intramolecular mechanism involves the classical rearrangement of a secondary butyl carbenium ion to tert-butyl carbenium ion over a protonated cyclopropane intermediate.[4] The intermolecular mechanism, as observed for n-butane isomerization in the presence of sulfated zirconia, in the first step involves alkane dehydrogenation followed by the formation of a C_8 intermediate and the subsequent β-elimination of the product.[5]

To achieve high activities and selectivities the promotion with a noble metal is essential. Platinum containing zeolitic materials favors the isomer formation according to a bifunctional mechanism (dehydrogenation/hydrogenation on platinum sites and isomerization on Brønsted acid site).[6,7] Many studies concerning detailed kinetic and mechanistic investigations revealed, that the rate-determining step is the skeletal rearrangement of carbenium ions on the acidic sites.[3,8] The concentrations of the catalytic functions have a strong impact on the catalytic reaction.[2,9] At low concentration of accessible noble metals, the formation of olefins is affected. With increasing the metal concentration to a certain level, dehydrogenation over the metal site is sufficiently fast so that the isomerization on Brønsted acid sites becomes rate limiting.[10] The addition of Pt to a sulfated ZrO_2 has been shown to enhance the hydride transfer and to increase the stability of the catalyst for the isomerization of butane and n-pentane at low temperature.[11,12] In previous published scientific reports based on various

experimental and theoretical studies, different mechanistic pathways for the alkane activation were proposed. Matsuhashi et al. reported three possible alkane activation modes over solid superacids.[13] According to Matsuhashi, the generation of carbenium ions can either occur via hydride abstraction over Lewis acid sites, proton addition over Brønsted acid sites with subsequent hydrogen elimination or via olefin protonation formed over metal sites.[13]

Given that the isomerization and hydride transfer are the main steps in alkylation reactions, it is necessary to get more detailed information about the ability of different catalysts to perform hydride transfer reaction. With this purpose, the catalytic activation ability of various lanthanum and platinum containing faujasite materials as well as Pt-SZ was studied in the hydroisomerization of n-pentane at 523 K and a pressure range of 5 to 25 bar. A detailed analysis of kinetic and mechanistic data along with catalytic performance studies of the selected materials enabled a better understanding of the hydride transfer step and their impact on the overall reaction mechanism. To describe the catalyst deactivation during hydroisomerization of n-alkanes, acid site properties before and after isomerization as well as coke deposition were analyzed.

4.2. Experimental

4.2.1. Materials

4.2.1.1. Catalyst preparation

The lanthanum, platinum and mixed lanthanum and platinum containing model catalysts were prepared from ultra-stable zeolite Y (H-USY, Grace Davison) with a Si/Al ratio of 3.1. Monometallic La-USY samples were obtained by treatment of H-USY with 0.5 M $La(NO_3)_3$ (solution to zeolite ratio of 7 mL/g) at 373 K for 4 h. After washing and drying at 373 K for 6 h, the resulting material was carefully calcined at 773 K (heating rate 10 K min^{-1}) in synthetic air (flow rate 200 ml min^{-1}) for 4 h. To replace the remaining sodium cations in the synthesized La-USY I material, an additional ammonium ion-exchange in a 5 M $NH_4(NO_3)$ solution was performed at 373 K for 4 h. In the final step, the material was extensively washed, dried and calcined. For the incorporation of higher La^{3+} in the ultra-stable zeolite Y the procedure of lanthanum ion-exchange was repeated for three times. This sample is denoted as La-USY II.

Monometallic Pt-USY and Pt-USY II was prepared by dropwise addition of the appropriate amount of $Pt(NH_3)_4(OH)_2$ and NH_4OH to a warm solution of H-USY under vigorous stirring (500

rpm) at 313 K. The impregnated sample was filtrated, washed and dried at 373 K for 20 h priory to calcination in synthetic air at 773 K (heating rate 10 K min^{-1}) for 4 h.

For the preparation of bimetallic La-Pt-USY samples, the proton form of the parent material was firstly ion-exchanged with $La(NO_3)_3$ and then with $Pt(NH_3)_4(OH)_2$ following the same procedures as described. Finally, all the synthesized materials were rehydrated at 343 K.

4.2.1.2. Platinum promoted Sulfated Zirconium Oxide (Pt-ZS)

A sulfur-doped zirconium hydroxide sample (XZO1249/01) provided by Magnesium Electron Inc. was calcined in synthetic air at 873 K for 3 h (heating rate of 10 K min^{-1}).[14] Following calcination, 13 g of the sulfated zirconium oxide was impregnated with 30 ml $Pt(NH_3)_4(NO_3)_2$ (2110 mg/L) solution and stirred for 4 h. After the impregnation and water removal, the sample was dried at 383 K overnight and calcined in synthetic air at 873 K for 3 h (heating rate of 10 K min^{-1}).

4.2.2. Physicochemical characterization

The concentration of sodium, aluminum and silicon were determined by atomic absorption spectroscopy using a Solaar M5 Dual Flammen-Graphitrohr AAS from ThermoFisher. The concentration of incorporated lanthanum was determined by ICP-OES using a FTMOA81A Spectrometer from Spectro-Analytica Instruments. CHNS analysis of the samples was performed on elemental analysis instrument *Vario EL* from *Elementar Analysesysteme GmbH*.

The crystallinity of the materials was analyzed by powder X-ray diffraction (XRD) patterns using a Philips X'pert diffractometer having a X'celerator module with CuKα radiation. Measurements were performed from 5 to 75° 2Θ with a step size of 0.033°. The dimensions of the unit cell was calculated from the X-ray diffraction patterns of the zeolite material mixed with 5 % of silicon using the silicon reflections as reference.[15] Therefore, the standard test method of the American Society for Testing and Materials was applied.

The apparent surface area was estimated by applying the Brunauer–Emmett–Teller (BET) theory[16] to the adsorption isotherms over a relative pressure range from 0.01 to 0.09. The micropore volumes were obtained by the t-plot method according to Halsey.[17] Because of the limitations of the PMI instrument, the isotherms were measured at relative partial pressures higher than 10^{-5} p/p^0.

^{27}Al MAS NMR measurements were performed on a Brucker AV500 spectrometer (B_0 = 11.7 T) and a spinning rate of 12 kHz. All the samples were fully hydrated before packing into a 4 mm ZrO_2 rotor. For ^{27}Al MAS NMR measurements 2400 scans were recorded for the single pulse experiment using a recycle time of 0.25 s. An excitation pulse with a length of 0.46 µs corresponding to a π/12-pulse was applied. All the recorded spectra are reported relative to an external standard of solid $Al(NO_3)_3$ (δ = -0.5427 ppm).

The concentration of different acid sites was analyzed by infrared spectroscopy of adsorbed pyridine. Infrared spectra of adsorbed pyridine were measured using a *Thermo Nicolet 5700* spectrometer. All the samples were pressed into self-supporting wafers and activated in vacuum (10^{-6} mbar) at 723 K for 1 h with a heating rate of 10 K min^{-1}. Pyridine was adsorbed at 423 K at a pressure of 0.1 mbar until no changes were observed in the spectrum. To remove all of the physisorbed pyridine, the system was outgassed for 1 h at 423 K. The density of strong acid sites was examined by increasing the temperature to 723 K for 0.5 h. The concentration of Brønsted and Lewis acid sites was determined based on the integrals of the IR bands at 1540 cm^{-1} and 1450 cm^{-1}. For quantification, the molar extinction coefficient of 0.73 for Brønsted acid sites and 0.96 for Lewis acid sites were used, respectively. These were determined for a standard material using combination of microgravimetric measurements of the thermal stability of pyridine and infrared spectroscopy of adsorbed pyridine.

4.2.3. Catalytic reactions

The catalytic n-pentane hydroisomerization was performed in a fixed bed stainless steel tubular reactor (inner diameter 8 mm; length 300 mm, shown in Fig. 4.1). The catalyst bed was prepared as follows: a mixture of catalyst (100 mg; 150-250 µm) and silicon carbide (1.90 g; 350-500 µm) was occluded on the top and on the bottom with 1.0 g pure silicon carbide and fixed with quartz wool inside the reactor. N-pentane was tempered in two consecutive saturation flasks while a third empty flask was used as a droplet precipitator. The partial pressure of n-pentane was adjusted at respective temperatures according to vapor pressure calculations using Antoine parameters and the Clausius-Clapeyron equation. Lines downstream the saturators were isolated and tempered independently from the reactor in order to prevent n-pentane condensation. The product distribution was analyzed online by a HP 6890 gas chromatograph (GC) with a HP-PLOT/Al_2O_3 (50 m × 0.32 mm × 8 µm) capillary column connected to a flame ionization detector (FID).

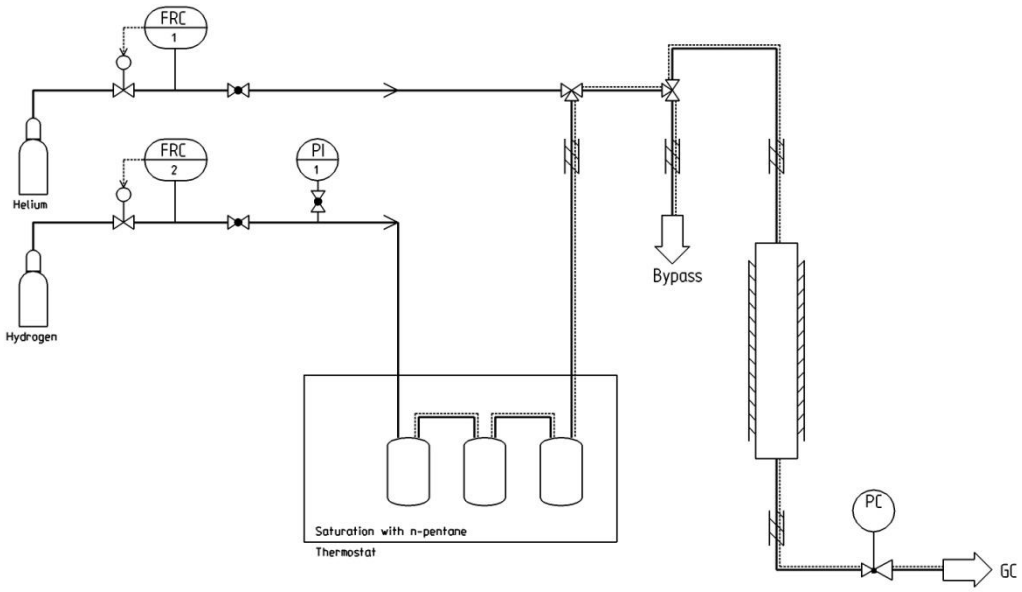

Figure 4.1: General configuration of the hydroisomerization set-up

All the lanthanum containing materials were thermally activated at 673 K (10 K min^{-1}) under helium flow (30 ml min^{-1}) at atmospheric pressure for 1 h and then cooled at the reaction temperature. Platinum containing samples were reduced *in situ* at 573 K (10 K min^{-1}) under hydrogen atmosphere (50 ml min^{-1}) for 4 h priory to use. After the reactants were cooled at the reaction temperature, the mixture was passed through the catalyst bed with a total flow of 50 ml min^{-1}.

The catalyst stability was tested under operating conditions (50 ml min^{-1} continuous hydrogen flow, 450 mbar partial pressure of n-pentane and 10 bar total pressure) at 523 K for 20 h.

For the kinetic experiments, the catalytic activity was determined under the experimental conditions described. The reaction order with respect to hydrogen was estimated at a total pressure range from 5-25 bar. Activation energies were determined from 483 K to 533 K.

4.3. Results

4.3.1. Chemical composition and physicochemical properties

The chemical composition and the physicochemical properties of the studied materials are compiled in Table 4.1.

Table 4.1: Physicochemical properties of the used catalysts

	H-USY	La-USY I	La-USY II	Pt-USY I	Pt-USY II	LaPt-USY I	LaPt-USY II	Pt-SZ
Si [mmol/g]	10.50	10.45	7.97	9.48	8.30	9.52	12.12	-
Al [mmol/g]	3.38	2.61	2.62	3.35	3.15	3.29	2.05	-
Na [mmol/g]	0.18	0.04	0.05	0.19	0.14	0.13	0.05	-
La [mmol/g]	-	0.19	0.47	-	-	0.02	0.10	-
Pt [mmol/g]	-	-	-	0.10	0.32	0.01	0.01	0.02
Si/Al	3.11	4.00	3.04	2.83	2.63	2.89	5.91	-
Na/Al	0.05	0.02	0.02	0.06	0.04	0.04	0.02	-
La/Al	-	0.07	0.18	-	-	0.01	0.05	-
S_{BET} [m^2/g]	759	712	740	721	713	750	641	188
$V_{Micropore}$ [cm^3/g]	0.28	0.26	0.26	0.26	0.26	0.27	0.23	0.07
Unit cell [nm]	2.46	2.45	2.45	2.45	2.45	2.45	2.43	-

Extended lanthanum and platinum incorporation was accompanied by a considerable decrease in the total aluminum and silicon content. While following La^{3+} ion-exchange almost in all the cases the maximum exchange degree in the zeolite is reached, in LaPt-USY I and II only a very low amount of platinum (0.01 mmol/g) was incorporated. According to the synthesis procedure, Na^+ cations present as charge compensating species are mainly replaced by La^{3+} and Pt^{2+} cations. The remaining Na^+ located in less accessible parts of the zeolite (hexagonal prisms and six-membered ring openings) cannot completely be removed since these places are inaccessible for most of the molecules.

Sulfated zirconium oxide has different surface species (SO_3, H_2SO_4, HSO_4^-, SO_4^{2-}) depending on the dehydration state of the sample.[18-20]

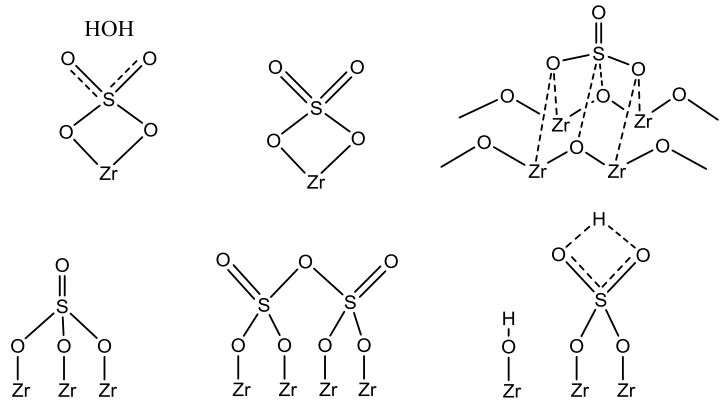

Figure 4.2: Proposed structures for sulfated zirconia from Ref. [18-20]

In the stepwise preparation of Pt-ZS consisting in the impregnation of sulfated zirconium oxide with $Pt(NH_3)_4(NO_3)_2$ solution followed by calcination step lead to the insertion of 0.02 mM Pt^{2+} per gram ZrO_2-SO_4 and the formation of a highly active and stable Pt-ZS with a complex structure (see Figure 4.2). The microporous Pt-SZ sample prepared has a 30 % higher BET specific surface area (188 m^2/g) compared to the Pt-SZ materials reported (133 m^2/g published by Comelli,[21] 114 m^2/g reported by K. Ebitani[22] and 98 m^2/g by Grau[23]).

Considering the parent USY material with a BET specific surface area of 759 m^2/g and micropore volume of 0.28 cm^3/g, the incorporation of metal cations led in all the cases to a gradually decrease in micropore volume, while the BET specific surface area was only slightly modified. This is in good agreement with the XRD analysis, which indicated no significant changes in the crystallinity patterns and in the unit cell size of the zeolitic materials over modification. The small decrease in unit cell size and micropore volumes for lanthanum exchanged samples is related with structural contortions implicated with the incorporation of polyvalent cations.[24]

^{27}Al MAS NMR measurements were performed for all faujasite materials in order to obtain more detailed structural information on the local environment of aluminum atoms in the faujasite type zeolites. The spectra, which are a time average of 2400 scans recorded with a 0.46 µs pulse and corrected for probe background signal, are shown in Figure 4.3.

The total concentration and coordination of aluminum species are shown in Table 4.2. ^{27}Al MAS NMR spectra of all the studied materials mainly consist of two main peaks one around 0 ppm corresponding to octahedrally coordinated extra-framework aluminum and one about 40-60 ppm typical of tetrahedrally coordinated framework aluminum atoms. AlO_4^- content in the selected materials is influenced by various La^{3+} cationic species present in ion-exchanged materials. The decrease of peak area integral at 0 ppm and the subsequent increase of the peak area integral at 60 ppm, as shown in spectra (a), (b) and (c), suggests an important decrease of extra-framework aluminum and an increase in the tetrahedrally coordinated framework aluminum content with increasing lanthanum concentration. The peak corresponding to octahedral aluminum in the spectrum of La-USY is sharp and almost symmetric. In previous publications similar peaks have been assigned to aluminum cations with a higher flexibility.[25] We assume that these species are present as charge compensating Al cations in the zeolite pores.

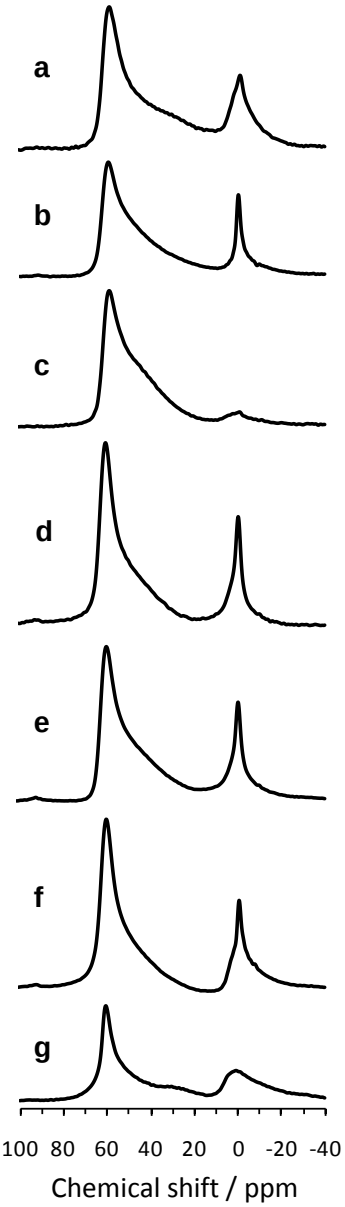

The broad peak at 0 ppm in the ^{27}Al MAS NMR spectra of H-USY originates from separate extra-framework aluminum phase located outside the zeolite pores.[24] A more accurate comparison of the peak corresponding to tetrahedral aluminum showed the presence of a shoulder at 50 ppm that became more significant with increasing lanthanum concentration.

The increasing peak intensity corresponding to the tetrahedral aluminum species (50 ppm) with increasing lanthanum concentration in La-USY I and La-USY II materials evidenced a more pronounced effect on the local environment of the framework aluminum species.

Figure 4.3: ^{27}Al MAS NMR spectra of a) H-USY, b) La-USY I, c) La-USY II, d) Pt-USY I, e) Pt-USY II, f) LaPt-USY I, g) LaPt-USY II

Despite the extended platinum ion-exchange, the framework and extra-framework aluminum was only marginally affected. Recorded ^{27}Al MAS NMR spectra for the Pt-USY I and Pt-USY II showed that platinum incorporation caused a less pronounced broadening of the peak assigned to AlO_4^- species compared to lanthanum ion-exchange. Bimetallic LaPt-USY I have the same content of octahedral aluminum as the parent material H-USY. Due to the low lanthanum content of LaPt-USY I no distinctive shoulder at about 50 ppm corresponding to tetrahedral aluminum was observed. An additional peak at 35 ppm was attributed to the penta-coordinated aluminum[25-27] and distorted tetrahedral aluminum species.[28,29] LaPt-USY II featured the lowest concentration of total aluminum and the highest fraction of octahedral aluminum.

Table 4.2: Amount of tetrahedral and octahedral aluminum determined by AAS and ^{27}Al MAS NMR

Sample	Total amount Al [mmol/g]	Tetrahedral Al [mmol/g]	Octahedral Al [mmol/g]
H-USY	3.38	2.54	0.84
La-USY I	2.61	2.11	0.49
La-USY II	2.62	2.38	0.24
Pt-USY I	3.35	2.55	0.80
Pt-USY II	3.15	2.43	0.72
LaPt-USY I	3.29	2.45	0.84
LaPt-USY II	2.05	1.36	0.69

Although the total aluminum and the extra-framework aluminum content generally decreased in a parallel manner with the increase of lanthanum ion-exchange degree, it is significant that the amount of framework aluminum remain rather unaffected. The incorporation of higher lanthanum and platinum amount in LaPt-USY II caused a more severe decrease of the total aluminum content.

The acidity of the samples was tested by pyridine adsorption and the incorporation of both lanthanum and platinum led to an increase in LAS and a decrease in BAS, as shown in Table 4.3.

Table 4.3: Composition of total and strong acid sites according to FTIR spectroscopy with adsorbed pyridine. Measurements were newly performed at 423 K after the samples were activated at 723 K for 1 h (10 K min^{-1}). Total acid sites are defined to retain pyridine at 423 K, strong acid sites are defined to retain pyridine at 723 K for 0.5 h

	Lewis acid sites [mmol/g]		Brønsted acid sites [mmol/g]		Strong Brønsted acid sites/ total acid sites
	total	strong	total	strong	
H-USY	0.32	0.15	1.38	1.17	0.69
La-USY I	0.53	0.44	1.16	0.90	0.53
La-USY II	0.52	0.27	0.78	0.50	0.38
Pt-USY I	0.66	0.54	1.01	0.72	0.43
Pt-USY II	0.71	0.58	0.98	0.59	0.35
LaPt-USY I	0.67	0.60	0.72	0.71	0.51
LaPt-USY II	0.21	0.14	0.25	0.25	0.54
Pt-SZ	0.50	0.25	0.37	0.25	0.29

The infrared spectra of adsorbed pyridine on Pt-ZS indicate that both Brønsted and Lewis acid sites are present. By comparing the effect of pyridine adsorption on the OH region of the infrared spectra, it was observed that lanthanum and platinum exchange increased the LAS. The concentration of Brønsted acid sites (BAS) as well as the highest ratio of strong Brønsted acid sites (SBAS) to total acid sites was found for the parent material. The Pt-SZ material has a similar concentration of LAS but a considerably lower concentration of BAS compared to the lanthanum exchanged USY materials.

4.3.2. Catalytic reaction

Apparent activation energies were determined from the temperature dependence (483 K to 533 K) of the initial conversion rates. For the determination of reaction orders with respect to hydrogen, the catalyst was contacted with hydrogen (50 ml min^{-1}) in a total pressure range of 5-25 bar at 523 K and a partial pressure of n-pentane of 450 mbar. For the determination of reaction orders with respect to hydrogen, the catalyst deactivation during the measurement was considered. Important kinetic parameters are compiled in Table 4.4.

Table 4.4: Values of apparent activation energies, reaction orders and calculated initial rates of n-pentane isomerization

	Initial rate		Ea	Pre-exponential factor		Reaction order in H_2
	10^{-7} [mol/(g_{cat}·s)]	10^{-4} [mol/(mol_{SBAS}·s)]	[kJ mol^{-1}]	[mol/(g_{cat}·s·bar)]	[mol/(mol_{SBAS}·s·bar)]	
H-USY	0.4	0.3	69	$6.7 \cdot 10^{-1}$	$1.3 \cdot 10^{3}$	0.33
La-USY I	2.1	2.3	97	$3.4 \cdot 10^{3}$	$3.8 \cdot 10^{6}$	0.44
La-USY II	-	-	72	2.4	$4.0 \cdot 10^{3}$	0.64
Pt-USY I	0.8	1.1	176	$7.9 \cdot 10^{10}$	$1.1 \cdot 10^{14}$	-0.61
Pt-USY II	-	-	178	$2.1 \cdot 10^{11}$	$3.6 \cdot 10^{14}$	-0.62
LaPt-USY I	0.8	1.1	164	$4.1 \cdot 10^{9}$	$5.8 \cdot 10^{12}$	-0.55
LaPt-USY II	0.4	1.6	121	$1.2 \cdot 10^{5}$	$4.9 \cdot 10^{8}$	-0.53
Pt-SZ	23.0	92	97	$2.1 \cdot 10^{4}$	$8.4 \cdot 10^{7}$	0.34

For the parent material H-USY and the lanthanum modified catalysts a positive reaction order with respect to hydrogen was found. The positive tendency became more significant over the catalysts with larger amount of lanthanum. For all the platinum modified ultra-stable zeolite Y a negative reaction order with respect to hydrogen was determined, though the order was not affected by the increasing platinum content. In line with the previously published work of Lanewala et al.,[10] the skeletal isomerization reactions over acid sites were proposed as rate limiting step when the hydrogenation and dehydrogenation reactions on platinum sites are in equilibrium. For the platinum containing mordenite catalyzed hydroisomerization of n-pentane Holló et al. reported a similar negative reaction order (-0.81).[8] In contrast, for the Pt-ZS catalyzed hydroisomerization of n-pentane a positive reaction order with respect to hydrogen was found.

Hydroisomerization over platinum exchanged zeolites proceeds via a bifunctional mechanism.[4,6,7,30-32] This is verified by the negative reaction order with respect to hydrogen observed for the Pt-USY I and Pt-USY II catalyzed reactions. The generation of an olefinic intermediate by dehydrogenation on platinum sites is hindered by increasing partial pressures of hydrogen due to a shift in the thermodynamic equilibrium of the alkane - alkene reaction.[4] With decreasing concentrations of olefins, the rate of isomerization declines resulting in a negative reaction order regarding hydrogen.

The values of the apparent activation energies over the selected catalysts were derived from the initial rates by the linear fits of the respective Arrhenius plots. With the catalysts used in this study the apparent activation energy values were found to vary from 72 kJ/mol for La-USY II till 178 kJ/mol for Pt-USY II. The lowest value was found, however, for the non-modified H-USY (69 kJ/mol). For the platinum containing catalysts the apparent activation energy values ranged from 121 kJ/mol for LaPt-USY II to 178 kJ/mol for Pt-USY II. Zeolites differing only in content of platinum (Pt-USY I = 176 kJ/mol, Pt-USY II = 178 kJ/mol) showed similar activation energies. The bimetallic materials exhibited activation energies ranging between the values determined for the monometallic samples. With increasing lanthanum content in bimetallic catalysts a decrease in activation energy for the isomerization reaction of n-pentane was observed indicating that the presence of La^{3+} stabilizes and facilitates the transition state. The activation energy of n-pentane isomerization over Pt-SZ was identical to the value obtained over lanthanum exchanged sample La-USY I.

In the following, the catalytic performances of a set of lanthanum and platinum containing catalysts were studied for the hydroisomerization of n-pentane at 523 K, 10 bar total pressure, 450 mbar partial pressure of n-pentane in 50 ml min^{-1} hydrogen for 20 h. Formation rates of various isomerization, cracking and dehydrogenation products are shown in Figure 4.4.

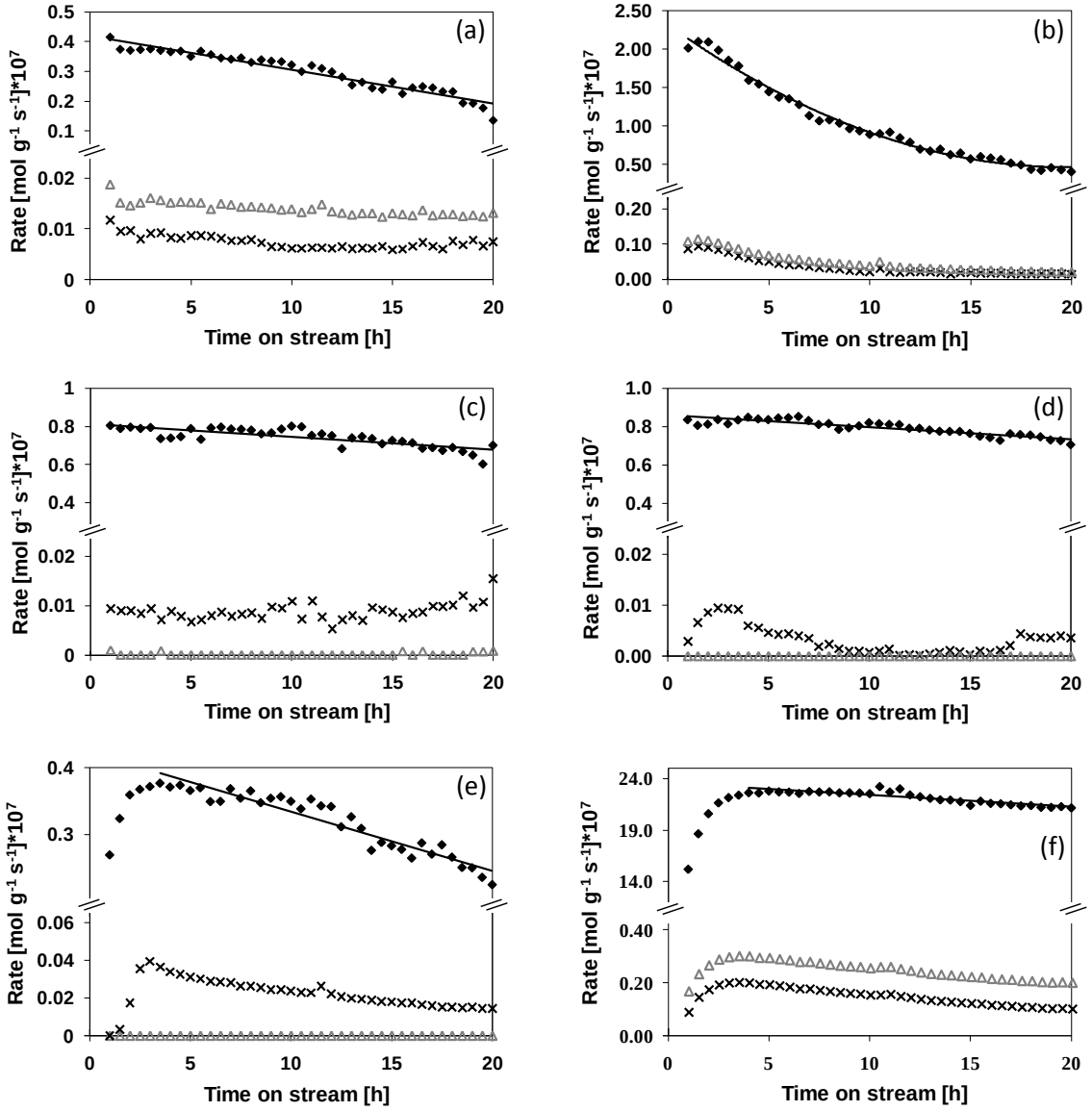

Figure 4.4: Formation rates of iso-pentane (♦), cracking products (×) and dehydrogenation products (△) over H-USY (a), La-USY I (b), Pt-USY I (c), LaPt-USY I (d), LaPt-USY II (e) and Pt-SZ (f)

The comparison of the activities of the parent (H-USY, Figure 4.4 a) and modified catalysts (Figure 4.4 b-e) shows the positive effect of modification on the catalytic iso-pentane formation. For all the samples, the rate of iso-pentane formation decreased slowly and steadily throughout the entire reaction time. The most accentuated decrease was found for the parent material H-USY and for the La-USY I material where about 50 % of the initial activity was lost

after the first 20 h on stream. When platinum was introduced in the zeolitic framework, the catalyst deactivation was greatly suppressed since platinum is able to catalyze the hydrogenation of carbonaceous deposits. The rates of by-products formation (dehydrogenation and cracking products) were insignificantly low and remained almost constant under working conditions.

The selectivities of the catalysts for the iso-pentane formation measured during these experiments and the calculated deactivation factors are summarized in Table 4.5.

Table 4.5: Selectivity for the iso-pentane formation determined at the beginning and end (after 20 h) of the catalytic reaction and corresponding deactivation factors

Sample	Selectivity [%]		Deactivation factor
	initial	20 h	
H-USY	0.93	0.90	0.53
La-USY I	0.92	0.93	0.84
Pt-USY I	0.99	0.98	0.17
LaPt-USY I	1.00	1.00	0.14
LaPt-USY II	1.00	0.95	0.37
Pt-SZ	0.98	0.99	0.07

The isomerization selectivity of the reaction on each catalyst is higher than 90 %. Beside the dominant target product iso-pentane, C_1-C_4 cracking and dehydrogenation side products are observed. Additional promotion of the ultra-stable zeolite Y by modification with 0.10 mmol/g platinum leads to an enhancement of the n-pentane conversion corresponding to an iso-pentane selectivity of almost 99 %.

The comparison of the experimental data for La-USY I and LaPt-USY II shown in Figure 4.4 and summarized in Table 4.5 demonstrates clearly that the incorporation of lanthanum significantly enhances the formation of cracking products while the n-pentane isomerization over LaPt-USY II is unchanged compared to the parent USY material. This findings are in good agreement with the experimental data for n-hexane and n-heptane isomerization over USY zeolites and platinum promoted zeolite Y reported by Roldán et al. and Wang et al.[3,33]

The Pt-ZS catalyst is considerably more active than the faujasite type ultra-stable zeolites Y. The considerable increase in the rate of iso-pentane formation (Figure 4.4 f) for the first hours on time on stream is attributed to the accumulation of n-pentane on the surface. The high selectivity in iso-pentane obtained with Pt-ZS in this study agrees well with the results of Matsuhashi et al.[13] on n-pentane isomerization over platinum promoted sulfated zirconia catalyst. In both cases the formation of side-products was negligible.

The catalyst deactivation behavior is described by the deactivation factor defined by the following rate-approximation equation.

$$Deactivation\ factor = \left(\frac{r_0 - r_d}{r_0}\right)$$

Whereas r_0 represents the initial reaction rate of iso-pentane formation and r_d the rate of iso-pentane formation after 20 h on stream.

In case of LaPt-USY II and Pt-SZ the initial iso-pentane rate formation, r_0 was replaced with r_3 representing the rate for iso-pentane formation after 3 h on stream, where the product formation rate became constant. The results compiled in Table 4.5 clearly demonstrate that the platinum promoted catalysts are considerably more stable than the parent H-USY and La-USY I materials.

Following the detailed analysis of the individual catalyst residues collected from the fixed bed stainless steel tubular reactor after 20 h on stream, the correlation between the acidity and their performance in the hydroisomerization is addressed. All examined materials were active and selective hydroisomerization catalysts. Absolute concentrations of LAS and BAS, defined as the difference in the ratio of strong BAS to total AS, carefully determined at the beginning of the hydroisomerization and after 20 h on stream, are included in Table 4.6.

Table 4.6: Acid site concentration and acid strength distribution as determined by pyridine desorption at 423 K

Sample*	Lewis acid sites [mmol/g]		Brønsted acid sites [mmol/g]		SLAS/ total AS	SBAS/ total AS	Difference (prior-after reaction)	
	total	strong	total	strong			SLAS/ total AS	SBAS/ total AS
H-USY	0.30	0.14	0.63	0.36	0.15	0.39	0.06	-0.30
La-USY I	0.36	0.23	0.68	0.29	0.22	0.28	-0.04	-0.25
Pt-USY I	0.46	0.30	0.54	0.41	0.30	0.41	-0.02	-0.02
LaPt-USY I	0.49	0.44	0.60	0.59	0.40	0.54	-0.03	0.03
LaPt-USY II	0.09	0.04	0.11	0.13	0.20	0.65	-0.10	0.11
Pt-SZ	0.25	0.09	0.07	0.03	0.28	0.09	-0.01	-0.20

*Prior analysis, all the samples were activated at 723 K for 1 h (10 K min^{-1})

For all catalysts the concentration of total acid site decreased with time on stream. The Lewis acidity in the H-USY material stayed constant. The comparison of the data shown in Table 4.6 demonstrates clearly that the total and the SBAS concentration decreased for all lanthanum and platinum modified zeolites with the time on stream. A more pronounced decrease in the SBAS concentration was observed for H-USY, La-USY I and Pt-SZ while the only platinum exchanged zeolites showed a nearly unaffected SBAS/total AS ratio. The ratio of SLAS to total AS remained almost constant and was comparable for all the materials.

Table 4.7 allows the comparison of the concentration and distribution of acidic sites in the Pt-SZ following the synthesis, reduction and after 2, 4 and 20 h on stream.

Table 4.7: Acid sites concentration and acid strength distribution in Pt-SZ as determined by pyridine desorption at 423 K

Pt-SZ	Lewis acid sites [mmol/g]		Brønsted acid sites [mmol/g]	
	total	strong	total	strong
synthesis	0.50	0.25	0.37	0.25
reduction	0.26	0.15	0.15	0.07
2 h on stream	0.29	0.15	0.18	0.07
4 h on stream	0.28	0.17	0.20	0.11
20 h on stream	0.25	0.09	0.07	0.03

Prior analysis, all the samples were activated at 723 K for 1 h (10 K min^{-1})

In concrete, the most accentuated decrease of the concentration of total acid sites, SLAS and SBAS in Pt-SZ occurred during reduction at 573 K (10 K min^{-1}) under hydrogen atmosphere (50 ml min^{-1}) for 4 h. During hydroisomerization the acidity of Pt-ZS was only affected at extended time on stream.

Following hydroisomerization of n-pentane the content of carbonaceous deposits was experimentally determined by elemental analysis. Table 4.8 lists the content of deposited carbon on the studied catalysts up to 20 h on stream.

Table 4.8: Deposited carbon content of used samples determined by CHNS analysis

Sample	Carbon content [mmol/g]		
	after 2 h	after 4 h	after 20 h
H-USY	-	-	6.37
La-USY I	-	-	3.88
Pt-USY I	-	-	0.61
LaPt-USY I	-	-	0.17
LaPt-USY II	-	-	0.33
Pt-SZ	< 0.08	< 0.08	1.29

CHNS results show that the deposition of carbon from gaseous reactant molecules during the first 4 h on stream is negligible low. In general, lanthanum and platinum modified zeolites have considerably less carbonaceous deposits on the catalyst surface after 20 h on stream compared to the parent material H-USY. The lowest carbon content was found for the materials with the highest catalytic activity, *i.e.*, platinum exchanged zeolites and Pt-SZ, respectively. It can be seen that the total amount of carbon deposited on the active surface of LaPt-USY II was twice as high as found for the LaPt-USY I, indicating differences in the reaction pathways leading to the formation and/or location of coke in the two catalysts.

4.4. Discussion

In recent literature, a continuously growing number of theoretical and experimental studies are focused on the correlations between the catalytic performance and the physicochemical properties, in particular, acid-base properties, of the solid acid catalysts. The introduction of highly charged cations by ion-exchange influences the properties of zeolites in a complex way. Lanthanum and platinum-exchange result in a noticeable loss of silicon, aluminum and, in case of lanthanum ion-exchange, of sodium. Due to the lower aluminum content of the lanthanum exchanged zeolitic materials, these samples exhibit higher Si/Al ratios as compared to the platinum exchanged faujasite materials. Additional incorporation of either lanthanum or platinum after a certain concentration has only marginal impact on the remaining sodium concentration, which if still present, are mainly located in hexagonal prisms or in sodalite cages and could not be removed with additional exchange procedures.[34] According to Pan et al. platinum has a preference to form small clusters within the zeolitic framework.[35] These single crystals are not able to replace sodium atoms present in the zeolitic framework resulting in a higher content of remaining sodium in platinum exchanged zeolites compared to lanthanum exchanged samples. While the consequential Si/Al ratios in lanthanum and platinum containing materials are rather small, the additional ion-exchange procedures do not have a great impact on the overall acid-base properties of the catalysts.

Polyvalent cation incorporation (La^{3+} or Pt^{2+}) into the zeolitic material decreases the Brønsted acid site concentration. The simultaneous increase in LAS is attributed to the intrinsic Lewis acidic character of lanthanum and platinum. Additional lanthanum incorporation in the framework of ultra-stable zeolite Y (La-USY II) did not led to further increase of LAS, since repeated ion-exchange simultaneously decreases the content of extra-framework aluminum acting as Lewis acid sites. Since transition metal cations such as Pt^{2+} are readily reduced at elevated temperatures, only a certain amount of the metal will be bounded to the zeolite structure, the remaining atoms form metallic platinum particles, for example in the sodalite cage.[34] Higher content of LAS in platinum exchanged zeolites is explained by higher aluminum content, in particular octahedral coordinated aluminum, compared to the lanthanum exchanged samples. Incorporation of polyvalent cations (La^{3+} and Pt^{2+}) distort the zeolitic structure by increasing the Si-O-Al and Si-O-Si angles.[36] Additional temperature programmed desorption of adsorbed ammonia measurements on different aluminum and lanthanum containing FAU materials show only marginal differences in the strength distribution of the

acid sites.[37] The concentrations of total and strong BAS for platinum and lanthanum containing materials are comparable. The catalysts containing both components, lanthanum and platinum, exhibit only strong BAS. It is proposed that the distinction between weak and strong BAS, as done in the IR measurements with adsorbed pyridine, is not enough to demonstrate the actually existing distribution of Brønsted acid sites.

By analyzing the ^{27}Al MAS NMR spectrum of lanthanum modified ultra-stable zeolite Y marked differences were observed for the aluminum atoms with tetrahedral coordination while platinum exchange had only a marginal impact. By extended lanthanum exchange the transformation of octahedral aluminum into tetrahedral aluminum was observed. In LaPt-USY II a third type of Al was present. The formation of penta-coordinated aluminum[25-27] as well as of a more distinct distortion of tetrahedral Al[28] was observed due to the high concentration of lanthanum and the additional presence of platinum in the sample.

The experiments carried out so far clearly indicate that the hydroisomerization of n-pentane over ultra-stable zeolite Y, in the absence of noble metal components such as platinum, proceeds over skeletal isomerization involving hydride transfer. A first indication is given from the apparent energies of activation for the conversion of n-alkanes. In contrast to platinum containing materials, where a high apparent energy of activation was observed, for the H-USY and La-USY catalyzed reactions considerably lower energies of activation were determined. Note that a process involving hydride transfer avoids the energetically unfavorable step of olefin formation.[38] A modification of the USY material by additional platinum incorporation didn't result in an interference of activation energy which is in accordance with the consideration of equal transition states despite a changed metal concentration. The difference of about 30 kJ/mol considering H-USY and La-USY I can be explained by lattice contortion of the zeolite with the incorporation of lanthanum which also play a significant role for adsorption and polarization.[24,39] A second argument for the skeletal isomerization proceeding over hydride transfer can be drawn from the positive reaction order with respect to hydrogen for isomerization over H-USY and La-USY. An increase in partial pressure of hydrogen results in a fast hydride transfer and therefore shows an enhancement for skeletal isomerization. Compared to Pt-SZ, H-USY and La-USY I showed more pronounced deactivation rates. This is comprehensible, since a distinct spillover effect, which enhances catalytic stability, requires both hydrogen and platinum.[40] Due to the absence of platinum on these catalysts the spillover-effect as existing over Pt-SZ occurs in a much lower degree. Another evidence for the skeletal

isomerization proceeding over hydride transfer in H-USY and La-USY is the relative decline in SBAS with increasing time on stream. SBAS have already been identified as the active sites for hydride transfer in Pt-SZ. However, in platinum incorporated samples the relative proportion of SBAS remains constant. Despite lower concentrations of SBAS in La-USY I compared to H-USY a higher initial rate for isomerization over La-USY I was observed. Hence it is inferred that lanthanum incorporation enhance hydride transfer by polarization of the C-H bonds[37] resulting finally in a faster desorption of branched alkanes from the active sites, the incorporation of lanthanum also favors the formation of coke promoters which adsorb on the catalytic active sites leading to a faster deactivation rate of the catalyst at the beginning of the isomerization reaction.[3] The higher content of carbonaceous deposits in the H-USY residue compared to La-USY I residue could be related to the higher total acid sites in H-USY. Similar assumption was made by Zhao et al., who identified BAS as active sites for the coke formation in the alkylation of α-methylnaphthalene on lanthanum modified HY zeolites.[41] On the same way, BAS were considered as active sites for competing reactions, such as oligomerization and cracking.[42,43]

The suggested mechanism for hydroisomerization of n-pentane proceeding over H-USY and lanthanum exchanged catalysts is schematically presented in Figure 4.5.

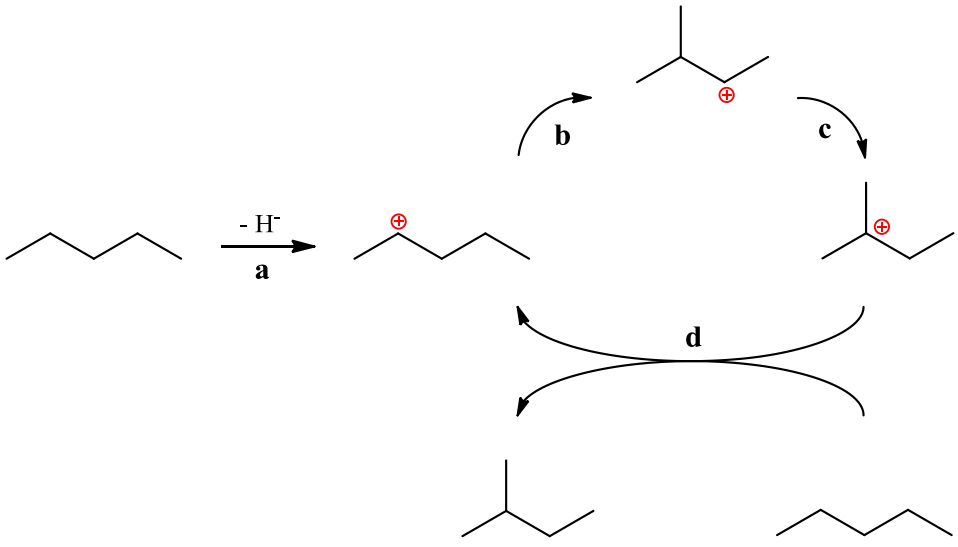

Figure 4.5: N-pentane isomerization via hydride transfer

In the first step, hydride abstraction over LAS leads to the formation of a secondary carbenium ion (a).[4,13] In the following step (b), the rearrangement of the formed secondary carbenium ion and the further formation of a protonated cyclopropane intermediate is proposed to occur. The in-situ formation of similar intermediate was already proposed by Brouwer et al. for the alkane isomerization reaction.[44] Due to their increased reactivity carbenium ions are short-lived intermediates and only exist as transition state in hydrocarbon conversion reactions over zeolites.[45] Further scientific studies performed by Kazansky et al. nearby the quantum mechanical study of Rigby et al. supported this consideration.[46] The rearrangement of the secondary carbenium ion (b) followed by a hydride shift results in the generation of a more stable tertiary carbenium ion (c). Following the hydride transfer step in the alkane isomerization over Pt-SZ materials[13] beside the formation of branched alkane the activation of further n-alkane (d) is expected.

Catalysts containing platinum featured constant activity and were found to be highly selective for n-pentane isomerization. Hydroisomerization over platinum exchanged zeolites proceeds via a bifunctional mechanism.[4,6,7,30-32] This is verified by the negative reaction order with respect to hydrogen observed for the Pt-USY I and Pt-USY II catalyzed reactions. The generation of an olefinic intermediate by dehydrogenation on platinum sites is hindered by increasing partial pressures of hydrogen due to a shift in the thermodynamic equilibrium of the alkane - alkene reaction.[4] With decreasing concentrations of olefins, the rate of isomerization declines resulting in a negative reaction order. Recently, it was shown that the constant activity ensues from the marginal amount of coke deposited on the platinum promoted zeolites, due to mostly suppressed cracking and the enhanced discharge of formed coke precursors on the surface in the presence of platinum.[5] In addition, the constant iso-pentane formation rate of platinum containing zeolitic materials throughout this study, despite decreasing concentration of total and strong acid sites, indicated that the metallic sites and not the acidic sites are accounting for the bifunctional mechanism. López et al. also concluded that acidity only plays a subordinate role in the reactivity for isomerization over platinum promoted catalysts.[6] According to Chao et al. a proper balance of hydrogenation activity and acidic activity is crucial in order to obtain high isomerization yield.[31] The dehydrogenation of n-pentane over platinum and the formation of an olefinic intermediate is a relevant step in the iso-pentane formation over the bifunctional mechanism but is not the rate determining step.[4,10] Considering the constant ratio of SBAS to the total acid sites it was possible to

demonstrate, that dehydrogenation enables a subsequent protonation over all available BAS without any specific requirements on acid strength. The observed activation energy for n-pentane isomerization over platinum promoted zeolites was rather high. This is related to the interim olefin formation associated with the energy-demanding step of dehydrogenation.[47] Similar values for the apparent Ea was reported by Xu et al. for dehydrogenation of propane over zeolite Y (173 kJ/mol).[48]

The existence of two different mechanisms in skeletal isomerization of n-pentane over lanthanum and platinum containing bimetallic zeolites is pointed out by the results obtained for the mixed metal zeolites LaPt-USY I and LaPt-USY II. On the one hand, considering the catalytic activity of LaPt-USY I, the synthesized catalyst seems to follow only platinum-zeolite behavior, since catalytic activity is constant and identical in rate for iso-pentane formation as achieved over Pt-USY I. On the other hand the activation energy is definitely lower than for Pt-USY I. A clear influence of lanthanum on present isomerization becomes visible. With increasing lanthanum concentration the activation energy decreases to even lower level as observed for LaPt-USY II, hydride transfer gains in importance due to increasing polarization through lanthanum. Similar observations were obtained on lanthanum incorporating zeolites with the addition of nickel.[49] The reaction orders of LaPt-USY I (-0.55) and LaPt-USY II (-0.53) with respect to hydrogen, coincide. An increase in reaction rate with increased hydride couldn't be evidenced, since the incorporation of lanthanum leads to a decrease of total acid site concentration. The results obtained for LaPt-USY II, however, confirm the coexistence of both pathways for isomerization, isomerization via bifunctional mechanism and via hydride transfer reaction. The bifunctional mechanism has to be regarded as dominating which can be seen in prevailing overall activation energy and reaction order with respect to hydrogen.

Hydroisomerization reaction performed in the presence of Pt-SZ followed different mechanistic pathways. Isomerization of n-butane proceeds over an intermolecular mechanism.[5] Hydroisomerization of n-alkanes (n(C)>4) followed an unimolecular mechanism involving hydride transfer.[11,12] In contrast to the bifunctional mechanism, no olefin intermediate was formed. Feller et al. suggested that strong BAS are the active sites which enable hydride transfer for alkylation of isobutane with n-butene by stabilizing the charge separation in the transition state.[50] The importance of strong BAS can be verified by considering the reduction of the proportion of SBAS to total acid sites during deactivation study as shown in Table 4.6. The fact that after reduction only few strong BAS are detected in

IR measurements of adsorbed pyridine shows that strong BAS are not exclusively responsible for the high catalytic activity. Manoli et al. identified few acidic sulfated-zirconia groups in the vicinity of platinum sites generated during calcination procedures as highly active centers and attributed the higher activity to these acid-metal interaction.[51] The presence of platinum significantly improves the selectivity and stability with time on stream in the hydroisomerization of n-pentane.[52,53]

In accordance with the work of Iglesia et al.[11] a positive reaction order of n-pentane hydroisomerization was observed. On the one hand this is due to the avoidance of an olefin intermediate formation and on the other hand this is because hydrogen acts as a hydride source and is in the same time the catalytic site in alkane isomerization catalysis in the presence of metals.[11,22] Therefore, hydrogen enhances the desorption of iso-pentane from SBAS accompanied with the transformation of another alkane into a secondary carbenium ion. The fact that the activation energy for hydroisomerization of n-pentane is found to be 97 kJ/mol and therefore to be lower than observed over platinum promoted zeolites, confirms the already introduced mechanism. The descent in activation energy originates from the prevention of olefin intermediates in the hydroisomerization over Pt-SZ. N-pentane conversion over Pt-SZ is also very selective towards isomerization, whereas the carbon content and concomitant deactivation in Pt-SZ is low. According to CHNS analyses coke deposits after 2 h respectively 4 h of reaction are negligible, therefore blocking of active sites in the initial period is excluded. Results concerning high catalytic activity and long lasting stability are in line with the work of Ebitani et al.[22] and Vaudagna et al.[40] They concluded the high and remaining activity is correlated with the presence of both hydrogen and platinum that cause the effect of “spillover hydrogen” resulting in the dissociation of hydrogen over platinum sites. The associated generation of hydride ions and protons results in a fast hydride transfer and thus high catalytic activity. The observed induction period over Pt-SZ on the one hand originates from the slight initial increase of active BAS. On the other hand it is suggested that the described spillover effect is not developed until a certain time on stream. It is likely that a certain concentration of hydride ions is needed to achieve maximum catalytic activity for hydroisomerization.

4.5. Conclusions

Hydroisomerization of n-pentane over USY zeolites proceeds over different mechanistic pathways depending on the nature of the incorporated metal. Platinum exchanged USY zeolites showed the highest activity and selectivity for n-pentane hydroisomerization within the series. Negative reaction orders with respect to hydrogen confirm the formation of an olefinic intermediate. Furthermore, the bifunctional mechanism was confirmed. According to the performed FTIR spectroscopic studies with adsorbed pyridine prior and after reaction, the unmodified proportion of strong Brønsted acid sites compared to the total acid sites of platinum exchanged zeolites excludes any strong dependence on acid strength for skeletal isomerization in platinum containing USY zeolites. Dehydrogenation of hydrocarbons over platinum enables a subsequent protonation over all available Brønsted acid sites. The formation of olefins has a high impact on activation energy. Activation energies for hydroisomerization over platinum exchanged zeolites (Pt-USY I = 176 kJ/mol) are considerably higher than over H-USY (69 kJ/mol), lanthanum exchanged zeolites (La-USY I = 97 kJ/mol) and Pt-SZ (97 kJ/mol).

Lanthanum containing USY zeolites exhibit enhanced initial rates for iso-pentane formation compared with H-USY and platinum promoted zeolites. However, enhanced activity is also associated with a more pronounced deactivation with increasing time on stream. Hydroisomerization of n-pentane over lanthanum exchanged USY zeolites and H-USY proceeds via hydride transfer as proposed for platinum promoted sulfated zirconia. Lanthanum incorporation distorts the zeolite lattice by withdrawing electron density from the framework.[36,54] In contrast to platinum which conduct (de)hydrogenation functions, incorporated lanthanum strongly polarize the C-H bond of the adsorbed hydrocarbon.[37] The alteration in the proportion of strong Brønsted acid sites compared to the total acid sites with increasing time on stream suggested that the isomerization of n-pentane proceeds only over strong BAS. Following the initiation, hydride abstraction over LAS, skeletal isomerization occurs over strong BAS and leads to the hydride transfer from another n-alkane to the branched carbenium ion. The isomerization process over lanthanum containing USY zeolites and H-USY therefore can be considered as chain reaction. Activation of n-alkanes and desorption of iso-alkanes is supposed to occur simultaneously. The low activation energy is a consequence of the avoidance of the energy demanding step of dehydrogenation. The strengthening in C-H

polarization on introduced hydrocarbons accelerates hydride transfer and is responsible for higher initial rates for isomerization in lanthanum exchanged zeolites.

The proceeding of isomerization via hydride transfer in Pt-SZ is verified by the positive reaction order with respect to hydrogen in iso-pentane formation and the particular decrease of strong BAS. In good agreement with other studies, Pt-SZ features high activity and selectivity for n-pentane isomerization, which remain on a high level throughout 20 h on stream. This is ascribed to the effect of "spillover hydrogen". The presence of hydrogen and platinum enhance the dissociation of hydrogen over platinum sites concomitantly accelerating the hydride transfer and finally resulting in a high, constant activity for hydroisomerization.[11,22]

In platinum and lanthanum containing mixed metal USY materials the formation of iso-pentane can follow both of the proposed mechanistic pathways. Due to the negative reaction orders with respect to hydrogen the bifunctional mechanism predominates within these materials. Lanthanum incorporation lowers activation energy and leads to less negative reaction orders.

4.6. Acknowledgements

The authors would like to thank Martin Neukam and Xaver Hecht for performing the AAS and BET measurements. We also gratefully acknowledge the financial support in the framework of IDECAT.

4.7. References

(1) Kinger, G.; Majda, D.; Vinek, H. *Appl. Catal. A-Gen.* **2002**, *225*, 301.

(2) Woltz, C.; Jentys, A.; Lercher, J. A. *J. Catal.* **2006**, *237*, 337.

(3) Roldán, R.; Romero, F. J.; Jiménez-Sanchidrián, C.; Marinas, J. M.; Gómez, J. P. *Appl. Catal. A-Gen.* **2005**, *288*, 104.

(4) Ono, Y. *Catal. Today* **2003**, *81*, 3.

(5) Wu, H.-C.; Leu, L.-J.; Naccache, C.; Chao, K.-J. *J. Mol. Catal. A: Chem.* **1997**, *127*, 143.

(6) López, C. M.; Sazo, V.; Pérez, P.; García, L. V. *Appl. Catal. A-Gen.* **2010**, *372*, 108.

(7) Deldari, H. *Appl. Catal. A-Gen.* **2005**, *293*, 1.

(8) Holló, A.; Hancsók, J.; Kalló, D. *Appl. Catal. A-Gen.* **2002**, *229*, 93.

(9) Woltz, C.; Jentys, A.; Lercher, J. A. Characterization of acidic properties of sulfated zeolite Beta. In *Stud. Surf. Sci. Catal.*; Elsevier, 2005; Vol. 158, Part 2; pp 1763.

(10) Lanewala, M. A.; Pickert, P. E.; Botton, A. P. *J. Catal.* **1967**, *9*, 95.

(11) Iglesia, E.; Soled, S. L.; Kramer, G. M. *J. Catal.* **1993**, *144*, 238.

(12) Liu, H.; Lei, G. D.; Sachtler, W. M. H. *Appl. Catal. A-Gen.* **1996**, *146*, 165.

(13) Matsuhashi, H.; Shibata, H.; Nakamura, H.; Arata, K. *Appl. Catal. A-Gen.* **1999**, *187*, 99.

(14) Li, X.; Nagaoka, K.; Simon, L. J.; Olindo, R.; Lercher, J. A. *J. Catal.* **2005**, *232*, 456.

(15) ASTM. Standard Test Method for Determination of the Unit Cell Dimension of a Faujasite-Type Zeolite. In *Annual Book of ASTM Standards*, 1985; Vol. D3942-85.

(16) Lippens, B. C.; Linsen, B. G.; De Boer, J. H. *J. Catal.* **1963**, *3*, 32.

(17) Halsey, G. *J. Chem. Phys.* **1948**, *16*, 931.

(18) Haase, F.; Sauer, J. *J. Am. Chem. Soc.* **1998**, *120*, 13503.

(19) Babou, F.; Coudurier, G.; Vedrine, J. C. *J. Catal.* **1995**, *152*, 341.

(20) Ward, D. A.; Ko, E. I. *J. Catal.* **1994**, *150*, 18.

(21) Comelli, R. A. *Catal. Lett.* **1996**, *40*, 67.

(22) Ebitani, K.; Konishi, J.; Hattori, H. *J. Catal.* **1991**, *130*, 257.

(23) Grau, J. M.; Parera, L. *Appl. Catal. A-Gen.* **1997**, *162*, 17.

(24) Sievers, C.; Liebert, J. S.; Stratmann, M. M.; Olindo, R.; Lercher, J. A. *Appl. Catal. A-Gen.* **2008**, *336*, 89.

(25) Omegna, A.; van Bokhoven, J. A.; Prins, R. *J. Phys. Chem. B* **2003**, *107*, 8854.

(26) Gilson, J.-P.; Edwards, G. C.; Peters, A. W.; Rajagopalan, K.; Wormsbecher, R. F.; Roberie, T. G.; Shatlock, M. P. *J. Chem. Soc., Chem. Commun.* **1987**, 91.

(27) Coster, D.; Blumenfeld, A. L.; Fripiat, J. J. *J. Phys. Chem.* **1994**, *98*, 6201.

(28) Kosslick, H.; Tuan, V. A.; Fricke, R.; Martin, A.; Storek, W. Study on the nature of aluminum in dealuminated zeolite ZSM-20. In *Stud. Surf. Sci. Catal.*; Elsevier, 1994; Vol. Volume 84; pp 1013.

(29) Remy, M. J.; Stanica, D.; Poncelet, G.; Feijen, E. J. P.; Grobet, P. J.; Martens, J. A.; Jacobs, P. A. *J. Phys. Chem.* **1996**, *100*, 12440.

(30) Sinfelt, J. H.; Hurwitz, H.; Rohrer, J. C. *J. Catal.* **1962**, *1*, 481.

(31) Chao, K.-J.; Wu, H.-C.; Leu, L.-J. *Appl. Catal. A-Gen.* **1996**, *143*, 223.

(32) Weisz, P. B. *Advances in Catalysis*; Academic Press: New York, 1963; Vol. 13.

(33) Wang, Z. B.; Kamo, A.; Yoneda, T.; Komatsu, T.; Yashima, T. *Appl. Catal. A-Gen.* **1997**, *159*, 119.

(34) Wright, P. A. *Microporous Framework Solids*; The Royal Society of Chemistry: Cambridge, 2008.

(35) Pan, M.; Cowley, J. M.; Chan, I. Y. *Ultramicroscopy* **1990**, *34*, 93.

(36) van Bokhoven, J. A.; Roest, A. L.; Koningsberger, D. C.; Miller, J. T.; Nachtegaal, G. H.; Kentgens, A. P. M. *J. Phys. Chem. B* **2000**, *104*, 6743.

(37) Schüßler, F.; Pidko, E. A.; Kolvenbach, R.; Sievers, C.; Hensen, E. J. M.; van Santen, R. A.; Lercher, J. A. *J. Phys. Chem. C* **2011**, *115*, 21763.

(38) van Santen, R. A.; Kramer, G. J. *Chem. Rev.* **1995**, *95*, 637.

(39) Sievers, C.; Onda, A.; Olindo, R.; Lercher, J. A. *J. Phys. Chem. C* **2007**, *111*, 5454.

(40) Vaudagna, S. R.; Comelli, R. A.; Canavese, S. A.; Fígoli, N. S. *J. Catal.* **1997**, *169*, 389.

(41) Zhao, Z.; Qiao, W.; Wang, G.; Li, Z.; Cheng, L. *J. Mol. Catal. A: Chem.* **2006**, *250*, 50.

(42) Guisnet, M.; Gnep, N. S. *Appl. Catal. A-Gen.* **1996**, *146*, 33.

(43) Corma, A.; Planelles, J.; Sánchez-Marín, J.; Tomás, F. *J. Catal.* **1985**, *93*, 30.

(44) Brouwer, D. M.; Hogeveen, H. *Prog. Phys. Org. Chem.* **1972**, *9*, 179.

(45) Kazansky, V. B.; Senchenya, I. N. *J. Catal.* **1989**, *119*, 108.

(46) Rigby, A. M.; Kramer, G. J.; van Santen, R. A. *J. Catal.* **1997**, *170*, 1.

(47) Bond, G. C. *Catal. Today* **1999**, *49*, 41.

(48) Xu, B.; Sievers, C.; Hong, S. B.; Prins, R.; van Bokhoven, J. A. *J. Catal.* **2006**, *244*, 163.

(49) Gray, J. A.; Cobb, J. T. *J. Catal.* **1975**, *36*, 125.

(50) Feller, A.; Zuazo, I.; Guzman, A.; Barth, J. O.; Lercher, J. A. *J. Catal.* **2003**, *216*, 313.

(51) Manoli, J.-M.; Potvin, C.; Muhler, M.; Wild, U.; Resofszki, G.; Buchholz, T.; Paál, Z. *J. Catal.* **1998**, *178*, 338.

(52) Essayem, N.; Ben Taârit, Y.; Feche, C.; Gayraud, P. Y.; Sapaly, G.; Naccache, C. *J. Catal.* **2003**, *219*, 97.

(53) Wen, M. Y.; Wender, I.; Tierney, J. W. *Energy Fuels* **1990**, *4*, 372.

(54) Carvajal, R.; Chu, P.-J.; Lunsford, J. H. *J. Catal.* **1990**, *125*, 123.

Chapter 5

Enhanced catalytic activity of alkaline treated FAU materials for isobutane/2-butene alkylation

Isobutane/2-butene alkylation was used to investigate the catalytic activity of ultra-stable H-USY, lanthanum exchanged La-USY and base treated La-USY materials. The influence of lanthanum incorporation and alkaline treatment on the pore size distribution, concentration and accessibility of catalytically active sites was studied in detail. Performed IR spectroscopic measurements of adsorbed pyridine showed that alkaline treatment of the USY materials improved the accessibility and concomitantly increased the concentration of hydroxylated lanthanum species. The performance of these catalysts was evaluated in terms of conversion, selectivity to trimethylpentanes (TMPs) and stability. Achieved results showed, that mild alkaline treatment and subsequent lanthanum exchange, led to the formation of a highly active catalyst with an improved stability under operating conditions. The catalytic activity of the synthesized materials in isobutane/2-butene alkylation increased in order: base treated La-USY > La-USY > H-USY. This sequence clearly shows the role of the structural features in the reaction along with the decrease in the transport limitation.

5.1. Introduction

Alkylation reaction of isobutane with light alkenes is an important refining process to produce highly branched alkanes as blending gasoline components.[1] Alkylation is currently catalyzed by anhydrous hydrofluoric acid or sulfuric acid. There might be commercial interest to replace the mineral acids by solid acid catalysts.[2] Zeolites are among the most promising candidates of choice, as they provide strong Brønsted acidity,[3] high thermal and mechanical stability. Practical zeolites (for the isobutane/2-butene alkylation only zeolites with large pores are of interest) contain not only micropores but also mesopores ranging from 2 nm up to 50 nm,[4] which may reduce mass transport limitation and grant fast access to the active sites of the zeolite.

The alkylation reaction requires a high concentration of Brønsted acid sites and, hence, only zeolites containing a high concentration of aluminum are suitable.[5-8] In a careful comparison Feller et al. showed that a high fraction of strong Brønsted acid sites (SBAS) significantly improves the catalyst productivity and life time. This has been affiliated with the better statistical partition between carbenium ions and available butene in the reactor, as well as to an enhanced hydride transfer and better stabilization of the transition state.[9]

Rare earth exchanged faujasites were previously shown to provide excellent activity and suitable selectivity for isobutane/2-butene alkylation. Lanthanum at ion-exchange positions of faujasite zeolites stabilizes their structure and further influence the concentration and strength of active acid sites through local distortion of the zeolite lattice.[6,10] This effect strongly depends on the concentration of aluminum in the zeolite lattice, being the more pronounced the higher the aluminum concentration is. The overall stabilization of the zeolite by La^{3+} cations especially in the presence of steam is well established. Note at this point that during regeneration high temperatures and the presence of steam cause the removal of lattice aluminum and thereby a reduction of the concentration of Brønsted acid sites.

Partial dealumination though may enhance the accessibility of the remaining acid sites by generating voids in the zeolite structure and so reducing the domains in which catalysis takes place. Steam treatment together with careful acid leaching will give rise to a physical structure of the catalyst particles, which combines facile transport through large pores with nano-domains of zeolites. Thus eventually the mesopores provide better access to the Brønsted acid sites minimizing so transport limitations.[11,12] Desilication by alkaline leaching seems to be a promising alternative to create further mesopores without removing more aluminum from the

lattice.[11-13] Thus, the combination of steaming and leaching procedures may lead to interesting catalysts. It should be kept in mind however at this point that the reduction of aluminum concentration inevitably will lead to a lower concentration of highly active lanthanum cations, as found in La-X.[14] The present study will address, therefore, the particular aspect of the isobutane/2-butene alkylation, i.e., the role of the pore structure in the catalyst deactivation.

Catalyst deactivation registration is the central problem for solid acid use inoculation. Widely impressive lifetimes have been reported,[15] these have been achieved only through frequent regenerations and have so reduced the catalyst productivity.[16] Under reaction conditions larger carbenium ions building slowly up in the pores of zeolites, but the critical deactivation occurs via a rapid blocking of the complete catalyst surface. It is speculated at present that the oligomers in the pores provide the basis for the rapid covering of the surface, while in the inner part of the zeolite particles still accessible and free Brønsted acid sites exist.[17,18] Conceptually, smaller particles and a very corrugated nature might allow suppressing or at least retarding the process of deactivation by a complete surface coverage.

It should however, also be kept in mind that reducing the concentration of larger carbenium ions would be beneficial by eliminating the bases for the surface growths. This latter concentration could be conceptually reduced by enhancing hydride transfer capabilities. As a positive side effect, this would also improve the selectivity to trimethylpentanes, the target product for iso-alkane/alkene alkylation.

Therefore, we explore in this study the activity, selectivity and stability of leached lanthanum exchanged USY zeolite in comparison to their parent material as catalyst for isobutane/2-butene alkylation. Especially, the influence of alkaline treatment to the accessibility of active sites and pore size properties in lanthanum ion-exchanged USY was studied in better understand the influence of pore structure and surface modification on isobutane/2-butene alkylation.

5.2. Experimental

5.2.1. Catalyst preparation

For the alkylation reaction of isobutane/2-butene relevant rare earth metal containing catalysts were prepared in a multiple step synthesis using a H-USY material provided by Grace Davison. In order to remove the remaining sodium from the parent material an additional ammonium ion-exchange, with 5 mol/L NH_4NO_3 solution, was performed over 4 h at 373 K.

For the La6.67%-USY catalyst the lanthanum ion-exchange was carried out using 0.5 M $La(NO_3)_3$ solution using a constant ratio of liquid to zeolite of 7 ml/g. The ion-exchange procedure was performed at 373 K under continuous stirring (500 rpm) for 4 h. The zeolite was thoroughly washed with bi-distilled water and dried at 373 K for 6 h. The dried material was calcined in flowing synthetic air (200 ml/min) up to 773 K with a heating rate of 10 K/min for 4 h. After calcination the material was rehydrated at 343 K. Afterwards, the exchange procedure was repeated for three more times followed by drying and calcination as described above.

Base treatment was performed according the procedure described in the literature,[19,20] using a NaOH solution (0.2 M for La-USY-L15, La-USY-L30 and La-USY-L360; 0.5 M for La-USY-0.5L30), with a base to zeolite ratio of 20 ml/g. The solution was continuously stirred with 200 rpm at 348 K for different treatment times (La-USY-LX; X=15, 30, 360 min). Afterwards the zeolite was filtered and washed several times with bi-distilled water. In order to remove remaining sodium, two additional ammonium exchange procedures in the presence of 0.5 M NH_4NO_3 solution with NH_4NO_3 to zeolite ratio of 50 ml/g were carried out. The solution was continuously stirred with a stirring rate of 400 rpm at 353 K for 1 h. After each ion-exchange step, the material was filtered, washed.[21] Finally, the samples were dried at 373 K over 4 h and calcined in a flow of air (200 ml/min) with a heating rate 10 K min^{-1} up to 773 K (4 h). After rehydration, one lanthanum ion-exchange step as described above was applied.

5.2.2. Physicochemical characterization

The aluminum, silicon and sodium contents of the synthesized materials were determined by means of atomic absorption spectroscopy using a Solaar M5 Dual Flammen-Graphitrohr AAS (ThermoFisher) spectrometer. The lanthanum content of the sample was determined by inductively coupled plasma – optical emission spectroscopy (ICP-OES) with SpectroFlame Typ FTMOA81A ICP-OES spectrometer from Spectro-Analytical Instruments.

Nitrogen physisorption isotherms were obtained by using a PMI automate sorptometer. The apparent surface area was calculated by applying the Brunauer–Emmett–Teller (BET) theory to the adsorption isotherms over a relative pressure range from 0.01 to 0.09.[22] The micropore volumes of used materials were calculated using the t-plot method according to Halsey.[23] The mesopore volumes were determined by the cumulative pore volume of pores with diameters ranging from 2 – 50 nm according to the BJH method.[23]

The crystallinity of the synthesized and modified samples was determined by powder X-ray diffraction on a Philips X'Pert Pro System (CuKα1-radiation, 0.154056 nm) at 40 kV / 45 mA diffractometer. Diffractograms were recorded from 5 to 75° 2Θ with a step size of 0.033°. The cell size dimension was calculated from the X-ray diffraction pattern of the zeolite mixed with 5 % of silicon using the silicon reflection as reference.[24] The relative crystallinity of synthesized faujasite materials was compared with the crystallinity of corresponding parent materials. For that, the intensity of eight peaks was evaluated according to the ASTM method D3906-03.[25,26] In order to evaluate the loss in crystallinity of the synthesized samples, the crystallinity of the starting material (H-USY) was considered to be 100 %.

For the determination of the Lewis and Brønsted acid sites concentration, IR spectra of adsorbed pyridine were measured using *Thermo Nicolet 5700 FT-IR* spectrometer in the transmission-absorption mode between 400 and 4000 cm^{-1} with a resolution of 4 cm^{-1}. The total concentration of acid sites was determined at 423 K after evacuating for one hour to remove physisorbed pyridine. Strong Lewis and Brønsted acid sites are classified to retain pyridine for 0.5 h at 723 K. For quantification the molar extinction coefficient (0.73 for Brønsted acid sites and 0.96 for Lewis acid sites) determined by a combination of microgravimetric measurements and infrared spectroscopic measurements of adsorbed pyridine, was used.

^{27}Al MAS NMR measurements were performed on a Bruker AV500 spectrometer (B_0 = 11.7 T) with a spinning rate of 12 kHz. The samples were fully hydrated before packing them into a 4 mm ZrO_2 rotor. In each case, single pulse ^{27}Al MAS NMR spectra were obtained by 2400 scans recorded with a recycle time of 0.25 s and an excitation pulse length (π/12-pulse) of 0.46 µs. The chemical shifts in all the recorded spectra are reported relative to an external standard of solid $Al(NO_3)_3$ (δ = -0.54 ppm). Samples prepared for ^{1}H MAS NMR measurements were activated in vacuum at 723 K for 15 h and afterwards packed in a 4 mm ZrO_2 rotor under nitrogen atmosphere. ^{1}H MAS NMR measurements were performed using a 90° excitation

pulse (3.8 µs) applied by a recycle time of 40 s. The chemical shift (δ = 1.78 ppm) of adamantane ($C_{10}H_{16}$; high symmetric cycloalkane) was used as standard for calibration. MFI zeolite containing 0.360 mmol H^+/g was selected as standard for the quantification of the experimental results.

The structure and particle size was studied with scanning electron microscopy (SEM) (JEOL JSM-5900LV) by analyzing the Au-sputtered samples at an acceleration voltage of 25 kV.

The influence of the alkaline treatment on the pore structure of the samples was analyzed with JEOL JEM-2010 transmission electron microscope at 120 kV. The pre-reduced catalyst samples were ground suspended in ethanol and ultrasonically dispersed. One drop of this suspension was placed on a copper grid with holey carbon film.

5.2.3. Isobutane/2-butene alkylation reaction

The alkylation reaction of isobutane and 2-butene was conducted in a 50 ml CSTR reactor (Autoclave Engineers) at 348 K and 25 bar.[10,17] The used olefin space velocity was 0.2 g_{butene} $g^{-1}_{catalyst}$ h^{-1}.[10] To avoid olefin addition on formed octane isomers before hydride transfer occurs, an isobutane to 2-butene ratio of 10/1 was used. The purity of isobutane was 99.9 % and 99.5 % for 2-butene, respectively. To provide optimized mixing conditions a Mahoney-Robinson spinning basket reactor (1600 min^{-1}) was used. All the catalysts were activated in situ in H_2 with a increment of 2 K min^{-1} up to 393 K for 4 h and up 453 K for further 14 h. The product distribution was analyzed online using a 50 m HP-1 column (ID = 0.32 mm, film = 0.52 µm) in a HP6890 gas chromatograph equipped with an FID detector.

5.3. Results

5.3.1. Characterization

The results of the physicochemical characterizations are shown in Table 5.1:

Table 5.1: Physicochemical properties of studied materials

	H-USY	**La6.67%-USY**	**La-USY-L15**	**La-USY-L30**	**La-USY-L360**	**La-USY-0.5L30**
Chemical composition [mmol/g]						
Si	10.50	7.97	8.93	7.59	6.45	7.47
Al	3.38	2.62	2.78	3.20	3.27	3.44
Na	0.18	0.05	0.06	0.05	0.08	0.12
La	-	0.48	0.45	0.41	0.47	0.50
Si/Al ratio	3.11	3.04	3.21	2.37	1.97	2.17
BET						
BET surface area [m^2/g]	759	726	736	730	720	734
Micropore volume [cm^3/g]	0.28	0.26	0.28	0.27	0.27	0.28
Mesopore volume [cm^3/g]	0.04	0.06	0.06	0.06	0.05	0.06
XRD						
Unit cell size [nm]	2.46	2.45	2.45	2.46	2.45	2.46
Relative Crystallinity [%]	100	52.97	51.72	52.44	50.69	49.61

As shown in Table 5.1, the lanthanum ion-exchange (at pH 6) led to a decrease in the aluminum concentration, whereas the alkaline treatment caused a loss of the framework silicon at longer treatment times, i.e., a significant decrease in the Si/Al ratio of USY was observed at prolonged alkaline treatment times. The lanthanum concentration was found to be similar (0.41 – 0.50 mmol/g) for all studied materials. The main differences between the materials listed in Table 5.1 are found in the number of repetitive ion-exchange steps required for the incorporation of identical lanthanum concentrations. For the La6.67%-USY sample, three additional ion-exchange steps were required in order to introduce the same lanthanum

concentration compared to the alkaline-treated USY material, where just a single ion-exchange step was required.

The BET surface area decreased slightly with lanthanum exchange (H-USY = 759 m^2/g, La6.67%-USY = 726 m^2/g), while alkaline treatment resulted in a minor increase of the BET surface area for short treatment times (La-USY-L15 = 736 m^2/g, La-USY-L30 = 730 m^2/g). At longer treatment time, a slight decrease of the surface area was observed (La-USY-L360 = 720 m^2/g). The micropore volume was affected neither by lanthanum incorporation nor by alkaline treatment (0.26 cm^3/g – 0.28 cm^3/g). Mesopore volumes increased following lanthanum exchange, while significant changes were not observed after alkaline treatment, most probably due to the silica removed from the zeolitic lattice, which remained in the pore system hindering the further increase in the mesopore volume.

As the XRD measurements exhibited, the unit cell size was not influenced by lanthanum ion-exchange and performed alkaline treatments. However, a gradual decrease in the crystallinity of the samples was observed by treating the samples with more concentrated alkaline solutions at longer contacting times. Moreover, parts of the structure (crystalline silicon debris) were destroyed in alkaline solution and washed out from the zeolitic pores. Relevant X-ray diffractograms of the studied ultra-stable zeolite Y are shown in Figure B 1.

IR spectroscopy of adsorbed pyridine indicated a decrease in the concentration of all Brønsted acid sites, while the concentration of Lewis acid sites increased for La^{3+} ion-exchanged samples. The concentration of strong Brønsted acid sites and strong Lewis acid sites remained unchanged for all the materials following the synthesis procedure described above, whereas the SBAS to SAS ratio stayed constant. A significant increase in the IR band corresponding to Si-OH stretching vibration at 3730 – 3736 cm^{-1} was observed for all the samples following alkaline treatment (see Fig. B 2 c-f). Furthermore, no changes on the bridging OH-groups in the zeolitic lattice were evidenced for the synthesized samples. All the studied ultra-stable zeolite Y materials showed two different IR bands corresponding to Lewis acid sites (EFAl at 1454 cm^{-1} and La-OH at 1446 cm^{-1}). Extended alkaline treatment times and higher base concentration increased the concentration of accessible La-OH species incorporated in the FAU supercages (see Fig. B 2 c-f). The quantitative determination of the different species is summarized in Table 5.2. These results are in good agreement with the ^1H MAS NMR results (Table 5.4).

Table 5.2: Brønsted (BAS) as well as Lewis (LAS) acid site concentration determined by infrared spectroscopy of adsorbed pyridine. Activation for 1 h at 723 K in vacuum. Adsorption at 0.1 mbar, outgassing for 1 h, all measurements were performed at 423 K. SBAS and SLAS are defined to retain pyridine at 723 K for 0.5 h

IR of ads. Pyridine [mmol/g]	**H-USY**	**La6.67%-USY**	**La-USY-L15**	**La-USY-L30**	**La-USY-L360**	**La-USY-0.5L30**
BAS	1.00	0.78	0.81	0.86	0.70	0.77
LAS	0.44	0.52	0.56	0.89	0.72	0.57
SBAS	0.51	0.50	0.47	0.71	0.55	0.60
SLAS	0.30	0.27	0.26	0.44	0.37	0.30
SLAS corresponding to La-OH	-	0.15	0.09	0.23	0.22	0.13
SLAS corresponding to EFAL	-	0.12	0.17	0.21	0.15	0.17
SBAS/SAS ratio	0.63	0.65	0.64	0.62	0.60	0.67

The scanning electron micrographs (Figure 5.1 a-c) showed that particle size and particle surface was not altered by La^{3+} ion-exchange procedure and alkaline treatment.

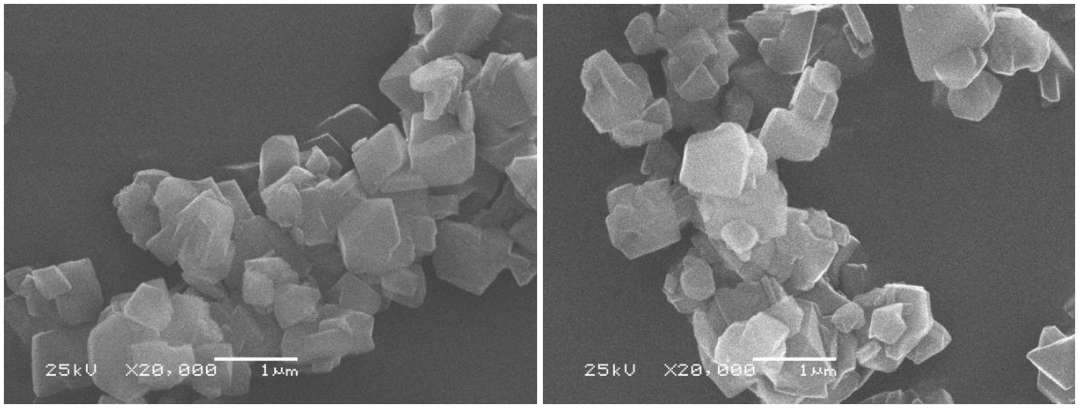

Figure 5.1 a: Scanning electron micrographs of H-USY (left) and La6.67%-USY (right)

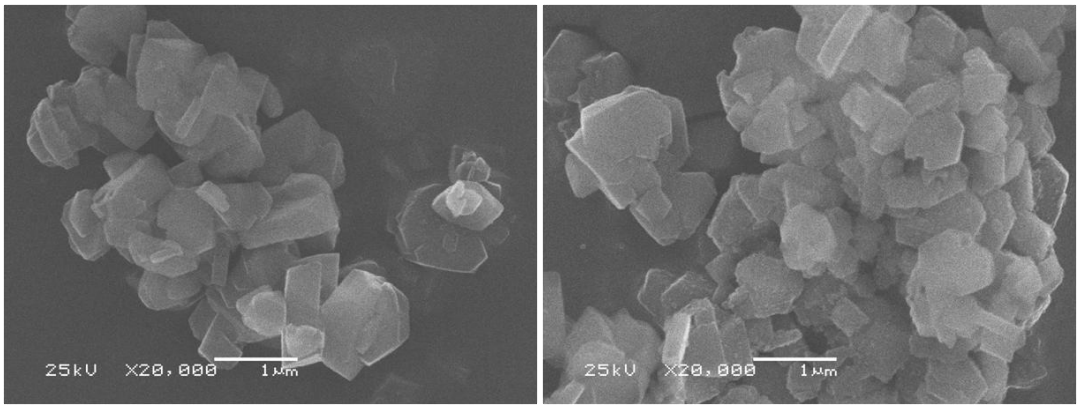

Figure 5.1 b: Scanning electron micrographs of La-USY-L15 (left) and La-USY-L30 (right)

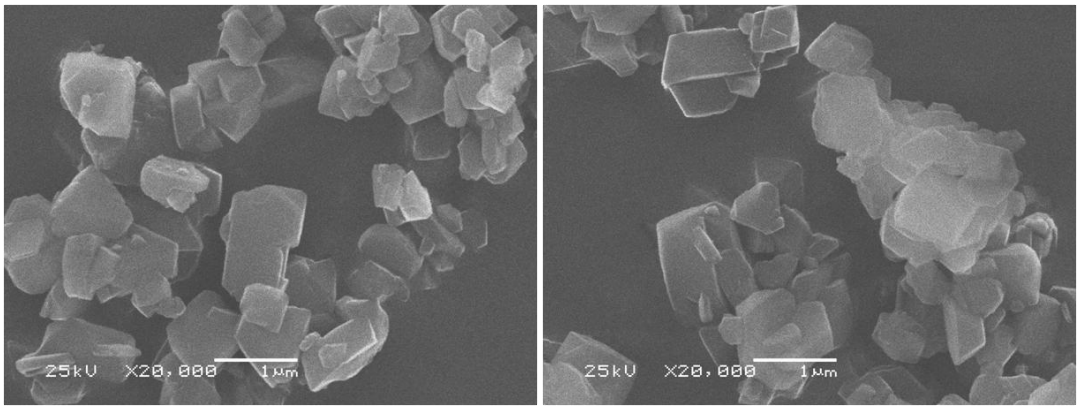

Figure 5.1 c: Scanning electron micrographs of La-USY-L360 (left) and La-USY-0.5L30 (right)

The transmission electron micrographs (Figure 5.2 a-f) indicate significant changes of the surface morphology after the ion-exchange procedures or alkaline treatment. Note that the parent material shows well defined edges, while these were more irregular structured and showed several fissures for La6.67%-USY. La6.67%-USY also showed variations in the thickness and strong unevenness of a surface layer. For La-USY-L15 and La-USY-L30 this was even more distinctive. For La-USY-L360 and La-USY-0.5L30, however, the surface of the materials did not change further.

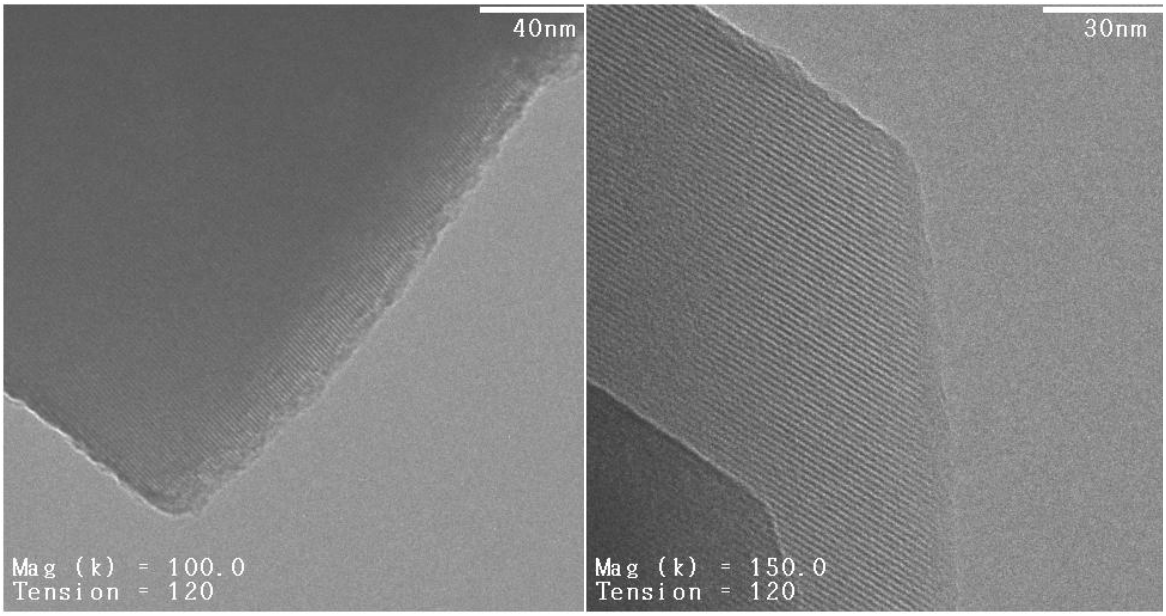

Figure 5.2 a: Transmission electron micrographs of H-USY

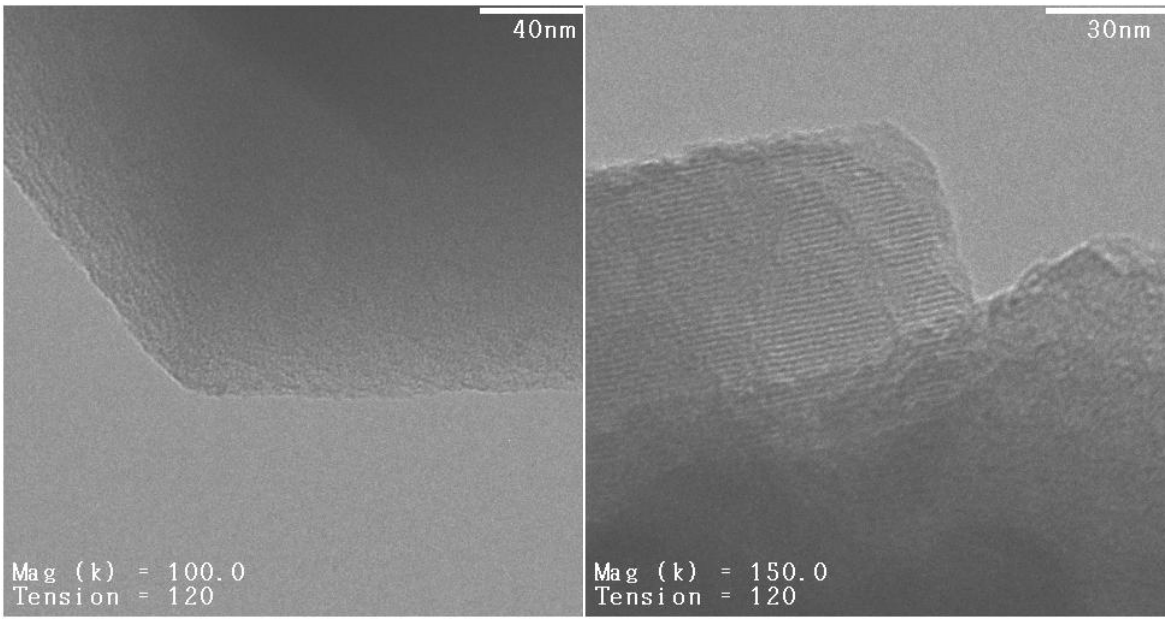

Figure 5.2 b: Transmission electron micrographs of La6.67%-USY

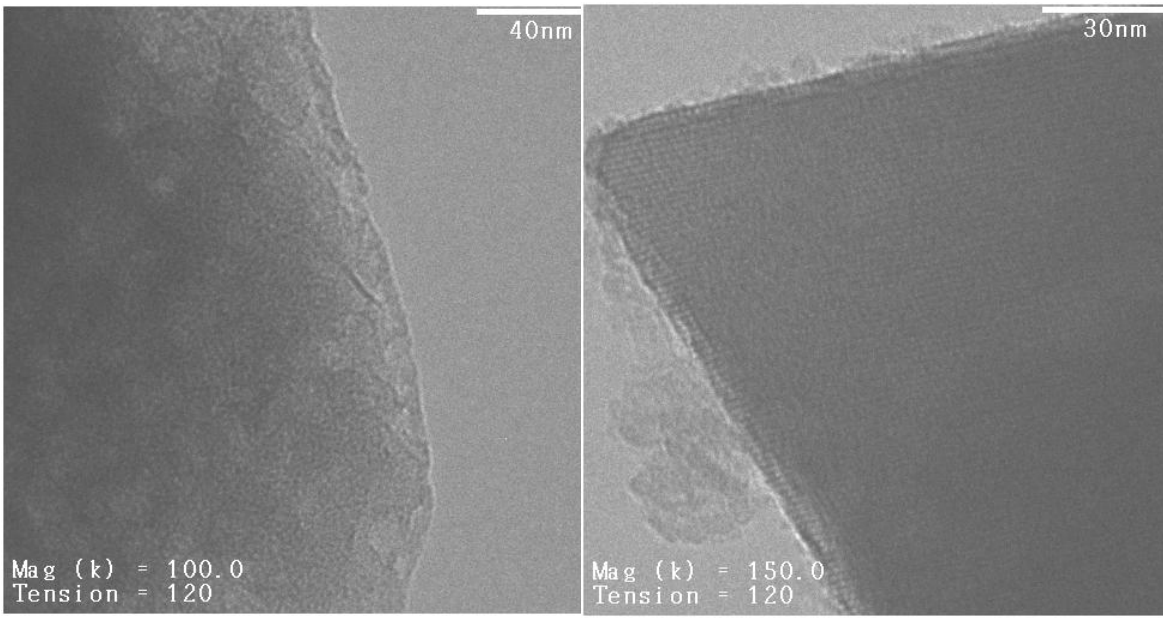

Figure 5.2 c: Transmission electron micrographs of La-USY-L15

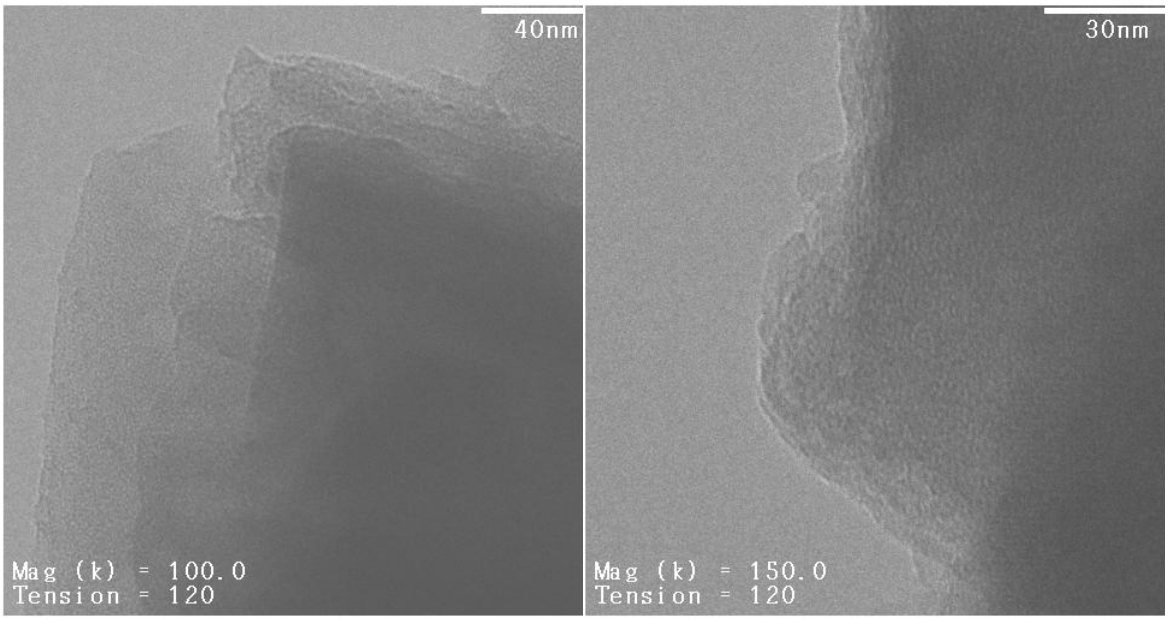

Figure 5.2 d: Transmission electron micrographs of La-USY-L30

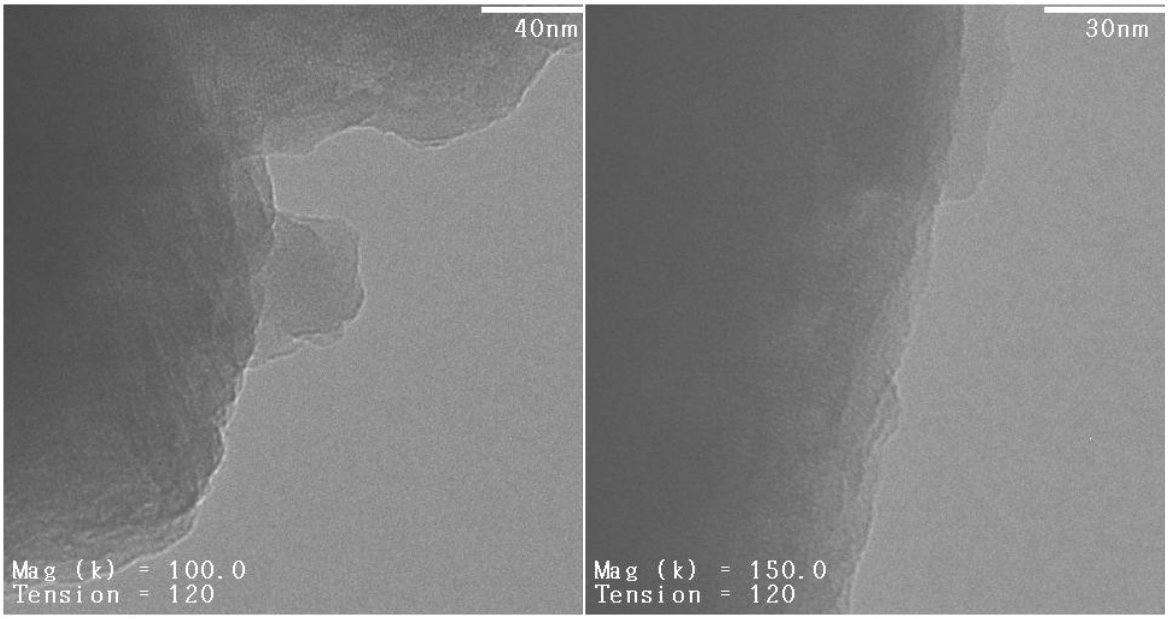

Figure 5.2 e: Transmission electron micrographs of La-USY-L360

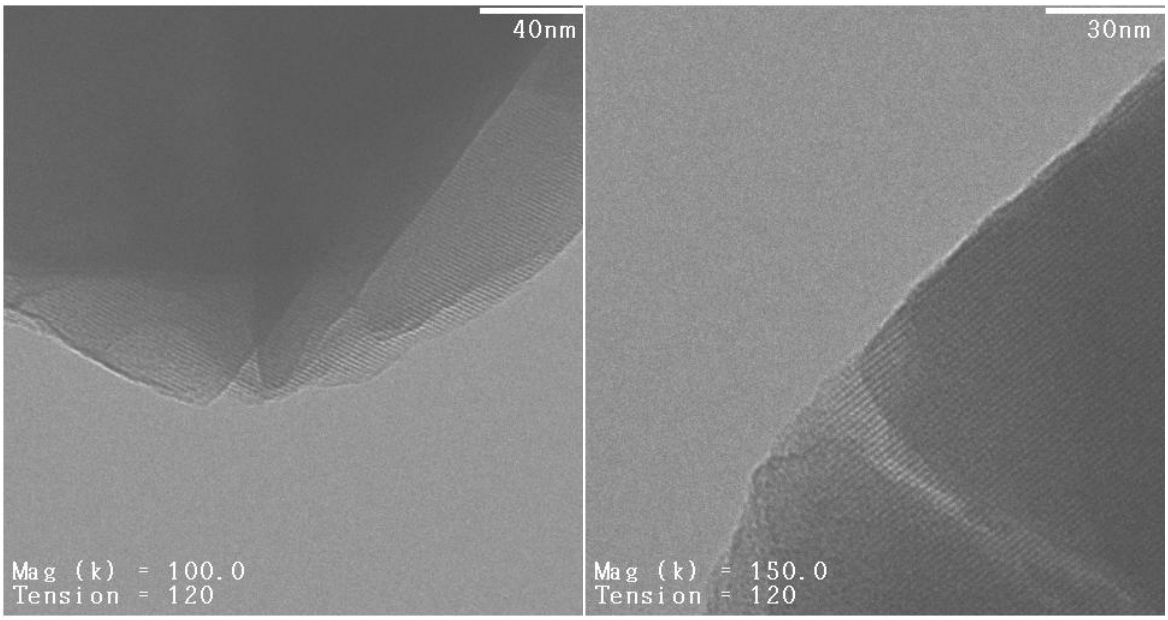

Figure 5.2 f: Transmission electron micrographs of La-USY-0.5L30

^{27}Al MAS NMR spectroscopic measurements were performed in order to study the influence of the ion-exchange and alkaline treatments on the tetrahedral framework aluminum (60-40 ppm) and octahedral coordinated aluminum (about 0 ppm), the latter corresponding to extra-framework aluminum (EFAl). Typical spectra of the studied materials are shown in Figure 5.3 and the data are summarized in Table 5.3. La^{3+} exchange led to a significant decrease in the concentration of EFAl-species, whereas alkaline treatment performed at different base concentrations and treatment times did only marginally influence EFAl (Figure 5.3 a-f and Table 5.3).

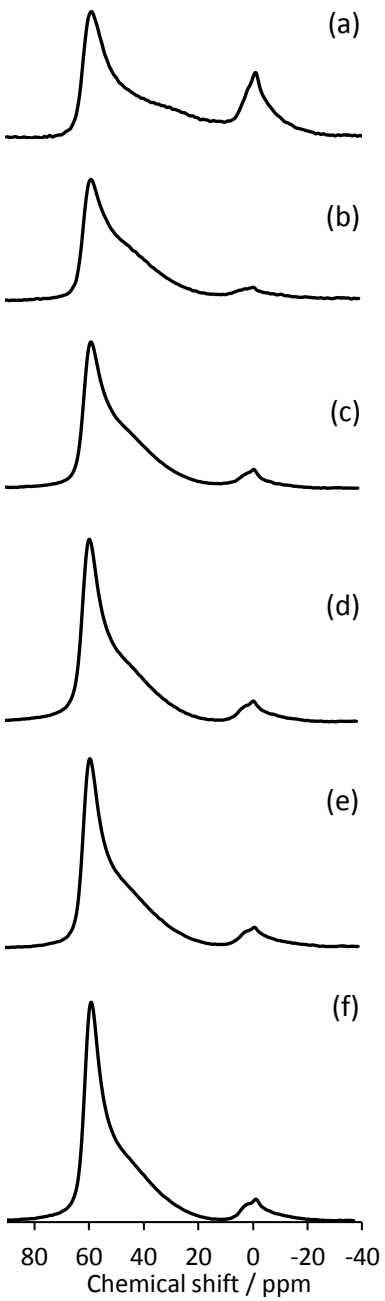

The sharp peak at 58 – 60 ppm, corresponding to the tetrahedral framework aluminum in close proximity to protons or sodium,[27] was not influenced by the La^{3+} exchange. An apparent increase in the tetrahedral framework aluminum concentration was observed with the lanthanum exchanged as well as alkaline treated materials. The increasing intensity of the peak corresponding to tetrahedrally coordinated aluminum and the parallel decrease of the signal intensity at 0 ppm indicate that EFAl-species were most probably dissolved and reinserted into zeolitic framework in a tetrahedral coordination environment.[28] A more pronounced increase in the concentration of the reinserted framework Al species was observed following the alkaline treatment at higher base concentration.

The peak at approximately 50 ppm represents framework aluminum in the vicinity of lanthanum cations.[29] This signal in the NMR spectra increased for La^{3+} exchanged materials, while it was unchanged for the alkaline treated samples.

Figure 5.3: ^{27}Al MAS NMR spectra of a) H-USY, b) La6.67%-USY, c) La-USY-L15, d) La-USY-L30, e) La-USY-L360, f) La-USY-0.5L30

Table 5.3: Tetrahedral and octahedral coordinated aluminum determined by ^{27}Al MAS NMR

Catalyst	H-USY	La6.67%-USY	La-USY-L15	La-USY-L30	La-USY-L360	La-USY-0.5L30
Framework Al [%]	75.1	88.8	90.1	88.2	87.5	92.9
EFAl [%]	24.9	11.2	9.9	11.8	12.5	7.1
Framework Al [mmol/g]	2.54	2.33	2.50	2.82	2.86	3.20
EFAl [mmol/g]	0.84	0.29	0.28	0.38	0.41	0.24

The summary of the detailed ^{1}H MAS NMR structural study of the zeolitic materials is shown in Table 5.4. The total concentration of bridging OH groups in USY determined by ^{1}H MAS NMR measurements were much higher compared to results from IR spectra of adsorbed pyridine. As the kinetic diameter of pyridine is 0.6 nm,[30] the molecule is not able to enter the six-membered ring window (0.25 nm) of the faujasite sodalite cages. In case of all lanthanum ion-exchanged materials, the total concentration of bridging OH-groups determined by ^{1}H MAS NMR was lower compared to the results of IR spectra of adsorbed pyridine. These differences might originate from the different coordination mode of La^{3+} cations in the zeolitic materials and needs further investigation. For the alkaline treated materials, a decrease in the concentration of bridging OH-groups located in large cavities was observed. All alkaline treated materials evidenced the presence of less La-OH groups, indicating the different coordination environment of the incorporated lanthanum cations, as shown in Table 5.4. The SiOH concentration was marginally increased with performed lanthanum exchange and alkaline treatment while the AlOH concentration decreased by performed alkaline treatments.

Table 5.4: Concentration of hydroxyl groups in zeolite materials determined by ^{1}H MAS NMR

Catalyst	LaOH		Bridging OH				AlOH		SiOH	
			Small cavities		Large cavities					
	[ppm]	[mmol/g]	[ppm]	[mmol/g]	[ppm]	[mmol/g]	[ppm]	[mmol/g]	[ppm]	[mmol/g]
H-USY	-	-	4.7	0.67	3.8	1.6	2.5	0.81	1.7	0.00
La6.7%-USY	6.0	0.29	4.5	0.21	3.9	0.43	2.7	0.96	1.7	0.14
La-USY-L15	6.0	0.14	4.6	0.27	3.9	0.29	2.7	0.63	1.8	0.14
La-USY-L30	6.0	0.15	4.6	0.31	3.9	0.35	2.7	0.63	1.8	0.13
La-USY-L360	5.9	0.16	4.6	0.20	3.8	0.26	2.7	0.56	1.9	0.12
La-USY-0.5L30	5.9	0.19	4.5	0.24	3.8	0.24	2.7	0.72	1.8	0.12

5.3.2. Catalytic performance

Alkylation of isobutane/2-butene

Isobutane/2-butene alkylation was performed in a CSTR reactor using high back-mixing ratio of isobutane/2-butene of 10. The 2-butene conversion was selected as benchmark for the catalyst activity under operating conditions.

The parent ultra-stable zeolite Y showed just a moderate stability under operating conditions, i.e., deactivation already starts after five hours. The incorporation of lanthanum cations significantly resulted in an improved catalyst lifetime. The lifetime of the synthesized La6.67%-USY was considerably higher (stable over eight hours) compared to the parent material. A further extension of the catalyst lifetime was achieved by short time alkaline treatment in case of La-USY-L15, while after longer treatment the catalyst lifetime decreased again (see Table 5.5). It is noteworthy, that among the studied zeolite materials, the alkaline treated zeolites had the longest catalyst lifetime.

The product fractions are classified as C_{5-7}, C_8 and C_{9+}. The C_{5-7} fraction contains cracking products, while the C_{9+} fraction consists of oligomerization products. Selectivity to 2,2,3-TMP, the primary alkylation product, as well as 2,3,3-TMP, 2,2,4-TMP and 2,3,4-TMP was used to characterize hydride transfer. A schematic representation of the alkylation reaction mechanism accounting for the protonation of 2-butene, hydride abstraction, alkene addition and hydride transfer is illustrated in Figure 5.4.

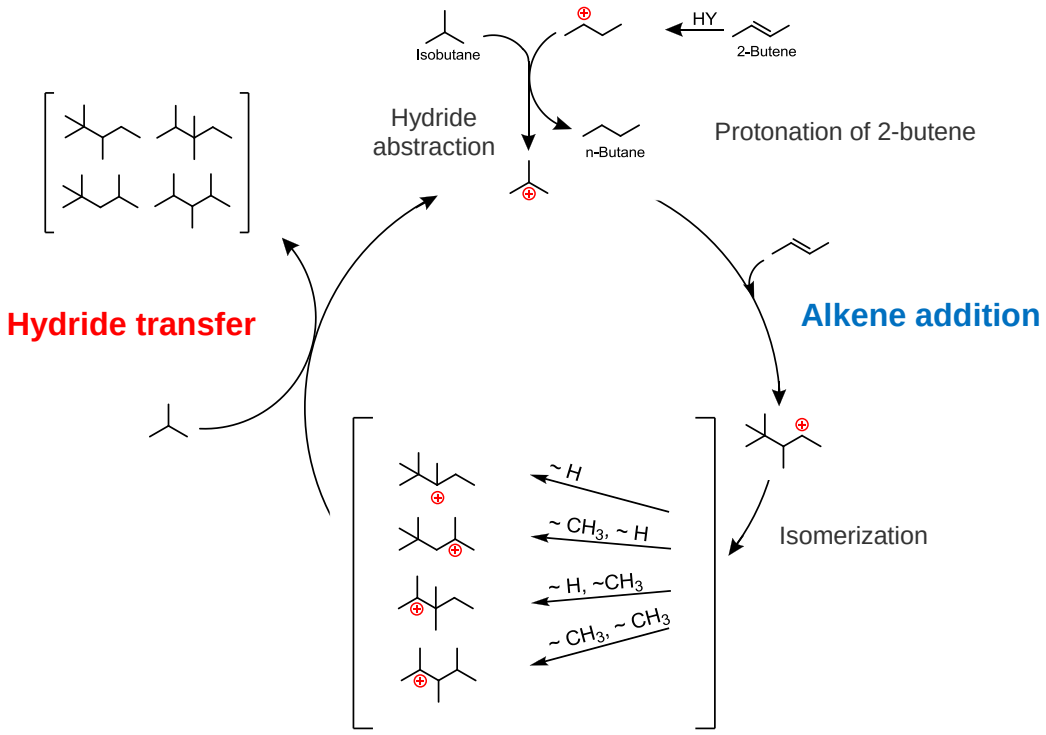

Figure 5.4: Alkylation reaction cycle of isobutane/2-butene

La^{3+} exchange doubled the C_8 fraction (H-USY: 1.69 g, La6.67%-USY: 3.36 g). The highest yield of C_8 (5.54 g) was found with La-USY-L15. Prolonged alkaline treatment, however, led to a significant decrease in the alkylation product formation, as illustrated in Table 5.5 and Figure 5.5.

Table 5.5: Catalyst lifetime study and product distribution in isobutane/2-butene alkylation reaction on USY type zeolites*

	Lifetime [h]	Products [g]	C_{5-7} [g]	C_8 [g]	C_{9+} [g]
H-USY	5	2.36	0.26	1.69	0.41
La6.67%-USY	8	4.68	0.54	3.36	0.78
La-USY-L15	16	7.78	0.83	5.54	1.41
La-USY-L30	12	6.63	0.78	4.79	1.06
La-USY-L360	10	5.90	0.64	4.30	0.96
La-USY-0.5L30	10	5.17	0.57	3.75	0.85

* Activation procedure: in situ in H_2, 4 h at 393 K and 14 h at 453 K, heating ramp: 2 K min^{-1}. Reaction conditions: reaction temperature = 348 K, isobutane/2-butene = 10, OSV = 0.2 g_{butene} $g^{-1}_{catalyst}$ h^{-1}, rpm = 1600 min^{-1}

It is important to note that the formation of cracking (C_5 – C_7) and oligomerization products (C_{9+}) varied in parallel the alkylation products. Shorter alkaline treatment times resulted in a significant increase in the catalytic activity and lifetime of the synthesized materials while at prolonged treatment times a less stable material was obtained.

In the presence of La6.67%-USY two times as much (0.54 g) cracking product was produced than in the case of H-USY (0.26 g). However, the highest amount of cracking products (0.83 g) was obtained in the presence of La-USY-L15, while lower amounts of the C_5 – C_7 products were obtained for La-USY-L30 (0.78 g) followed by La-USY-L360 (0.64 g). The lowest amounts of cracking products (0.57 g) were isolated in the presence of La-USY-0.5L30.

The yield of oligomerization products varied analogously. It was enhanced in the presence of La-USY-L15 (1.41 g), while La6.67%-USY (0.78 g), La-USY-L30 (1.06 g) and La-USY-L360 (0.96 g) led to lower yields of C_{9+}. The lowest amount of oligomerization products (0.85 g) was isolated in the presence of La-USY-0.5L30 when the highest base concentration was applied for the alkaline-treatment of the parent material.

The selectivity of 2,2,3-TMP, 2,2,4-TMP, 2,3,4-TMP and 2,3,3-TMP was used as indicator for the hydride transfer ability of the catalysts. The hydride transfer ability is best described by the change of the 2,2,3-TMP selectivity, as this is the primary product, which is further converted to other TMPs via methyl-shift reactions.[9,10] As the yield of 2,2,3-TMP cannot be separated from the yield of 2,5-dimethylhexane (DMH), the variation of the selectivity of DMH and methylheptanes (MHp) will be discussed. As shown in Table 5.6, the selectivity towards MHps

is not influenced by La^{3+} ion-exchange and alkaline treatment and varies between 1.03 % and 1.28 %.

Lanthanum exchange and alkaline treatment had only minor influence on the selectivity towards DMHs. The selectivity to 2,3-DMH and 3,4-DMH was similar for all materials used. La^{3+} ion-exchange increased the selectivity towards 2,4-DMH from 2,49 % (H-USY) to 3.63 % (La6.67%-USY). Alkaline treatment did hardly influence the 3,4-DMH formation. A slight decrease was noticeable only for La-USY-0.5L30.

The formation of $C_{8=}$ products was lower for the lanthanum incorporated and alkaline treated materials. Long alkaline treatment times and a high base concentration increased the amount of $C_{8=}$ formed.

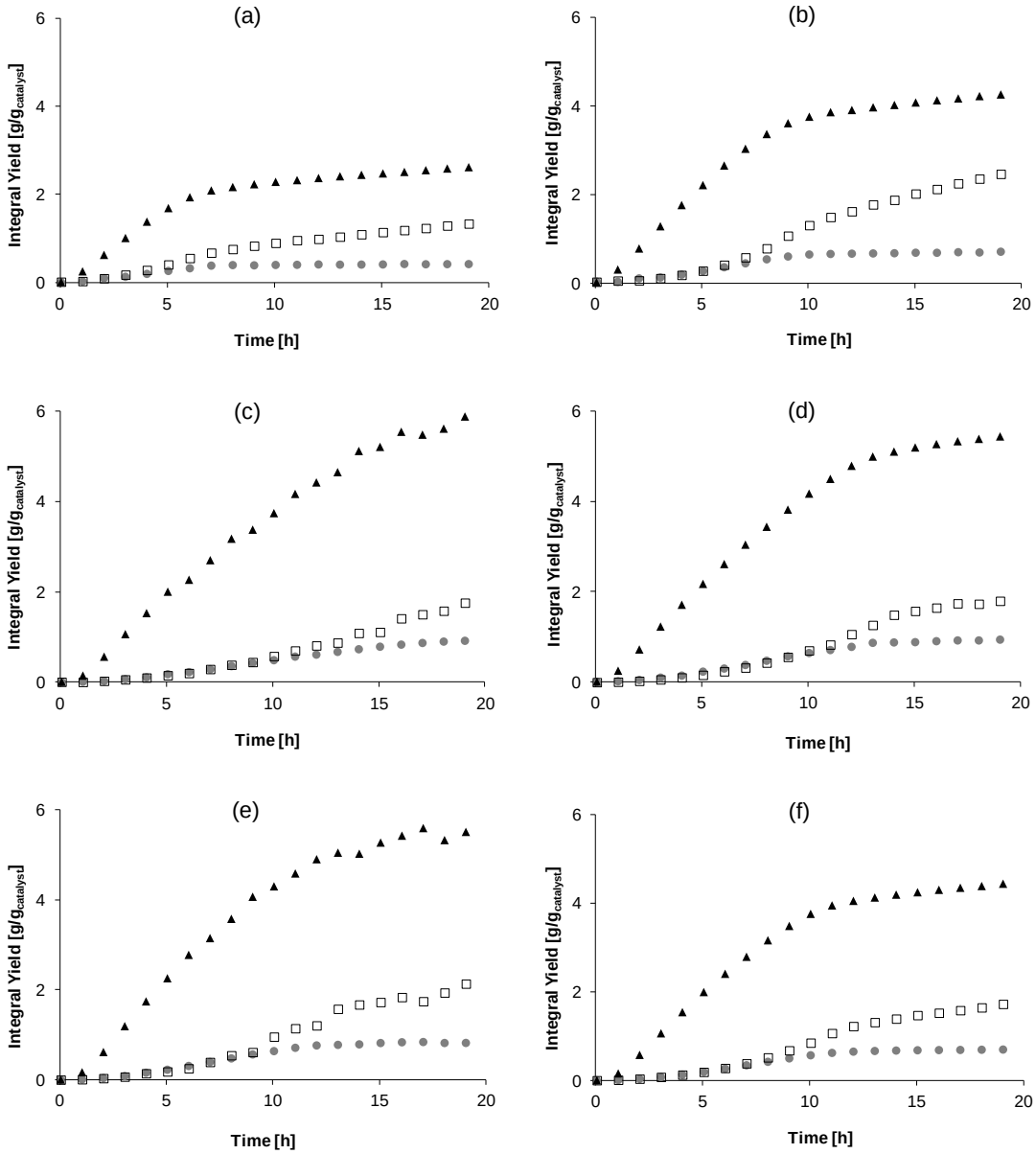

Figure 5.5: Integral product yield of C_5-C_7 (●), C_8 (▲) and C_{9+} (□) over H-USY (a), La6.7%-USY (b), La-USY-L15 (c), La-USY-L30 (d), La-USY-L360 (e) and La-USY-0.5L30 (f). Activation procedure: in situ in H_2, 4 h at 393 K and 14 h at 453 K, heating ramp = 2 K min^{-1}. Reaction conditions: reaction temperature = 348 K, isobutane/2-butene = 10, OSV = 0.2 g_{butene} $g^{-1}_{catalyst}$ h^{-1}, rpm = 1600 min^{-1}

Table 5.6: DMH and MHp formation in the solid acid catalyzed isobutane/2-butene alkylation. Activation procedure: in situ in H_2, 4 h at 393 K and 14 h at 453 K, heating ramp = 2 K min^{-1}. Reaction conditions: reaction temperature = 348 K, isobutane/2-butene = 10, OSV = 0.2 g_{butene} $g^{-1}_{catalyst}$ h^{-1}, rpm = 1600 min^{-1}

Selectivity	H-USY [%]	La6.67%-USY [%]	La-USY-L15 [%]	La-USY-L30 [%]	La-USY-L360 [%]	La-USY-0.5L30 [%]
2,4-DMH	2.49	3.63	3.56	3.79	3.46	3.16
2,3-DMH	5.35	5.50	5.38	5.31	5.25	5.29
2-MHp	0.01	0.21	0.21	0.22	0.17	0.12
4-MHp (3,4-DMH)	0.92	0.84	0.87	0.77	0.79	0.85
3,4-DMH (4-MHp)	0.71	0.97	0.88	0.93	0.90	0.77
3-MHp	0.10	0.19	0.20	0.22	0.19	0.17
$C_{8=}$	0.69	0.49	0.35	0.38	0.41	0.62
Σ DMH	8.55	10.10	9.82	10.03	9.61	9.22
Σ MHp	1.03	1.24	1.28	1.21	1.15	1.14

As summarized in Table 5.7, the change in catalyst selectivity towards 2,2,3-TMP/2,5-DMH formation is mainly determined by the alteration of the selectivity for 2,2,3-TMP. La^{3+} exchanged La6.67%-USY showed an increased selectivity of 8.15 % towards the 2,2,3-TMP formation in comparison with the parent material H-USY of 5.94 %. Higher selectivity to 2,2,3-TMP was also achieved for alkaline treated materials La-USY-L15, La-USY-L30, but slightly lower selectivity toward 2,2,3-TMP was observed for La-USY-L360 and La-USY-0.5L30 catalysts under the same experimental conditions.

All the studied solid acid catalysts showed a similar variations in the catalyst selectivity toward 2,2,4-TMP and 2,2,3-TMP formation, while exactly the opposite was observed for 2,3,3-TMP and 2,3,4-TMP, the main products formed following methyl-shift-isomerization.

Table 5.7: Selectivity of TMPs formed in solid acid catalyzed isobutane/2-butene alkylation. Activation procedure: in situ in H_2, 4 h at 393 K and 14 h at 453 K, heating ramp = 2 K min^{-1}. Reaction conditions: reaction temperature = 348 K, isobutane/2-butene = 10, OSV = 0.2 g_{butene} $g^{-1}_{catalyst}$ h^{-1}, rpm = 1600 min^{-1}

Selectivity	H-USY [%]	La6.67%-USY [%]	La-USY-L15 [%]	La-USY-L30 [%]	La-USY-L360 [%]	La-USY-0.5L30 [%]
2,2,4-TMP	20.80	27.68	27.58	29.31	26.91	25.04
2,2,3-TMP / 2,5-DMH	5.94	8.15	8.51	9.07	8.27	7.48
2,3,4-TMP	29.37	21.23	21.13	19.99	21.42	23.00
2,3,3-TMP	33.62	31.11	31.35	30.01	32.23	33.51

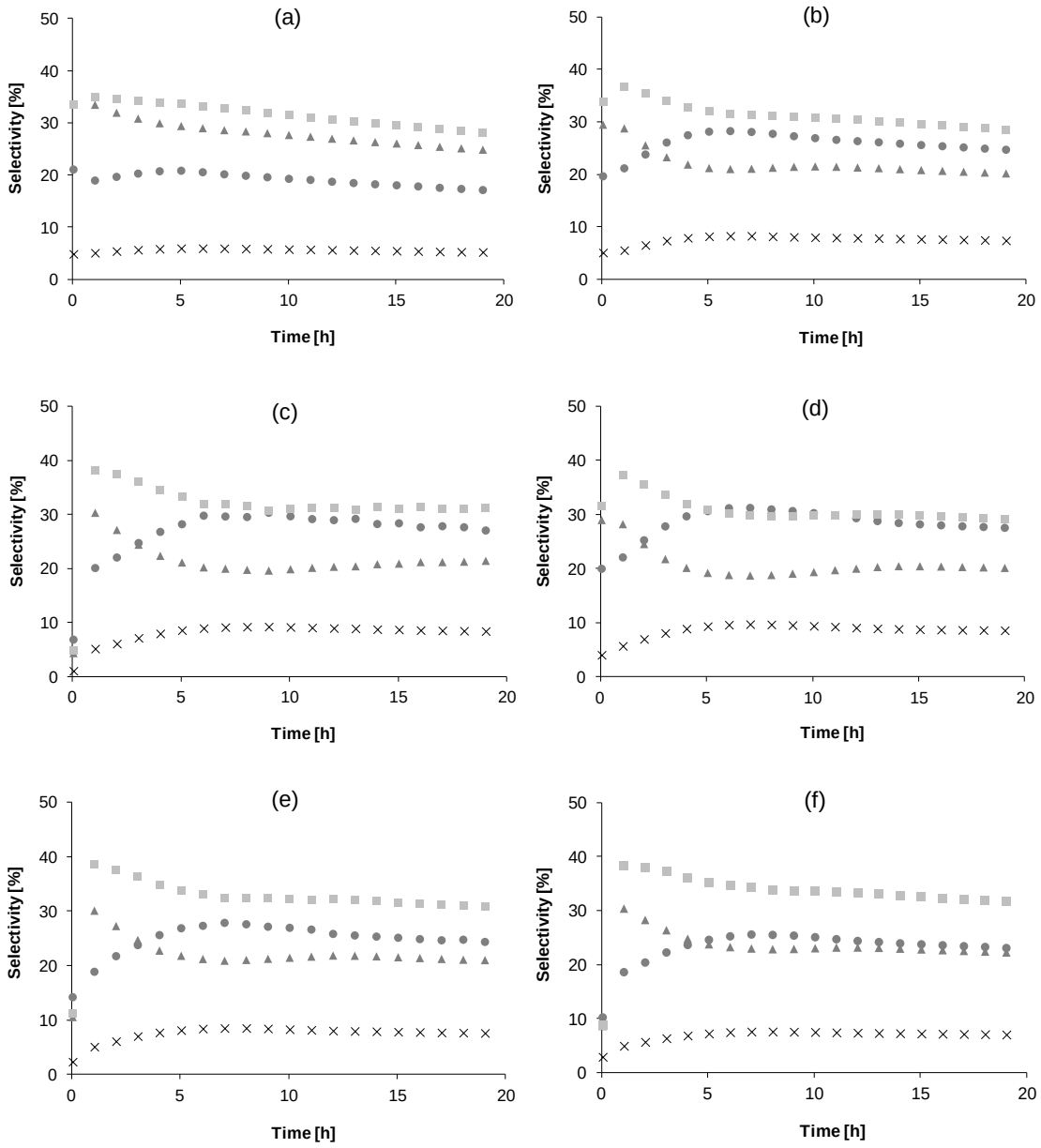

Figure 5.6: Selectivity of 2,5-DMH/2,2,3-TMP (×), 2,2,4-TMP (●), 2,3,3-TMP (■) and 2,3,4-TMP (▲) over H-USY (a), La6.67%-USY (b), La-USY-L15 (c), La-USY-L30 (d), La-USY-L360 (e) and La-USY-0.5L30 (f). Activation procedure: in situ in H_2, 4 h at 393 K and 14 h at 453 K, heating ramp = 2 K min^{-1}. Reaction conditions: reaction temperature = 348 K, isobutane/2-butene = 10, OSV = 0.2 $g_{butene}g^{-1}_{catalyst}h^{-1}$, rpm = 1600 min^{-1}

5.4. Discussion

5.4.1. Influence of alkaline treatment and lanthanum incorporation on physicochemical properties

The outstanding catalytic activity of alkaline treated La^{3+} ion-exchanged faujasites more than justifies the study on the complex structure and physicochemical properties of the ultra-stable zeolitic materials. In this study, different alkaline treatment times (up to 360 minutes) and base concentrations (0.2 - 0.5 M of NaOH) were used to prepare a series of La^{3+} ion-exchanged USY materials. In contrast to previous studies on high silica containing zeolites,[31-33] alkaline-treatment on low silica containing USY materials had no influence on the mesopore volume. Under alkaline conditions, the removal of SiO_2 improved the interconnection of the zeolitic channels. At prolonged treatment times, significant changes in the structure morphology leading to the appearance of several fissures and variations in the thickness beside the creation of a strong unevenness on the zeolitic surface (see Fig. 5.2 a-f) was observed.

Alkaline treatment of the parent material, led to a significant decrease in the concentration of Na^+ cations, however, it was not possible to completely wash out from the samples even after repeated alkaline treatments with concentrated basic solutions, due to their location in rather inaccessible parts of the zeolitic framework. Moreover, an increase in the Na^+ concentration (see Table 5.1) at extended alkaline treatment times occurred due to the reinsertion of sodium cations into the zeolitic lattice.

High base concentrations along with prolonged alkaline treatment times of high aluminum containing faujasite materials resulted in a substantial decrease of the Si/Al ratio, while at shorter treatment times no relevant changes were observed. Performed ^{27}Al MAS NMR measurements evidenced that over acidic La^{3+} ion-exchange most of the octahedral EFAl species were reinserted as tetrahedral coordinated aluminum species. In concentrated basic solution the reinsertion of EFAl ions became favorable. The removal of the octahedral EFAl out of the zeolitic pore systems is speculated to improve the mass transport inside the zeolitic pores.

Lanthanum incorporation into the non-alkaline treated USY materials led to the formation of $[La(OH)_n]^{(3-n)+}$ cationic species inside the supercages. To introduce the desired amount of lanthanum cations into the FAU supercages, a repetitive ion-exchange was required. The removal of silicon debris during alkaline-treatment increased the aluminum concentration in

the zeolitic framework and facilitated the insertion of La^{3+} ions with different coordination environment. By increasing the number of neighboring aluminum atoms, the number of charge compensating hydroxyl ligands coordinated at the La^{3+} ion decreased, consequently enabling a better accessibility of the reactive centers (reduced sterical hindrance). The improved accessibility of non-hydroxylated La^{3+} species led to a significantly increase of the intrinsic catalytic activity.

The incorporation of La^{3+} cations in the zeolitic framework resulted in a decrease of the total concentration of Brønsted acid sites and a considerable increase of the Lewis acid sites at pH = 6 (see Table 5.2). Lanthanum containing non alkaline-treated USY materials possess a high concentration of Lewis acidic sites due to the presence of EFAl and La-OH species. In alkaline solution, at short treatment times, the concentration of the strong Lewis acidic sites was decreased due to the increased number of neighboring aluminum atoms, enhancing the formation of non-hydroxylated lanthanum species (see Fig. B 2 and Table 5.2). Prolonged alkaline-treatment resulted in an increased number of hydroxylated lanthanum species with a pronounced Lewis acidic character.

The incorporation of La^{3+} ions into extra-framework positions in an optimized pore system improved the reactivity of alkaline treated materials.

5.4.2. Catalyst performance in isobutane/2-butene alkylation

The incorporation of different charge compensating lanthanum species inside the zeolitic framework enables a strong polarization of the hydrocarbon molecule[14] and improves the catalytic activity of the parent material. A further enhancement of the catalyst performance was achieved by performed alkaline-treatments leading to a better accessibility of the reactive sites inside the zeolitic channels.

Short alkaline-treatment of the materials led to the removal of silicon debris from the mesopores and further enhanced the reinsertion of EFAL as well as the incorporation of La^{3+} species resulting in a more active and stable alkylation catalyst (catalyst lifetime up to 16 h). At extended alkaline-treatment times, a considerable increase in the concentration of Lewis acid sites due to the higher fraction of accessible La-OH species caused a more pronounced formation of secondary oligomerization reaction products and a faster deactivation of the catalyst (catalyst lifetime to 10 h) (see Table 5.5).

The C_8 fraction of 2,3,3-TMP, 2,2,4-TMP and 2,3,4-TMP was used as an evidence for the

isomerization ability of the catalyst before the hydride transfer and desorption of Brønsted acid site occurred. Increasing hydride transfer reactions by improved mass transport in lanthanum as well as alkaline-treated materials increase the alkylation to oligomerization ratio and prolonged the catalyst lifetime. Improved mass transport inside the zeolitic material higher the selectivity of the 2,2,3-TMP primary alkylation product and reduces secondary reactions. Oligomerization reactions are facilitated by the isobutane adsorption on the in-situ formed TMP carbenium ion sites prior TMP desorbs and were reduced by increasing mass transport. Increasing alkaline concentration and time removes silicon debris and further attack the zeolite surface leading to a lifetime maximum.

Higher base concentration and longer contacting time lowered the catalyst selectivity toward the primary alkylation product 2,2,3-TMP (La-USY-0.5L30: 7.48 %) due to the significant changes in the inner pore structure by silicon removal of the treated zeolite and the formation of an increased number of interconnections within the zeolite pores. Similar to 2,2,3-TMP, the selectivity for the self-alkylation product (2,2,4-TMP) was changed over the studied materials. Yoo et al. showed that the pore topology plays an important role in the product distribution.[34] According to their study, a strong interconnected pore system promotes the formation of bulkier molecules that block the pores, enhancing the coking process. It was also shown, that an increased number of expansions caused a decrease in the 2,2,4/2,2,3-TMP to 2,3,3/2,3,4-TMP ratio. Similar effects were observed in our work using more intensive base-treatment and at the same time removal of silicon debris. The higher concentration of accessible La-OH species acting as Lewis acid site increases the oligomerization reaction caused by an increased formation of $C_{8=}$ and long-chained C_{9+} by-products that cannot desorb and therefore block the zeolitic pores, leading to a shorter catalyst lifetime. The higher oligomerization product formation lowers the accessibility of active acid sites and therefore the hydride transfer reaction. The hindered hydride transfer reaction consequently increase the selectivity to 2,3,3 and 2,3,4-TMP formed via methyl-shift isomerization in the alkylation reactions performed in the presence of materials exposed to longer alkaline treatment.

5.5. Conclusions

Alkaline-treatment of lanthanum ion-exchanged aluminum rich ultra-stable zeolite Y resulted in the removal of silica and the concomitant formation of a highly reactive and stable catalyst for isobutane/2-butene alkylation. During acidic lanthanum ion-exchange procedure aluminum ions were removed from the octahedral extra-framework positions and partially reinserted into the zeolitic framework upon prolonged alkaline-treatment times. Performed lanthanum ion-exchange and alkaline treatment caused no significant change in the SBAS/SAS ratio, i.e., it did not change the critical chemical parameter influencing the catalyst lifetime.

Alkaline treatment caused on the one hand a significant change in the surface morphology, whereas at long alkaline-treatment times, the inner pore structure was affected. We assume that a similar effect as described by Yoo et al.[34] is responsible for the product formation inside the zeolitic pores. Increasing hydride transfer ability through improved mass transport in alkaline-treated and lanthanum ion-exchanged materials increased the alkylation to oligomerization product ratio and improved the catalyst stability. For the samples exposed at extended alkaline-treatment times, the increased concentration of Lewis acid sites promoted the formation of C_{9+} leading to more accentuated cocking processes and, therefore, to a faster deactivation of the catalyst. These two processes are opposing, what results in the observed lifetime maximum for short alkaline-treated zeolitic materials. A decreasing 2,2,4/2,2,3-TMP to 2,3,3/2,3,4-TMP ratio observed for extended alkaline-treated samples, supports the theory of Yoo et al. Short alkaline-treatments of ultra-stable zeolite Y followed by the incorporation of lanthanum-ions led to the formation of highly efficient and stable catalysts for the isobutane/2-butene alkylation. Alkaline-treatment enhanced the incorporation of lanthanum ions and reduced the mass transport limitations.

5.6. References

(1) Weitkamp, J.; Traa, Y. *Catal. Today* **1999**, *49*, 193.

(2) Feller, A.; Zuazo, I.; Guzman, A.; Barth, J. O.; Lercher, J. A. *J. Catal.* **2003**, *216*, 313.

(3) Corma, A.; Martinez, A. *Catal. Rev. Sci. Eng.* **1993**, *35*, 483.

(4) Rouquerol, J.; Avnir, D.; Fairbridge, C. W.; Everett, D. H.; Haynes, J. H.; Pernicone, N.; Ramsay, J. D. F.; Sing, K. S. W.; Unger, K. K. *Pure Appl. Chem.* **1994**, *66*, 1739.

(5) Lercher, J.; Jentys, A. Catalytic Properties of Micro- and Mesoporous Nanomaterials. In *Dekker Encyclopedia of Nanoscience and Nanotechnology*; CRC Press, 2004; Vol. 6.

(6) Guzman, A.; Zuazo, I.; Feller, A.; Olindo, R.; Sievers, C.; Lercher, J. A. *Micropor. Mesopor. Mater.* **2005**, *83*, 309.

(7) Venuto, P. B.; Hamilton, L. A.; Landis, P. S. *J. Catal.* **1966**, *5*, 484.

(8) Ward, J. W. *J. Catal.* **1969**, *14*, 365.

(9) Feller, A.; Guzman, A.; Zuazo, I.; Lercher, J. A. *J. Catal.* **2004**, *224*, 80.

(10) Sievers, C.; Liebert, J. S.; Stratmann, M. M.; Olindo, R.; Lercher, J. A. *Appl. Catal. A-Gen.* **2008**, *336*, 89.

(11) Groen, J. C.; Sano, T.; Moulijn, J. A.; Pérez-Ramírez, J. *J. Catal.* **2007**, *251*, 21.

(12) Ogura, M.; Shinomiya, S.-y.; Tateno, J.; Nara, Y.; Nomura, M.; Kikuchi, E.; Matsukata, M. *Appl. Catal. A-Gen.* **2001**, *219*, 33.

(13) Suzuki, T.; Okuhara, T. *Micropor. Mesopor. Mater.* **2001**, *43*, 83.

(14) Schüßler, F.; Pidko, E. A.; Kolvenbach, R.; Sievers, C.; Hensen, E. J. M.; van Santen, R. A.; Lercher, J. A. *J. Phys. Chem. C* **2011**, *115*, 21763.

(15) Klingmann, R.; Josl, R.; Traa, Y.; Gläser, R.; Weitkamp, J. *Appl. Catal. A-Gen.* **2005**, *281*, 215.

(16) Rørvik, T.; Mostad, H.; Ellestad, O. H.; Stocker, M. *Appl. Catal. A-Gen.* **1996**, *137*, 235.

(17) Feller, A.; Barth, J.-O.; Guzman, A.; Zuazo, I.; Lercher, J. A. *J. Catal.* **2003**, *220*, 192.

(18) Sahebdelfar, S.; Kazemeini, M.; Khorasheh, F.; Badakhshan, A. *Chem. Eng. Sci.* **2002**, *57*, 3611.

(19) Groen, J. C.; Peffer, L. A. A.; Moulijn, J. A.; Pérez-Ramírez, J. *Colloids Surf., A* **2004**, *241*, 53.

(20) Groen, J. C.; Peffer, L. A. A.; Moulijn, J. A.; Pérez-Ramírez, J. *Micropor. Mesopor. Mater.* **2004**, *69*, 29.

(21) Melián-Cabrera, I.; Espinosa, S.; Groen, J. C.; v/d Linden, B.; Kapteijn, F.; Moulijn, J. A. *J. Catal.* **2006**, *238*, 250.

(22) Lippens, B. C.; Linsen, B. G.; De Boer, J. H. *J. Catal.* **1963**, *3*, 32.

(23) Halsey, G. *Chem. Phys.* **1948**, *16*, 931.

(24) ASTM. Standard Test Method for Determination of the Unit Cell Dimension of a Faujasite-Type Zeolite. In *Annual Book of ASTM Standards*, 1985; Vol. D3942-85.

(25) Ravenelle, R. M.; Schüßler, F.; D'Amico, A.; Danilina, N.; van Bokhoven, J. A.; Lercher, J. A.; Jones, C. W.; Sievers, C. *J. Phys. Chem. C* **2010**, *114*, 19582.

(26) ASTM. Standard Test Method for Determination of Relative X-ray Diffraction Intensities of Faujasite-Type Zeolite-Containing Materials. In *Annual Book of ASTM Standards*, 2008; Vol. D39 06-03.

(27) Klinowski, J. *Prog. Nucl. Magn. Reson. Spectrosc.* **1984**, *16*, 237.

(28) Omegna, A.; van Bokhoven, J. A.; Prins, R. *J. Phys. Chem. B* **2003**, *107*, 8854.

(29) Weihe, M.; Hunger, M.; Breuninger, M.; Karge, H. G.; Weitkamp, J. *J. Catal.* **2001**, *198*, 256.

(30) Bludau, H.; Karge, H. G.; Niessen, W. *Micropor. Mesopor. Mater.* **1998**, *22*, 297.

(31) de Lucas, A.; Canizares, P.; Durán, A.; Carrero, A. *Appl. Catal. A-Gen.* **1997**, *154*, 221.

(32) Groen, J. C.; Jansen, J. C.; Moulijn, J. A.; Pérez-Ramírez, J. *J. Phys. Chem. B* **2004**, *108*, 13062.

(33) Groen, J. C.; Zhu, W.; Brouwer, S.; Huynink, S. J.; Kapteijn, F.; Moulijn, J. A.; Pérez-Ramírez, J. *J. Am. Chem. Soc.* **2006**, *129*, 355.

(34) Yoo, K.; Burckle, E. C.; Smirniotis, P. G. *J. Catal.* **2002**, *211*, 6.

Chapter 6

Summary / Zusammenfassung

6.1. Summary

Acid catalyzed reactions are important refining processes. In these processes the heterogeneous catalysts are of enormous importance in case of separating the reactant/product feed from the catalyst. Further the accessibility to active sites in heterogeneous catalysts is of great interest. Large pore zeolites like faujasites show a great potential in this respect. Rare earth exchanged faujasites, especially lanthanum FAU, show an improved catalytic activity. Therefore, the understanding of nature, concentration and location of intrazeolitic lanthanum cations as well as the relations between their properties and the properties of the stabilizing zeolite matrices is crucial for the rationalization of the unique catalytic reactivity of low-silica zeolites.

In this study the C-H bond polarization of adsorbed hydrocarbons and the resulting hydride transfer reaction in Brønsted acid catalyzed reactions e.g. isobutane/2-butene alkylation, low temperature cracking of 2,2,4-trimethylpentane as well as high temperature cracking of propane, n-pentane and n-pentane isomerization were investigated. Therefore, FAU zeolites with varying aluminum concentration in protonic form and with incorporated extra-framework cations (platinum and lanthanum) were studied in detail. In aluminum rich faujasite materials (La-X) some of the lanthanum cations are located in SII sites slightly inside the supercage. Additional stabilization of these isolated La^{3+} species occurs via OH groups of the clustered lanthanum species within the adjacent sodalite cage. In high silica containing FAU materials (La-Y and La-USY) the lanthanum species within the supercage can only be stabilized in hydroxylated form. Polarization of adsorbed hydrocarbons is highest on isolated La^{3+} species accessible in supercage SII sites. The reduced polarization of adsorbed hydrocarbons in La-Y and La-USY is due to the sterical hindrance by shielding OH groups.

The high aluminum containing La-X material show highly improved catalytic performance in low temperature 2,2,4-trimethylpentane cracking. Lanthanum incorporation in USY material (La-USY), containing no isolated La^{3+} species located in supercage, showed no improvement in 2,2,4-TMP cracking. Consequently, accessible lanthanum cations located in the supercage polarize the C-H bond of adsorbed hydrocarbons very strong. This leads to an improved cracking reaction of formed octane isomers build in alkylation reaction resulting in an enhanced hydride transfer. The increased hydride transfer enhances the overall catalyst lifetime as well as the C_8 product yield in isobutane and 2-butene alkylation reaction.

Lanthanum containing FAU materials, showing an improved catalytic activity in isobutane/2-butene alkylation, were also investigated in n-pentane hydroisomerization. For discussion in hydride transfer capability and reaction mechanisms different lanthanum, platinum as well as platinum and lanthanum mixed metal containing FAU materials and platinum promoted sulfated zirconium oxide was investigated. Hydroisomerization reaction of n-pentane on lanthanum containing FAU materials exclusively occur on strong Brønsted acid sites. Hydroisomerization reaction on platinum containing materials follows a bifunctional mechanism including dehydrogenation/hydrogenation on platinum sites and skeletal isomerization on the Brønsted acid sites. In mixed metal containing faujasite materials both reaction mechanisms coexist.

Alkaline treatment of faujasite materials was investigated to discuss crystal surface modifications and transport properties of reactants and products in acid catalyzed reactions. It was evidenced that not only the concentration of active Brønsted acid sites is an important factor for the overall catalyst lifetime in alkylation reaction. Short alkaline treatment improves the accessibility of active sites and reduce mass transport limitations. Consequently, the overall catalyst lifetime was increased dramatically.

We can conclude that lanthanum containing faujasites are promising materials in Brønsted acidic catalyzed reactions. Especially isolated La^{3+} cations stabilized in accessible positions in supercages are highly polarizing C-H bonds of adsorbed hydrocarbons and therefore responsible for the enhanced catalytic activity. Moreover, a minimized transport limitation onto the catalyst active sites increases the overall catalyst productivity.

6.2. Zusammenfassung

In der Aufarbeitung von Erdöl sind sauer katalysierte Reaktionen von großer Bedeutung. In diesen Prozessen ermöglicht der Feststoffkatalysator eine leichte Separation des Katalysators vom Edukt, bzw. Produktstrom. Weiter ist die Zugänglichkeit aktiver Zentren von großem Interesse. Hier zeigen vor allem großporige Zeolithe, wie z. B. der Faujasit, großes Potential. Modifizierte Faujasite, ausgetauscht mit seltenen Erden, vor allem mit Lanthan, zeigen eine erhöhte katalytische Aktivität. Um die katalytische Aktivität solcher Katalysatoren weiter zu verbessern, ist es von besonderem Interesse, die Bedeutung von Struktur, Konzentration und Lage der eingebrachten Lanthankationen in das Zeolithgitter, sowie deren Auswirkungen auf das Zeolithgitter, tiefergehend zu erforschen.

In dieser Arbeit wurde die Polarisierung von C-H Bindungen adsorbierter Kohlenwasserstoffe und die daraus resultierende Hydrid Transfer Reaktion in Brønsted sauer katalysierten Reaktionen, wie z. B. Alkylierung von Isobutan und 2-Buten, Cracken von 2,2,4-Trimethylpentan bei niedrigen Temperaturen, Cracken von Propan und n-Pentan bei hohen Temperaturen, sowie Isomerisierung von n-Pentan, untersucht. Hierfür wurden FAU Zeolithe mit unterschiedlichem Aluminiumgehalt in deren Protonenform, sowie mit Metallen (Platin und Lanthan) ausgetauscht, verwendet. In aluminiumreichen Faujasiten (La-X) koordinieren Anteile an Lanthankationen in SII Zentren leicht innerhalb des Superkäfigs. Eine weitere Stabilisierung dieser isolierten La^{3+} Kationen erfolgt dabei über OH Gruppen des Lanthan-Clusters innerhalb des Sodalith-Käfigs. In Zeolithen mit erhöhtem Silizium Anteil (La-Y sowie La-USY) kann die Stabilisierung des eingebrachten Lanthankations im Superkäfig nur in hydroxylierter Form erfolgen. Die Polarisierung adsorbierter Kohlenwasserstoffe ist dabei an isolierten La^{3+} Kationen in zugängigen SII Zentren im FAU Superkäfig am höchsten. Die geringere Polarisierung adsorbierter Kohlenwasserstoffe in La-Y sowie La-USY resultiert aus der sterischen Hinderung, hervorgerufen durch Hydroxylgruppen um das Lanthankation.

Beim Cracken von 2,2,4-Trimethylpentan bei niedrigen Temperaturen zeigen aluminiumreiche La-X Materialien stark verbesserte katalytische Eigenschaften. Materialien mit keinerlei isolierten La^{3+} Kationen (La-USY) zeigen im 2,2,4-Trimethylpentan Cracken bei niedrigen Temperaturen keine Verbesserung. Letztendlich wird dadurch die starke Polarisierung der C-H Bindungen adsorbierter Kohlenwasserstoffe an zugänglichen Lanthankationen im Superkäfig ersichtlich. Dies kann zu einem verbesserten Cracken, geformter Oktanisomere in der Alkylierungsreaktion und einem daraus resultierenden erhöhtem Hydrid Transfer führen.

Dabei erhöht der verbesserte Hydrid Transfer die Katalysatorlebenszeit, wie auch die C_8 Ausbeute in der Alkylierungsreaktion von Isobutan und 2-Buten.

Materialien, die in dieser Arbeit eine verbesserte katalytische Aktivität in der Alkylierung von Isobutan und 2-Buten gezeigt haben, wurden ebenso in der Hydroisomerisierung von n-Pentan getestet. Um hier den Hydrid Transfer sowie Reaktionsmechanismus zu diskutieren, wurden verschiedene Materialien mit Lanthan, Platin, sowie Lanthan-Platin Mischmetall-Materialien, sowie Platin modifiziertes Zirkonoxid verwendet. Die Hydroisomerisierungsreaktion von n-Pentan an La-FAU Materialien erfolgt ausschließlich an starken Brønsted Säure Zentren. Die Hydroisomerisierungsreaktion an Platin Materialien folgt einem bifunktionalen Mechanismus, wobei die Dehydrierung/Hydrierung am Platin, sowie die Skeletisomerisierung am Brønsted Säure Zentrum erfolgt. In Mischmetall Katalysatoren laufen beide Reaktionsmechanismen gleichzeitig ab.

Um den Zusammenhang der Beschaffenheit der Kristalloberfläche auf Transporteigenschaften von Edukt/Produkt in sauer katalysierten Reaktionen zu untersuchen, wurden Faujasit Materialien basisch behandelt. Dabei wurde gezeigt, dass nicht nur die Konzentration an aktiven Brønsted Säure Zentren die Katalysatorlebenszeit in der Alkylierungsreaktion von Isobutan und 2-Buten beeinflusst. Kurzes, basisches behandeln verbessert die Zugängigkeit zu aktiven Zentren und reduziert Stofftransportlimitierungen. Folglich erhöht sich die Katalysatorlebenszeit dramatisch.

Zusammenfassend kann gesagt werden, dass Faujasite, modifiziert mit Lanthan, vielversprechende Materialien für Brønsted sauer katalysierte Reaktionen darstellen. Vor allem isolierte La^{3+} Kationen, stabilisiert in zugänglichen Positionen im FAU-Superkäfig, polarisieren C-H Bindungen von adsorbierten Kohlenwasserstoffen sehr stark, was zu einer erhöhten katalytischen Aktivität führt. Eine minimierte Transportlimitierung an aktiven Zentren im Katalysator erhöht weiter die katalytische Produktivität.

Appendix

A. Appendix for Chapter 2

Quantitative determination of aluminum atoms in six rings into FAU type zeolite is made using the method described by Mikovsky et al. (see citation 50).

According to Mikovsky, in the first line a homogeneous aluminum distribution in FAU six ring windows is assumed. Furthermore, it is assumed that each tetrahedral aluminum belongs to two 6-membered ring. Therefore, in one cell unit are 64 6-membered rings containing 0,1,2 or 3 tetrahedral lattice aluminum atoms.

Table A 1: Temperature programmed desorption of ammonia

Catalyst	Acidity (TPD) [mmol/g]	Temperature maximum [K]
La-USY I	1.172	567
La-USY II	1.129	542
La-Y I	0.808	532
La-Y II	0.341	525
La-X I	0.751	524
La-X II	0.779	540

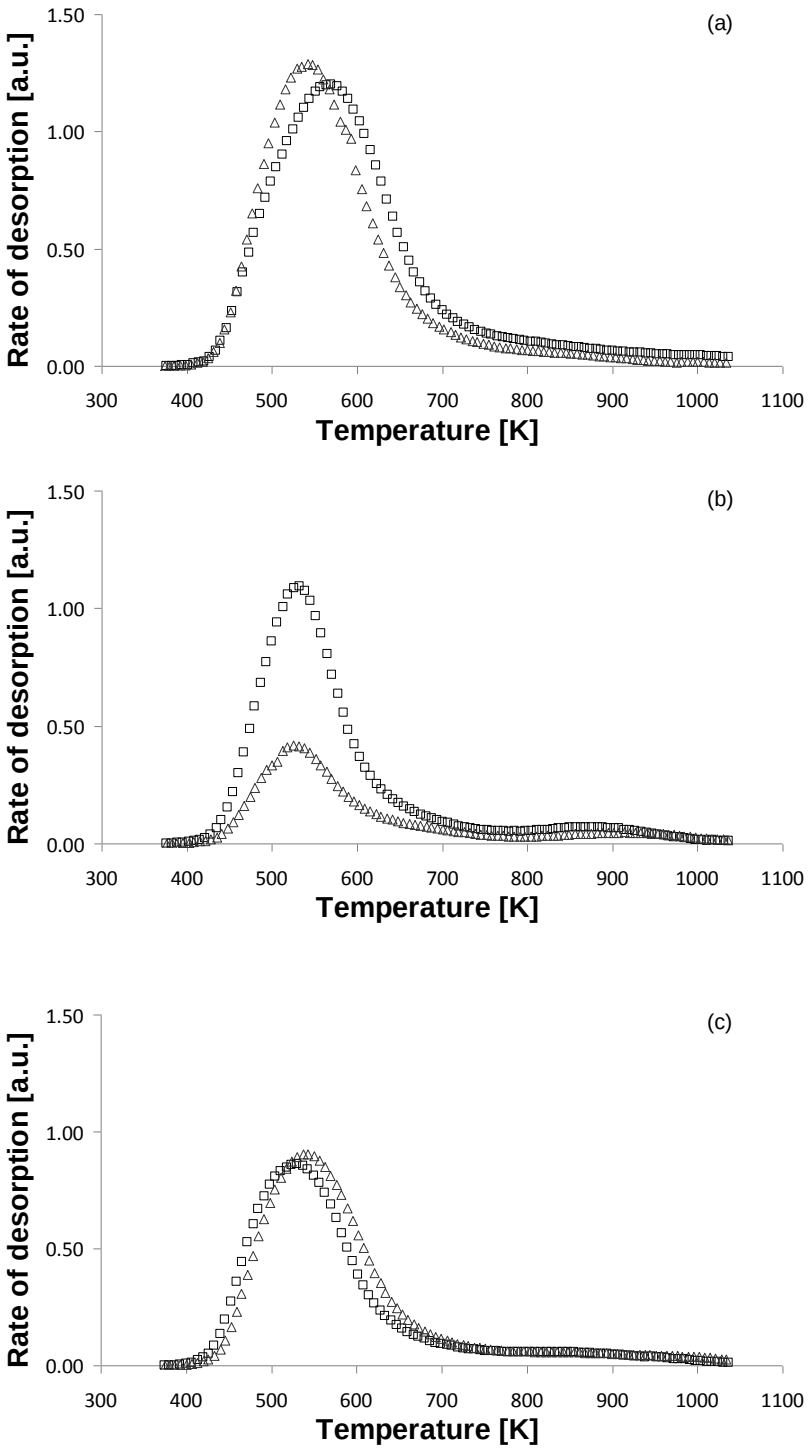

Figure A 1: Temperature programmed desorption of ammonia for La-USY (a), La-Y (b) and La-X (c) materials

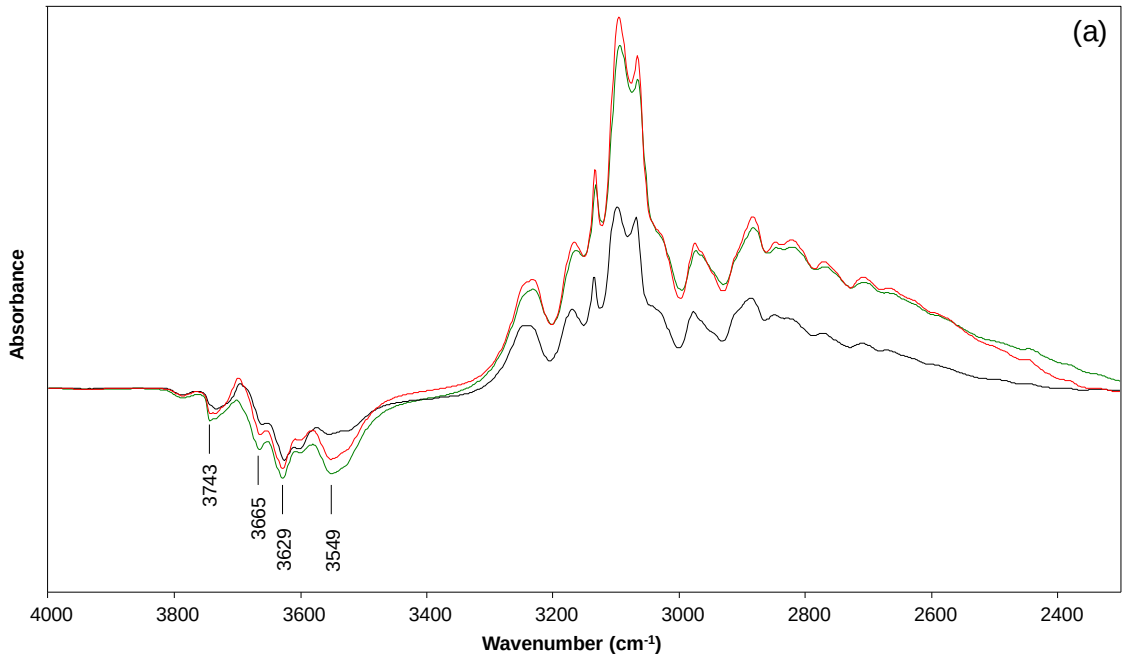
(a)
Absorbance
3743
3665
3629
3549
4000
3800
3600
3400
3200
3000
2800
2600
2400
Wavenumber (cm-1)

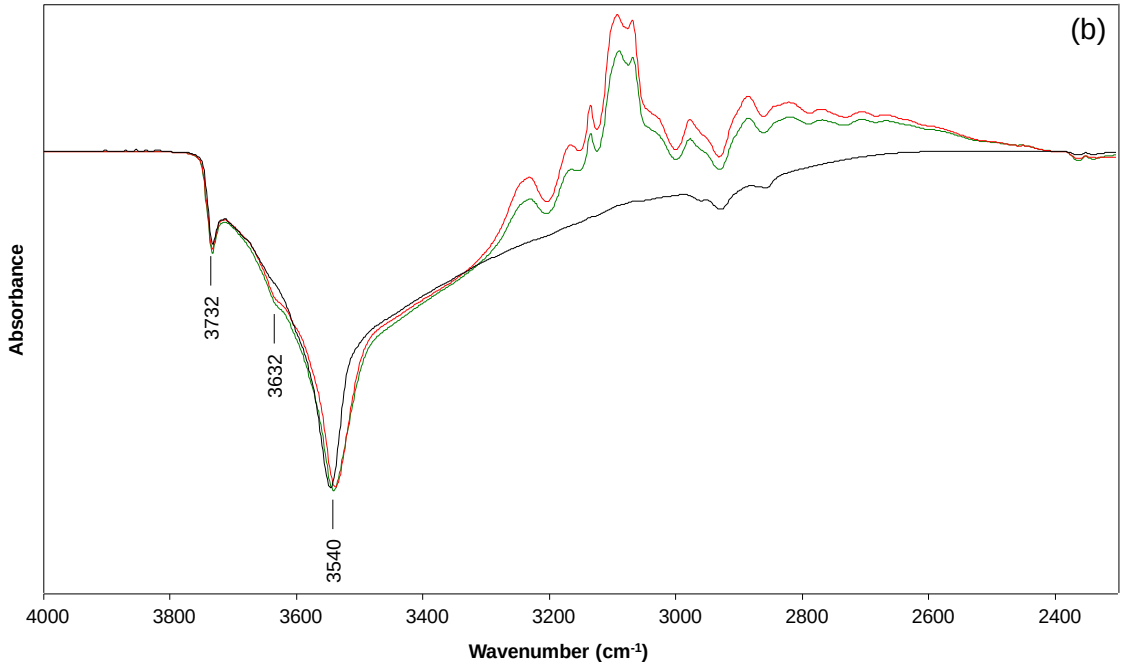
(b)
Absorbance
3732
3632
3540
4000
3800
3600
3400
3200
3000
2800
2600
2400
Wavenumber (cm-1)

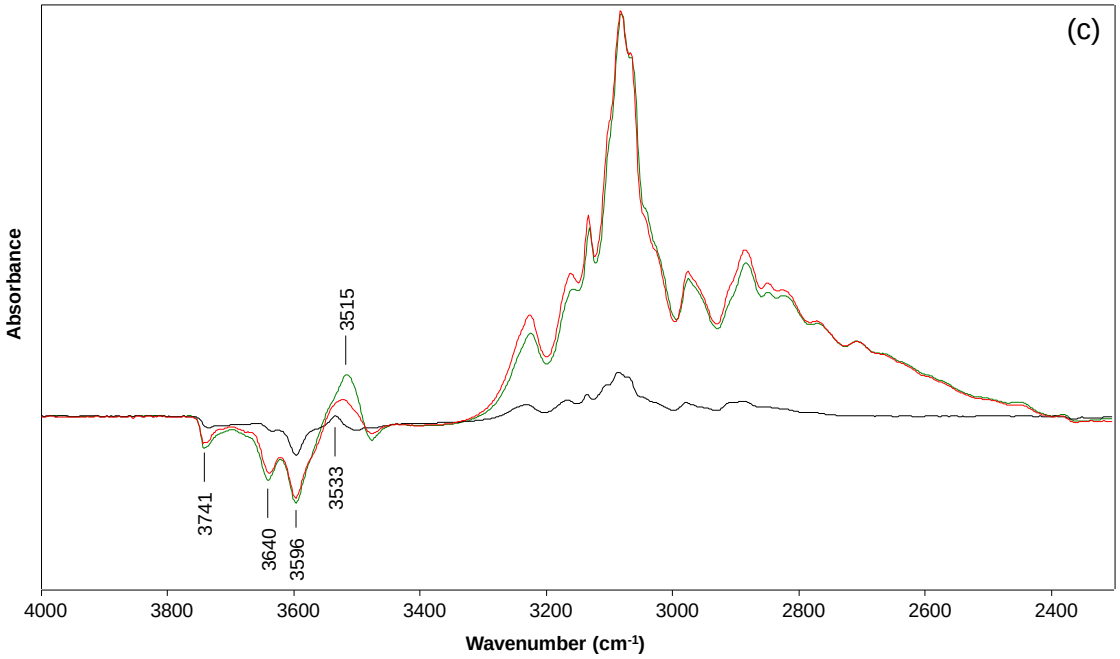

Figure A 2: Difference IR spectra of adsorbed pyridine at La-USY I (a), La-Y I (b) and La-X I (c); adsorption of one minute (green), after outgasing for 1 h (red) and desorption for 0.5 h at 723 K (black)

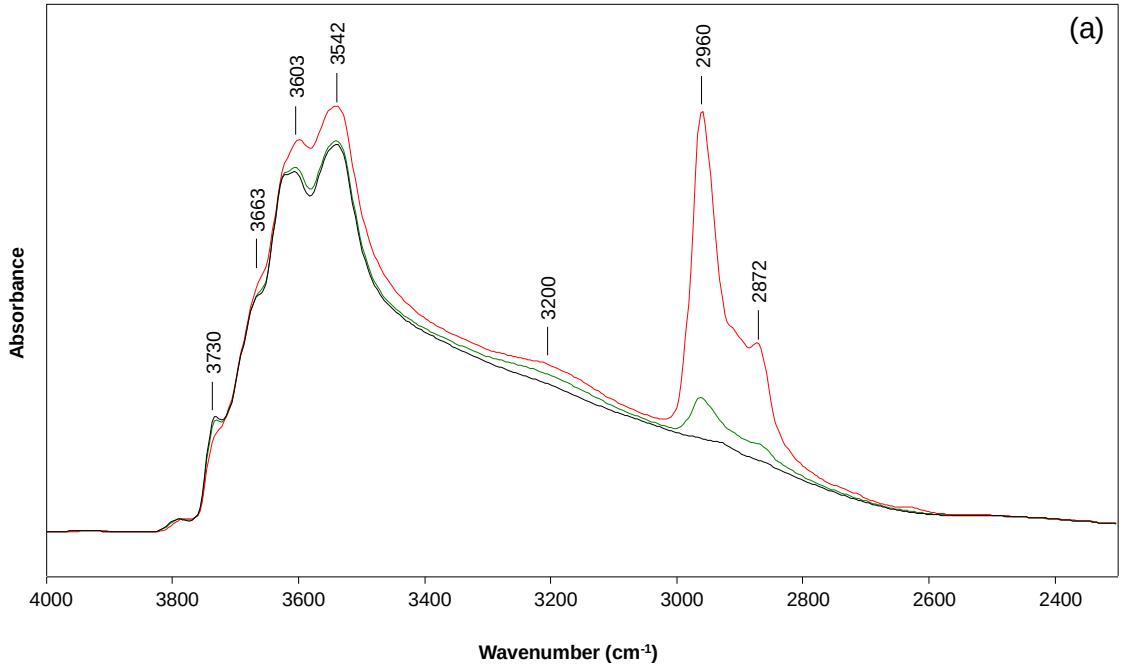
(a)
Absorbance
3730
3663
3603
3542
3200
2960
2872
4000
3800
3600
3400
3200
3000
2800
2600
2400
Wavenumber (cm-1)

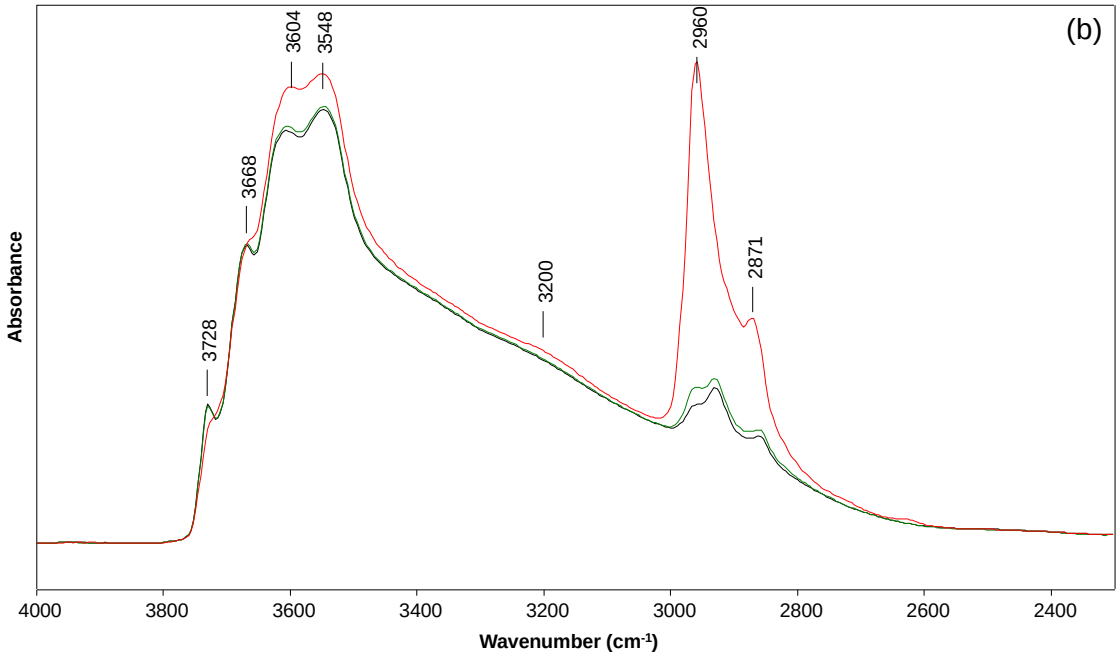
(b)
Absorbance
3728
3668
3604
3548
3200
2960
2871
4000
3800
3600
3400
3200
3000
2800
2600
2400
Wavenumber (cm-1)

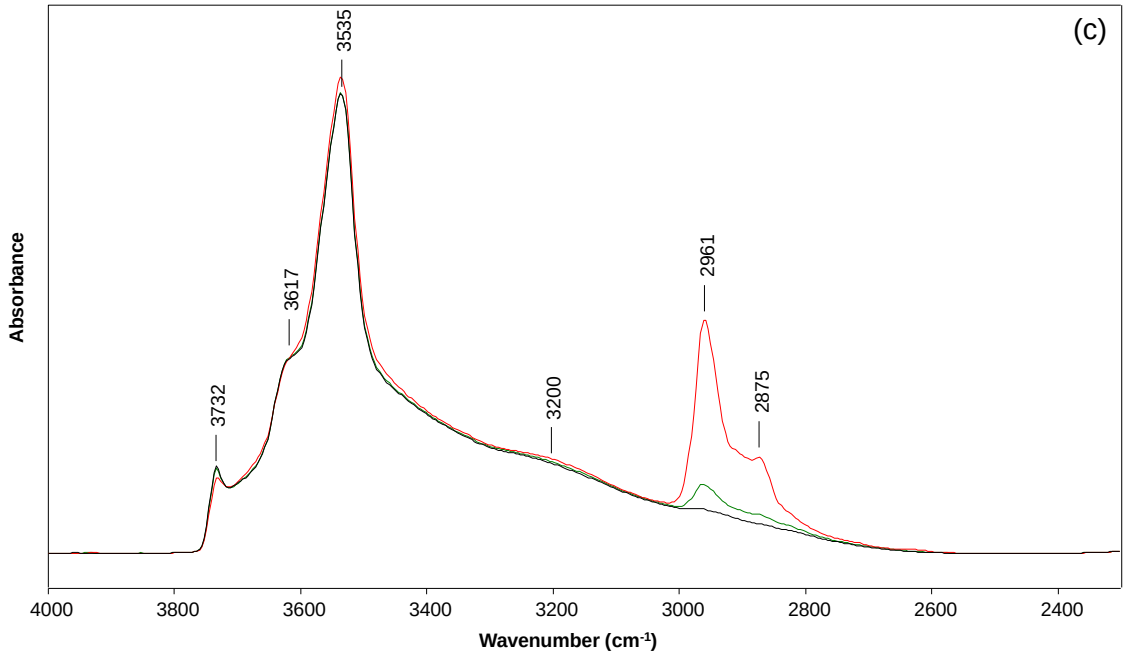
(c)
3535
3617
3732
3200
2961
2875
Absorbance
4000
3800
3600
3400
3200
3000
2800
2600
2400
Wavenumber (cm-1)

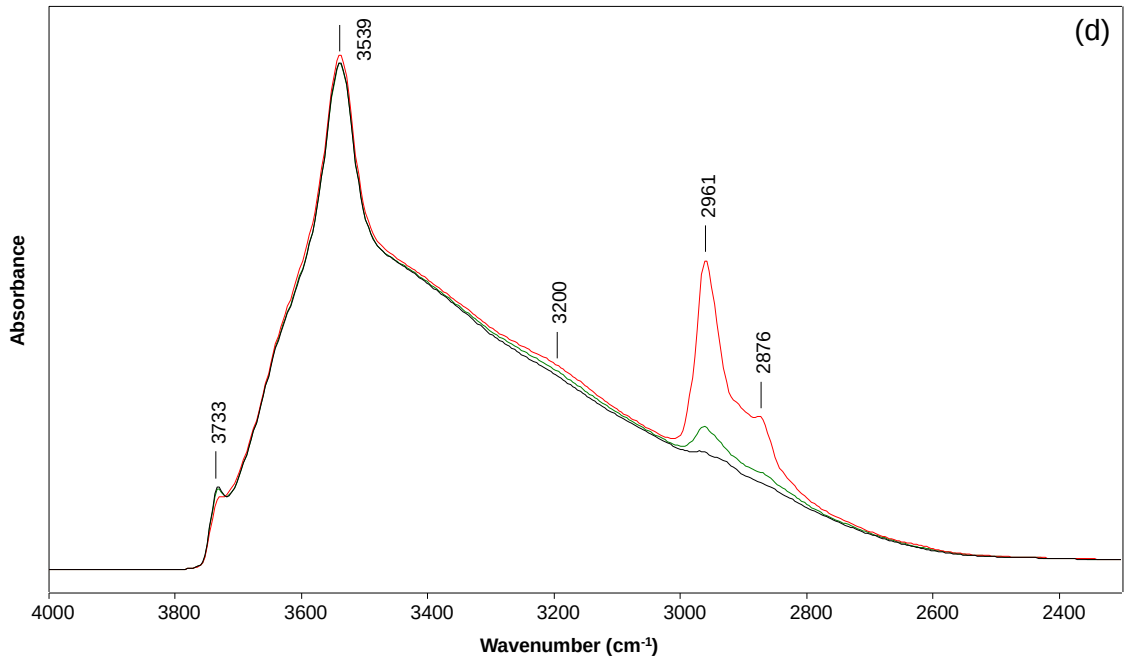
(d)
3539
3733
3200
2961
2876
Absorbance
4000
3800
3600
3400
3200
3000
2800
2600
2400
Wavenumber (cm-1)

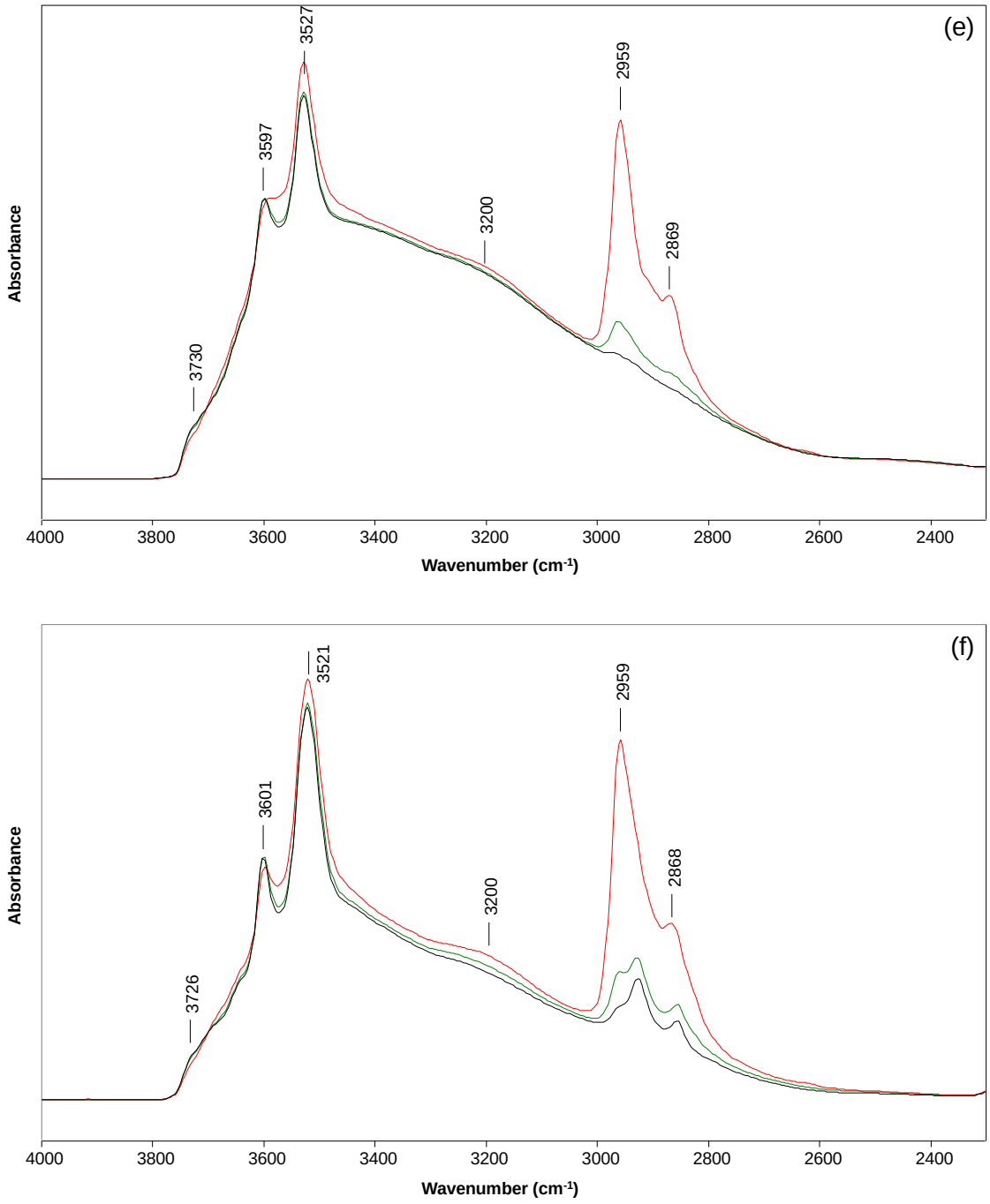

Figure A 3: IR spectra of adsorbed isobutane at La-USY I (a), La-USY II (b), La-Y I (c), La-Y II (d), La-X I (e) and La-X II (f); 0.1 mbar isobutane partial pressure (black), 1 mbar isobutane partial pressure (green) and 10 mbar isobutane partial pressure (red)

B. Appendix for Chapter 5

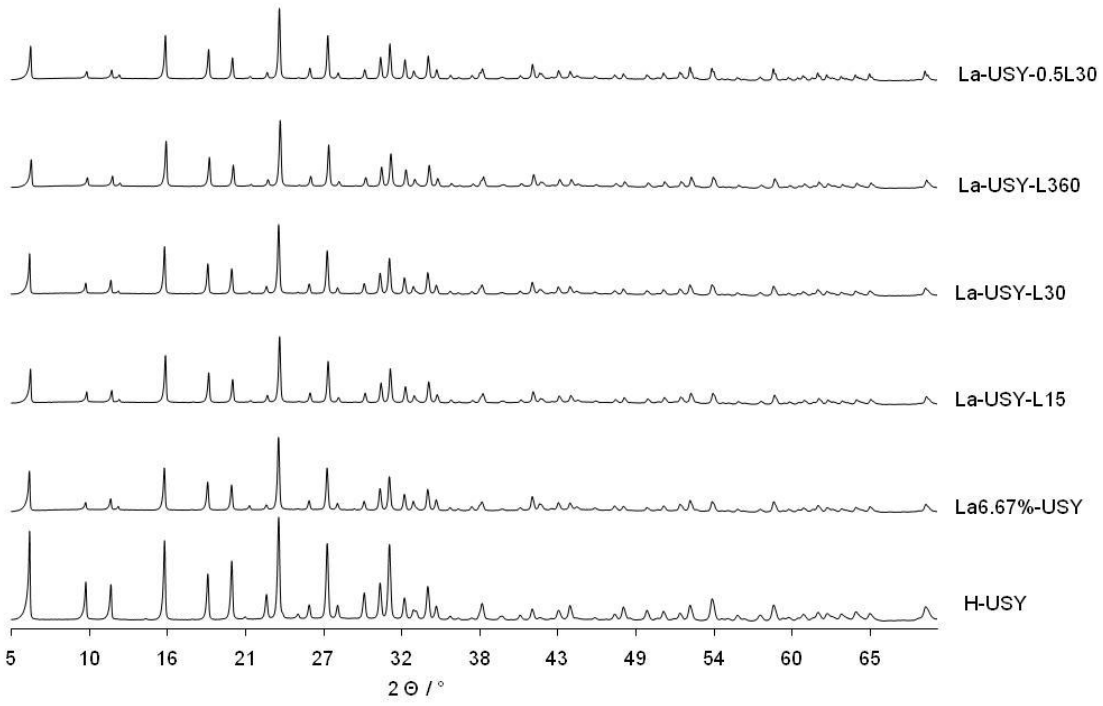

Figure B 1: X-ray diffractograms of all the studied zeolitic materials

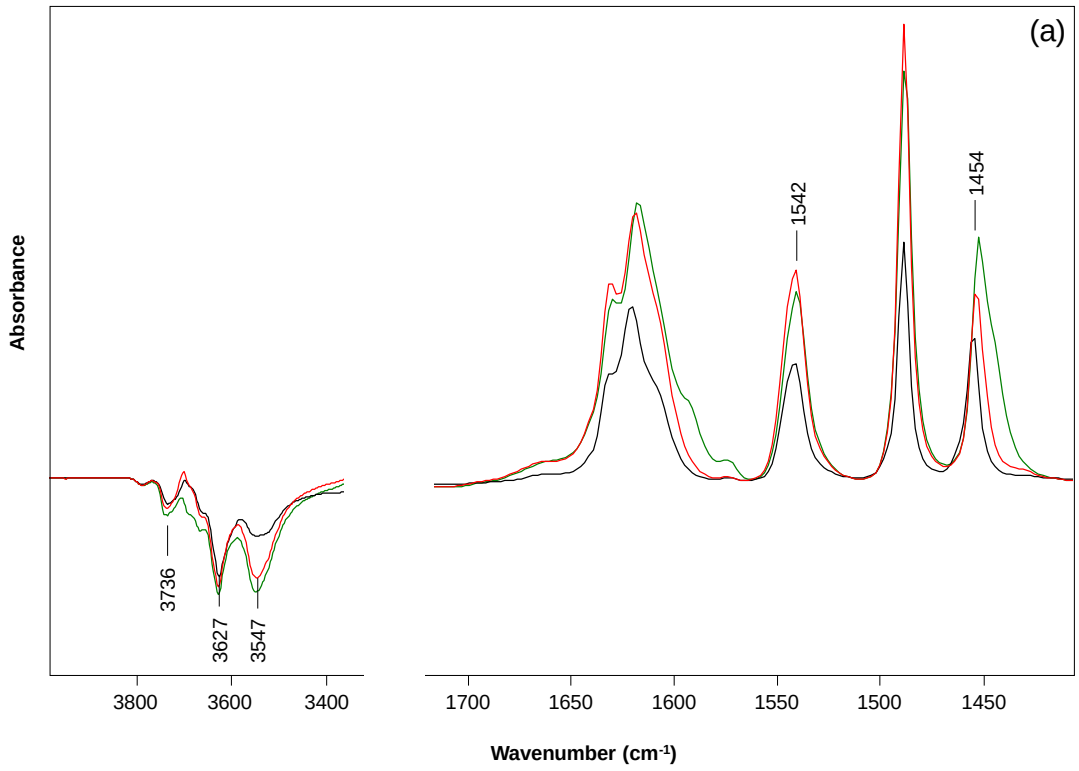
(a)
Absorbance
3736
3627
3547
1542
1454
3800
3600
3400
1700
1650
1600
1550
1500
1450
Wavenumber (cm-1)

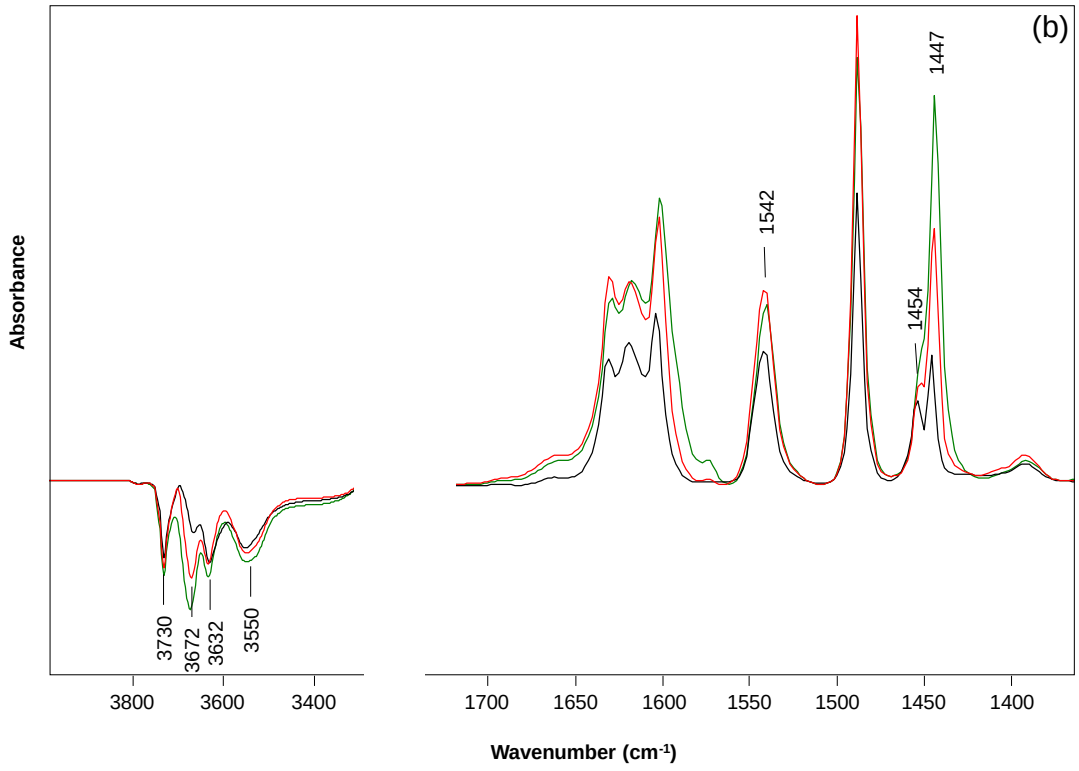
(b)
Absorbance
3730
3672
3632
3550
1542
1454
1447
3800
3600
3400
1700
1650
1600
1550
1500
1450
1400
Wavenumber (cm-1)

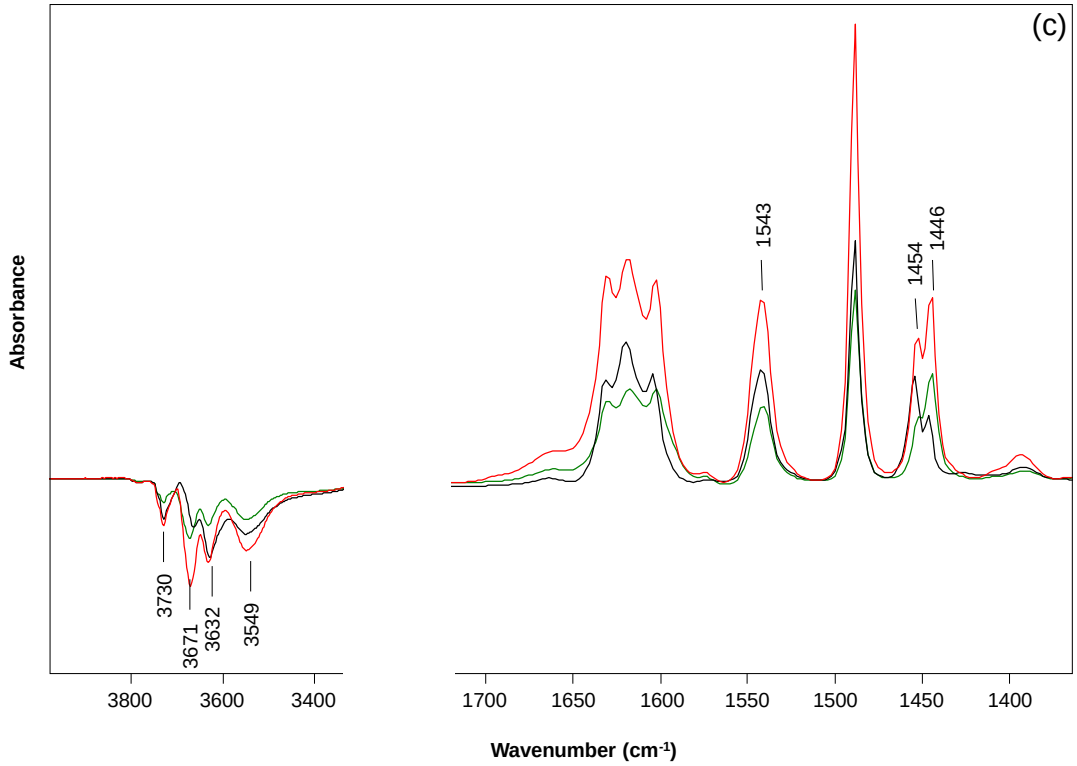
(c)
Absorbance
3730
3671
3632
3549
1543
1454
1446
3800
3600
3400
1700
1650
1600
1550
1500
1450
1400
Wavenumber (cm-1)

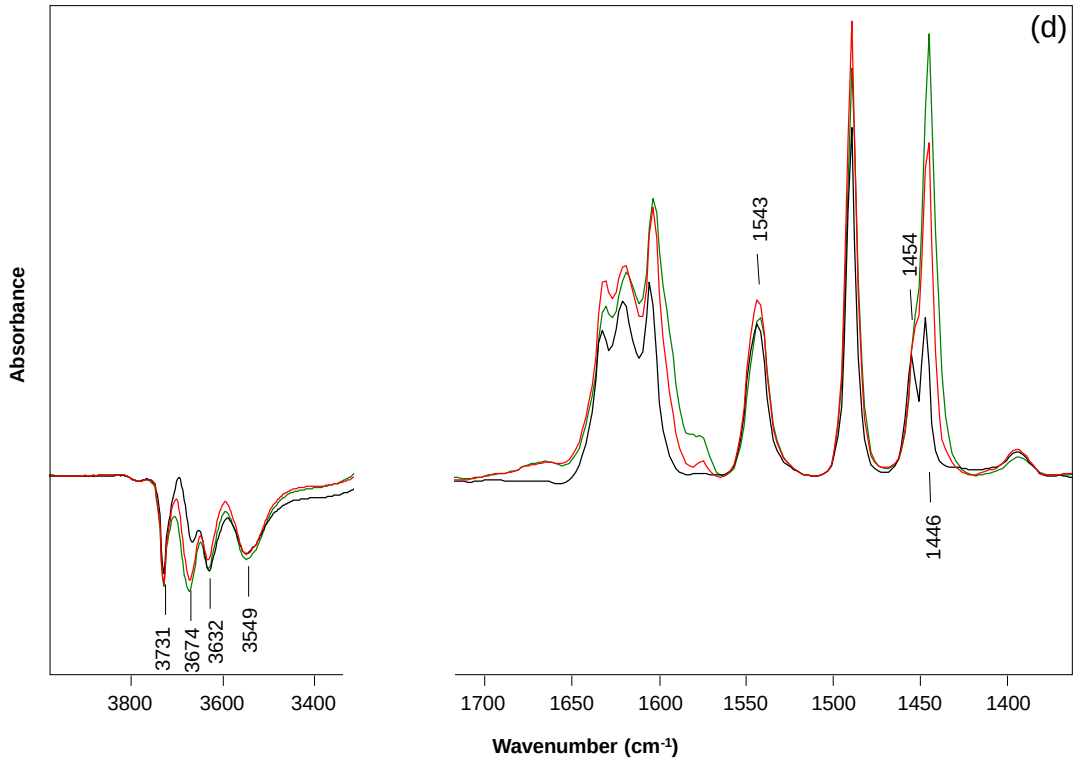
(d)
Absorbance
3731
3674
3632
3549
1543
1454
1446
3800
3600
3400
1700
1650
1600
1550
1500
1450
1400
Wavenumber (cm-1)

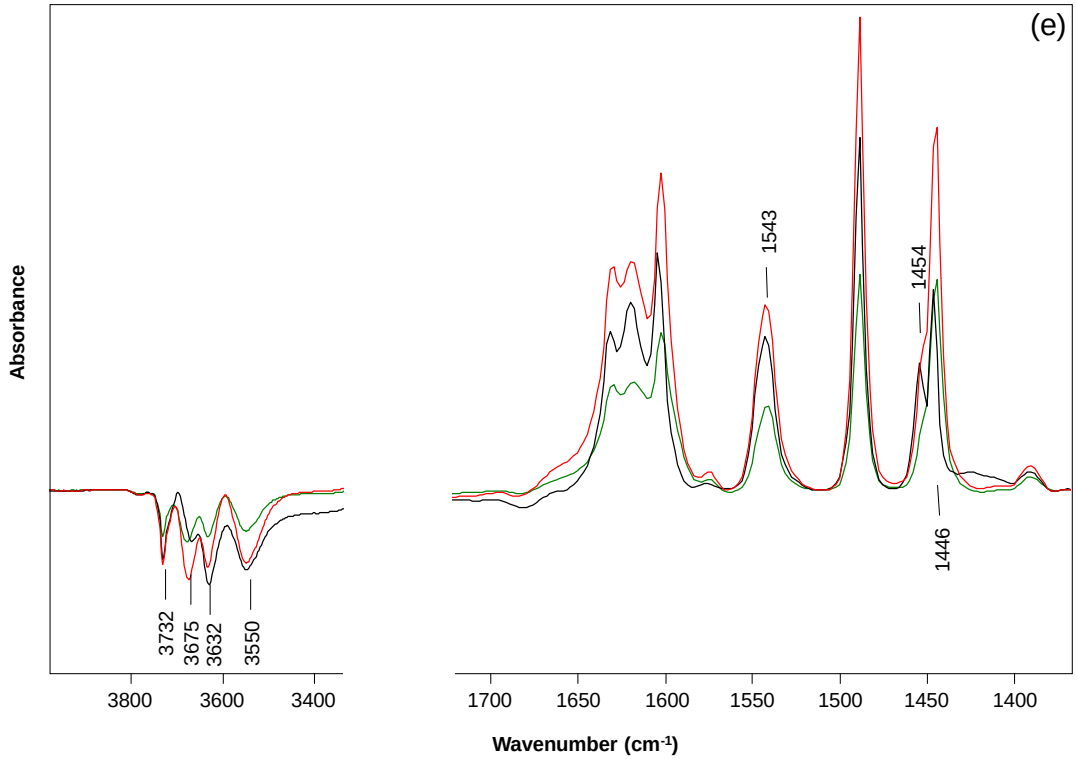
(e)
Absorbance
3732
3675
3632
3550
1543
1454
1446
3800
3600
3400
1700
1650
1600
1550
1500
1450
1400
Wavenumber (cm-1)

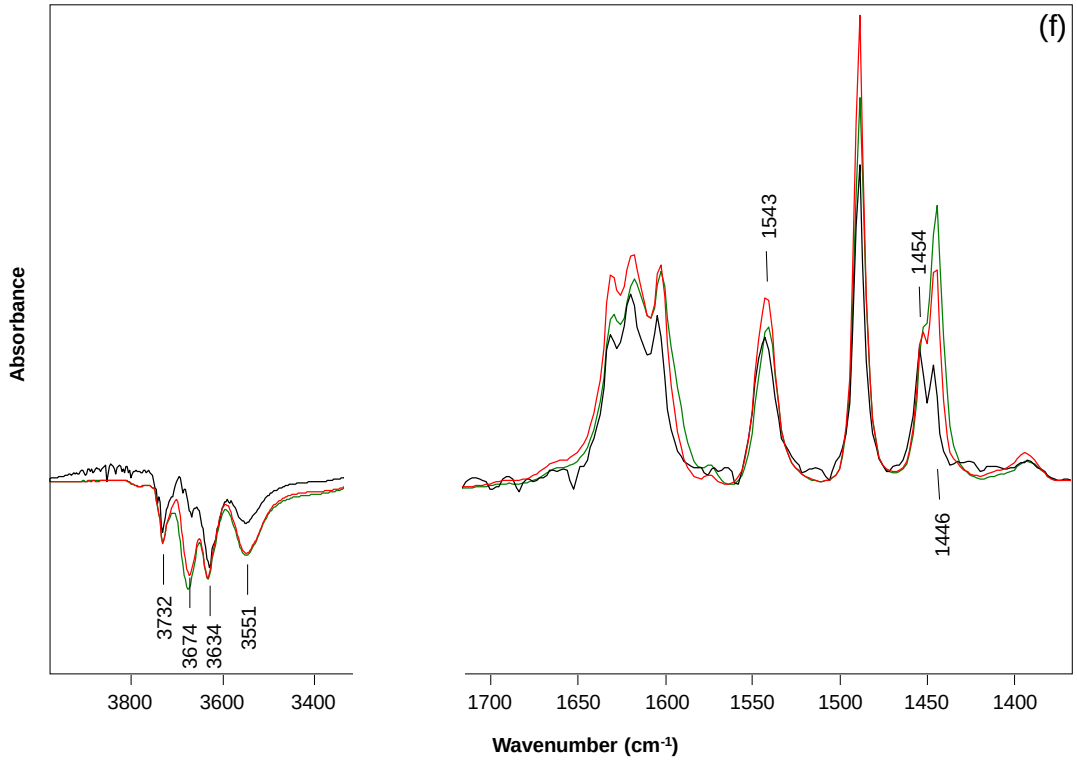
(f)
Absorbance
3732
3674
3634
3551
1543
1454
1446
3800
3600
3400
1700
1650
1600
1550
1500
1450
1400
Wavenumber (cm-1)

Figure B 2: Difference IR spectra of adsorbed pyridine at H-USY (a), La6.67%-USY (b), La-USY-L15 (c), La-USY-L30 (d), La-USY-L360 (e) and La-USY-0.5L30 (f); adsorption of one minute (green), after outgasing for 1 h (red) and desorption for 0.5 h at 723 K (black)

Publications

Journal publications

1. Ryan M. Ravenelle, Florian Schüßler, Andrew D'Amico, Nadiya Danilina, Jeroen A. van Bokhoven, Johannes A. Lercher, Christopher W. Jones, and Carsten Sievers, "Stability of Zeolites in Hot Liquid Water", J. Phys. Chem. C, 2010, 114, 19582-19595
2. Florian Schüßler, Evgeny A. Pidko, Robin Kolvenbach, Carsten Sievers, Emiel J.M. Hensen, Rutger A. van Santen, and Johannes A. Lercher, "Nature and Location of Cationic Lanthanum Species in High Alumina Containing Faujasite Type Zeolites", J. Phys. Chem. C, 2011, 115, 21763-21776
3. Sonja Kouva, Jaana M. Kanervo, Florian Schüßler, Roberta Olindo, Johannes A. Lercher and Outi Krause, "Sorption and diffusion parameters from vacuum-TPD of ammonia on H-ZSM-5", Chem. Eng. Sci., 2013, 89, 40-48
4. Florian Schüßler, Stefan Schallmoser, Hui Shi, Erika Ember and Johannes A. Lercher, "Influence of La^{3+} cations in zeolites for acid catalyzed alkane reactions", (paper ready for submission)
5. Florian Schüßler, Stefanie Simson, Arne Holtz and Johannes A. Lercher, "Mechanistic Studies on the Hydroisomerization of n-pentane over Lanthanum and Platinum Ion Exchanged Faujasites and Platinum Promoted Sulfated Zirconium Oxide", (in preparation)
6. Florian Schüßler, Sabine Wilhelm, Erika Ember and Johannes A. Lercher, "Enhanced catalytic activity of alkaline treated FAU materials for isobutane/2-butene alkylation", (in preparation)

Conference Contributions – Posters

1. F. Schüßler, C. Sievers, X. Li, J.A. Lercher, “Comparison of LaX and ZnX zeolites with different exchanging degrees”, 42. Jahrestreffen Deutscher Katalytiker, 2009, Weimar, Germany
2. C. Sievers, A. D’Amico, F. Schüßler, N. Danilina, J.A. van Bokhoven, C.W. Jones, “Modification of Zeolite HY in Hot Liquid Water”, 2009, Salamanca, Spain
3. F. Schüßler, X. Li, J.A. Lercher, “Comparison of different La-FAU catalysts for Brønsted acid-catalyzed reactions”, 43. Jahrestreffen Deutscher Katalytiker, 2010, Weimar, Germany
4. S.K. Kouva, J.M. Kanervo, A.O.I. Krause, F. Schüßler, R. Olindo, J.A. Lercher, “Determination of ammonia sorption kinetics using TPD data”, IDECAT workshop “Advanced utilisation of temperature-programmed experiments in catalysis research”, 2010, Espoo, Finland
5. F. Schüßler, X. Li, J.A. Lercher, “Concerted activation of alkanes in lanthanum exchanged Faujasites”, 16th International Zeolite Conference, 2010, Sorrento, Italy
6. S.K. Kouva, J.M. Kanervo, A.O.I. Krause, F. Schüßler, R. Olindo, J.A. Lercher, “Using vacuum-TPD data in the extraction of a kinetic model for sorption of ammonia”, i-CATS conference, 2010, Messina, Italy
7. F. Schüßler, E.A. Pidko, R. Kolvenbach, C. Sievers, E.J.M. Hensen, R.A. van Santen, J.A. Lercher, “On the behavior of different Lanthanum species in Faujasite zeolites and their impact of adsorbed alkanes”, 44. Jahrestreffen Deutscher Katalytiker, 2011, Weimar, Germany

Conference Contributions – Talks

1. C. Sievers, R. Ravenelle, A. D'Amico, F. Schüßler, C.W. Jones, "Changes in Zeolite Structures Induced by Aqueous Biomass Solutions", AIChE Annual Meeting, 2009, Nashville TN, USA
2. F. Schüßler, X. Li, J.A. Lercher, "On the role of chemical composition of La^{3+} exchanged FAU for Brønsted acid-catalyzed reactions", 22. Deutsche Zeolith-Tagung, 2010, München, Germany
3. S.K. Kouva, J.M. Kanervo, A.O.I. Krause, F. Schüßler, R. Olindo, J.A. Lercher, "Using TPD data in determination of ammonia sorption kinetics on HZSM-5", 14^{th} Nordic Symposium in Catalysis, 2010, Helsingør, Denmark